

# Extensive longevity and DNA virus-driven adaptation in nearctic *Myotis* bats

Juan M Vazquez<sup>1†</sup>, M. Elise Lauterbur<sup>2,3†</sup>, Saba Mottaghinia<sup>4</sup>, Melanie Bucci<sup>2</sup>, Devaughn Fraser<sup>5,6</sup>, Genavieve Gray-Sandoval<sup>2</sup>, Léa Gaucherand<sup>7</sup>, Zeinab R Haidar<sup>8,9</sup>, Melissa Han<sup>10</sup>, William Kohler<sup>10</sup>, Tanya M. Lama<sup>11</sup>, Amandine Le Corf<sup>4</sup>, Sarah Maesen<sup>4</sup>, Dakota McMillan<sup>1,12</sup>, Stacy Li<sup>1,13</sup>, Johnathan Lo<sup>13</sup>, Carine Rey<sup>4</sup>, Samantha LR Capel<sup>6</sup>, Michael Singer<sup>14</sup>, Kathleen Slocum<sup>15</sup>, William Thomas<sup>16</sup>, Janet Debelak Tyburec<sup>17</sup>, Sarah Villa<sup>14</sup>, Richard Miller<sup>10</sup>, Michael Buchalski<sup>5</sup>, Jose Pablo Vazquez-Medina<sup>1</sup>, Sébastien Pfeffer<sup>7</sup>, Lucie Etienne<sup>4\*\*\*</sup>, David Enard<sup>2†\*\*</sup>, Peter H Sudmant<sup>1,13†\*</sup>

## Affiliations:

1. Department of Integrative Biology, University of California, Berkeley, Berkeley, CA USA
2. Department of Ecology and Evolutionary Biology, University of Arizona, Tucson, AZ USA
3. Current affiliation: Department of Biology, University of Vermont, Burlington, VT USA
4. Centre International de Recherche en Infectiologie (CIRI), Inserm U1111, UCBL1, CNRS UMR5308, Ecole Normale Supérieure ENS de Lyon, Université de Lyon, Lyon, France
5. Wildlife Genetics Research Unit, Wildlife Health Laboratory, California Department of Fish and Wildlife, Sacramento, CA, United States
6. Current affiliation: Wildlife Diversity Program, Wildlife Division, Connecticut Department of Energy and Environmental Protection, Burlington, CT, United States
7. Université de Strasbourg, Architecture et Réactivité de l'ARN, Institut de Biologie Moléculaire et Cellulaire du CNRS, Strasbourg, France.
8. Department of Biology, California State Polytechnic University, Humboldt, Arcata, CA USA
9. Current affiliation: Western EcoSystems Technology Inc, Cheyenne, WY USA
10. Department of Pathology and Clinical Laboratories, University of Michigan, Ann Arbor, MI USA
11. Department of Biological Sciences, Smith College, Northampton, MA USA
12. Department of Science and Biotechnology, Berkeley City College, Berkeley, CA USA
13. Center for Computational Biology, University of California, Berkeley, Berkeley, CA USA
14. Department of Molecular and Cellular Biology, University of California, Berkeley, Berkeley, CA USA
15. Bat Conservation International, Austin, TX USA
16. Department of Ecology and Evolution, Stony Brook University, Stony Brook NY USA
17. Bat Survey Solutions, LLC, Tucson, AZ USA

† Contributed equally as first authors

‡ Contributed equally as senior authors

\* Correspondence: [psudmant@berkeley.edu](mailto:psudmant@berkeley.edu)

\*\* Correspondence: [denard@arizona.edu](mailto:denard@arizona.edu)

\*\*\* Correspondence: [lucie.etienne@ens-lyon.fr](mailto:lucie.etienne@ens-lyon.fr)

**Keywords:** Aging, Bats, Cancer, Evolutionary Biology, Functional Genomics, Immunity, Infectious Disease

## Abstract

The rich species diversity of bats encompasses extraordinary adaptations, including extreme longevity and tolerance to infectious disease. While traditional approaches using genetic screens in model organisms have uncovered some fundamental processes underlying these traits, model organisms do not possess the variation required to understand the evolution of traits with complex genetic architectures. In contrast, the advent of genomics at tree-of-life scales enables us to study the genetic interactions underlying these processes by leveraging millions of years of evolutionary trial-and-error. Here, we use the rich species diversity of the genus *Myotis* - one of the longest-living clades of mammals - to study the evolution of longevity-associated traits and infectious disease using functional evolutionary genomics. We generated reference genome assemblies and cell lines for 8 closely-related (~11 MYA) species of *Myotis* rich in phenotypic and life history diversity. Using genome-wide screens of positive selection, analysis of structural variation and copy number variation, and functional experiments in primary cell lines, we identify new patterns of adaptation in longevity, cancer resistance, and viral interactions both within *Myotis* and across bats. We find that the rapid evolution of lifespan in *Myotis* has some of the most significant variations in cancer risk across mammals, and demonstrate a unique DNA damage response in the long-lived *M. lucifugus* using primary cell culture models. Furthermore, we find evidence of abundant adaptation in response to DNA viruses, but not RNA viruses, in *Myotis* and other bats. This is in contrast to these patterns of adaptation in humans, which might contribute to the importance of bats as a reservoir of zoonotic viruses. Together, our results demonstrate the utility of leveraging natural variation to understand the genomics of traits with implications for human health and suggest important pleiotropic relationships between infectious disease tolerance and cancer resistance.

## Introduction

Bats (order *Chiroptera*) represent approximately 20% of all known mammalian species and are one of the most phenotypically diverse clades of mammals<sup>1,2</sup>. Since their emergence 60 million years ago<sup>3-5</sup>, many bat lineages have independently evolved a wide variety of life history strategies and phenotypic traits, including exceptional changes in longevity, viral tolerance, and immune defense<sup>6-11</sup>. Such systems, in which shared traits have evolved *de novo* multiple times, are powerful resources for dissecting the genetic basis of phenotypes. Rigorous approaches to studying these traits, however, depend on high-quality, well-annotated genomes to test evolutionary and genomic hypotheses, and on experimental functional systems to validate these hypotheses.

The largest genus of bats - *Myotis* - is estimated to have emerged approximately 33 million years ago<sup>12,13</sup>, and encompasses over 139 described species spanning six continents and a wide range of ecological niches<sup>1,12-14</sup>. Extraordinary changes in lifespan have independently evolved multiple times in *Myotis*, including the most extreme variation in lifespan amongst mammals<sup>6,15-18</sup>. There exists a six-fold difference in lifespan between the longest-lived species (*M. brandtii*, 42 years<sup>15,19</sup>, **Figure 1A**) and the shortest-lived species (*M. nigricans*, 7 yrs<sup>15,20</sup>) which diverged approximately 10.6 million years ago<sup>5,14,21,22</sup>. In addition, *Myotis* species have been used as systems for investigating virus tolerance and other pathogen resistance<sup>23-25</sup> associated with the expansion and contraction of antiviral defenses<sup>26-29</sup>, which have contributed to bats' ecological role as zoonotic reservoirs<sup>10,11,30-33</sup>.

The origin, evolution, and functional basis of these phenotypes have been studied using two major approaches: comparative evolutionary methods, and model organism-based experimental work. The power of comparative evolutionary studies is constrained by several factors including incomplete phylogenetic coverage;

77 poor temporal resolution; the quality and composition of gene annotations; and availability of functional data and  
78 tools for validation. Rapidly evolving genes, such as those associated with adaptations to pathogens<sup>34–36</sup>,  
79 present particular challenges for homology and alignment based methods. Similarly, poor phenotypic resolution  
80 and long divergence times between study species hinders the power of statistical approaches to identify patterns  
81 of selection and diversification<sup>37–40</sup>. Meanwhile, model organism-based approaches contribute a different,  
82 complementary perspective and provide the power of functional analyses; however, these studies can suffer  
83 from issues related to the suitability and diversity of the model species' genotype and phenotype.

84 For example, many studies of the genetic basis of vital processes such as longevity are based on short-  
85 lived model organisms<sup>41,42</sup>. While these studies have been crucial for identifying and dissecting several key aging  
86 pathways, comparative studies of exceptionally long-lived organisms have uncovered novel genes and  
87 pleiotropic effects governing lifespan<sup>36,41,43–53</sup>. The comparative approach, however, has historically been  
88 hindered by limitations in available genomic resources and genetic tools for study. Similarly, studies of infectious  
89 disease response are common and powerful in model organisms, but the lack of diversity and inbred lines limits  
90 their scope. Bats in particular present an important case study in, and opportunity to study, variation in virus  
91 adaptation strategies due to their role as zoonotic reservoirs and their specific resistance to viruses<sup>36,54</sup>. While  
92 previous studies have shown unique infectious disease adaptations in bats, including loss of important  
93 inflammatory genes and expansions of and adaptation in some immune gene families<sup>54–56</sup>, they are typically  
94 hampered by the breadth and number of species analyzed, and only rarely functionally validate results from  
95 genomic analyses.

96 Here we combined comparative and functional approaches in *Myotis* to uncover strong genomic and  
97 functional evidence of adaptation to both aging-related and infectious diseases. We present for the first time a  
98 robust quantification of relative intrinsic cancer risk across mammals, finding that *Myotis* are overrepresented at  
99 the extreme of increased cancer risk. Consistent with this observation, we identified pervasive selection of genes  
100 in longevity- and cancer-related processes, especially in lineages which have undergone the greatest changes  
101 in lifespan. Furthermore, we found strong evidence of adaptation in response to DNA viruses in *Myotis* and other  
102 bats. Genome-wide enrichment of adaptation being driven by DNA viruses is unique to bats in comparison with  
103 other large groups of mammals. Finally, using near-complete assemblies, we identified structural variations  
104 encompassing stress response, immunity, and inflammation genes, including a trans-species copy number  
105 polymorphism of protein kinase R (PKR). Together, our results suggest that pleiotropy and co-evolution of traits  
106 in *Myotis* has played a key role in the evolution of exceptional longevity and infectious disease resistance.

## 107 Results

### 108 High quality chromosome-level assemblies of 8 *Myotis* bat species

109 To study how lifespan and viral response have evolved in *Myotis*, we collected skin punches and derived  
110 primary cell lines from several North American (“Nearctic”)<sup>21</sup> species (**Figure 1A,C**), including one of the longest-  
111 lived mammals, *Myotis lucifugus*<sup>15</sup>. Using these cell lines and flash frozen tissues we generated *de novo*  
112 haplotype-resolved, chromosome-scale genome assemblies for eight species (**Figure 1A**) using a combination  
113 of long-read PacBio HiFi sequencing and HiC scaffolding. These genomes are highly contiguous, with an  
114 average of 98.6% of nucleotide content assembled into 22-23 syntenic chromosome-scale scaffolds  
115 corresponding to the published karyotype<sup>57</sup> with an average QV of 66. These genomes have among the lowest  
116 auNG scores of any *Chiroptera* genome published to date (**Figure 1A, E; Table S1**). Across all 8 genomes, each

117 autosome has been completely assembled telomere-to-telomere (T2T) in at least one species (**Figure 1E**).  
118 Within assemblies, 29%-70% of chromosomes are fully assembled with an average of less than one gap per  
119 chromosome (**Table S1**). When comparing the assemblies of species generated from tissue samples versus  
120 primary cell lines, we found that they were broadly comparable and structurally similar. However, genomes  
121 assembled from cell lines had slightly improved statistics likely attributable to the increased quality and molecular  
122 weight of extracted DNA (**Figure 1A, D, E; Table S1**).

123 Genomes were annotated using well-established pipelines<sup>36</sup> leveraging multiple lines of evidence,  
124 including short-read RNAseq, gene prediction (AUGUSTUS-CGP<sup>58</sup>, GeneMark-ES<sup>59</sup>; gene projections<sup>60</sup>,  
125 TOGA<sup>61</sup>); and homology (miniprot<sup>62</sup>). In total, we identified an average of 27,536 protein coding genes per  
126 species. We benchmarked our annotations using BUSCO<sup>63,64</sup> (V5.4.3) mammalian ortholog sets indicating these  
127 annotations are 98.2%-98.5% complete (**Figure 1C**). We also annotated a recent assembly of *Myotis*  
128 *yumanensis*<sup>65</sup> for inclusion in downstream analyses. Overall, these fully annotated genomes represent some of  
129 the most contiguous *Laurasiatheria* assemblies to date.

## 130 Resolving the phylogeny and the evolution of body size and lifespan in 131 nearctic *Myotis*

132 The phylogenetic relationships within *Myotis* have been the subject of much debate, with a number of  
133 conflicting phylogenies described in the literature based on different choices of genetic markers<sup>14,66-69</sup>. To resolve  
134 the phylogeny of Nearctic *Myotis*, we identified single copy orthologs of 17,509 protein genes present in at least  
135 4 of our 536 mammalian genomes using *miniprot*<sup>62</sup> and the SwissProt database<sup>70</sup>, resulting in 30.6M aligned  
136 nucleotides. These alignments were used to build a maximum likelihood tree of *Eutheria*. The *Chiroptera* sub-  
137 clade was then time-calibrated using *mcmctree*<sup>71,72</sup> and available fossil-based node calibrations (**Figure 1B**;  
138 **Figure S1; Table S2**). Our results conclusively recapitulate known sister species pairs including *M. lucifugus*  
139 and *M. occultus*; *M. yumanensis* and *M. velifer*, and *M. evotis* and *M. thysanodes*. Our proposed phylogeny resolves  
140 the complex relationship between these sister taxa, with 100% bootstrap support at all nodes throughout  
141 *Chiroptera*.

142 Using our resolved Nearctic *Myotis* phylogeny, we re-examined the evolution of body size and lifespan  
143 in *Chiroptera*. In mammals and other metazoans, there is a strong allometric scaling (positive correlation with  
144 body size) of lifespan. Bats have been noted as an exception to this rule: they are exceptionally long-lived for  
145 their body size<sup>17,18,73</sup>, and this exceptional longevity has evolved *de novo* multiple times<sup>6,73,74</sup>. However, these  
146 observations have not been tested using phylogenetically corrected statistics, leveraging well-resolved  
147 phylogenies. To test the hypothesis of non-allometric scaling of lifespan in bats, we modeled the evolution of  
148 body size and lifespan across a supertree of over 1000 placental mammals (*Eutheria*)<sup>67</sup> (**Figure 2; Table S2**). In  
149 agreement with previous studies in vertebrates<sup>7,17,46,51,75-83</sup>, changes in body size are pervasive across mammals,  
150 with extreme changes seen in whales (*Cetacea*)<sup>81,82</sup>, elephantids (*Proboscidea*)<sup>44,46,75</sup>, and in sloths and  
151 armadillos (*Xenarthra*)<sup>76,83-85</sup>. Within bats, major changes in body size are only observed at the root of the lineage  
152 and within *Yinpterochiroptera* (megabats including genera *Pteropus*, *Eidolon*, *Megaderma*, and *Rhinolophus*).  
153 Outside of these clades, only minor changes in body size were observed (**Figure 2A**). The evolution of lifespan  
154 across mammals mirrors the evolution of body size, with additional variability. Branches with large increases in  
155 body size (e.g. *Cetacea* ancestor, *Primate* ancestor) have also experienced large increases in lifespan (**Figure**  
156 **2B**), leading to an overall positive association between lifespan and body size (**Figure S2A**). However, despite  
157 little change in body size in bats (**Figure 2A, C**), we observed some of the largest changes in lifespan across



mammals towards the tips of the tree (**Figure 2B, D**), consistent with the theory of multiple independent increases in lifespan across bats. This is especially true in *Myotis*, where we saw many of the fastest increases in lifespan, including for *Myotis grisescens* (4.15x increase, 100th percentile), *Myotis brandtii* (2.25x increase, 100th percentile), *Myotis lucifugus* (1.56x, 98th percentile), *Myotis myotis* (1.1x increase, 79nd percentile), and the *Myotis* common ancestor (1.26x increase, 92rd percentile) (**Figure 2D**; **Figure S2C**; **Table S2**). We next used phylogenetically-corrected generalized linear models and ANCOVA to study the relationship between body size and lifespan across mammals. While we find that non-bat mammals experience a 0.159% increase in lifespan per 1% increase in body size, bats experience a 0.223% increase in lifespan years per 1% increase in body size; these rates were not significantly different, however, suggesting that lifespan allometry is conserved in bats after accounting for phylogeny (**Figure S2E-F**; pANCOVA,  $p=0.29$ ).

Rapid changes in body size and lifespan can have major implications for the evolution of cancer risk and resistance across mammals. The lifetime cancer risk of an individual is modeled as the product of body size (i.e. the number of cells within an individual), lifespan, and a constant representing the intrinsic cancer risk per cell and unit time. Within species, lifetime cancer risk scales linearly with body size, and with lifespan by a power-law of exponent  $6^{86-89}$ . In contrast to this within-species relationship, there is no significant correlation between these traits across species<sup>89-92</sup> - a phenomenon known as Peto's Paradox. The observation of similar lifetime cancer incidence rates across mammals<sup>76,92,93</sup> implies that species possess distinct intrinsic cancer risks per cell to compensate for changes in lifespan and/or body size. Thus, large bodied, long lived mammals must evolve increased *cancer resistance* proportional to their increased *cancer risk* to avoid increased rates of cancer and death (**Figure 2E**).

We thus hypothesized that the very rapid evolution of increased lifespan in *Myotis* would result in a dramatic increase in their expected cancer risk compared to other mammals. Given consistent cancer rates across mammalian clades<sup>76,92,93</sup>, the Reduced Intrinsic Cancer Risk per cell (RICR) between an extant mammal and its most recent ancestor can be calculated as the log ratio of body size and lifespan between the two nodes (**Figure 2E**)<sup>46,89</sup>. We thus used our estimates of body size and lifespan across *Eutheria* to quantify changes in (RICR) across placental mammals (**Figure 2F**)<sup>46</sup>. We found that bats were slightly overrepresented at the top 10% of RICR, with an odds ratio of 1.15 at the highest extreme, highlighting the impact of rapid lifespan evolution on cancer risk. Importantly, the longest-lived *Myotis* (*M. grisescens*, 39 yrs & 1st pct; *M. brandtii*, 42 yrs & 2nd percentile; *M. lucifugus*, 36 yrs & 4th pct) and their most recent common ancestors (*lucifugus-occultus*, ~26 yrs & 8th pct; *Myotis* common ancestor, ~22 yrs & 14th pct) demonstrated some of the most pronounced decreases in RICR among mammals (**Figure 2F**; **Figure S2D**; **Table S2**). Similar to other extreme cases of body size and lifespan in vertebrates<sup>46,48,51,53,76,94-97</sup>, the pronounced changes in RICR seen in *Myotis* imply an extraordinarily strong selective pressure to evolve cancer resistance mechanisms at multiple points across *Chiroptera* in general, and within *Myotis* in particular.

## Evolutionary signatures of cancer resistance in *Myotis*

We next set out to identify genes under positive selection across our phylogeny of Nearctic *Myotis*. We used aBSREL<sup>98</sup> to test for branch-specific positive selection among 15,734 single-copy orthologous genes identified in at least 4 of our 536 mammalian genomes. We found that on average, 22.7% of genes were under selection across the 9 nearctic *Myotis* species and their internal branches after multiple testing correction at  $FDR \leq 5\%$ ; and 5.23% of genes were significant and had omega values above 1, signaling positive selection (**Table S3**). These genes were enriched for several pathways involved in immunity, cancer, and aging (**Table S3**). Many of these genes lie at the intersection of these two processes, including members of the Cluster of

Differentiation (CD) family, Serpin family, insulin signaling pathway, redox repair, and iron storage (**Figure 3A; Table S3**), suggesting possible pleiotropic influences on genes under selection.

To test this, we quantified the contribution of genes under selection to pathways associated with the hallmark of cancer<sup>99-101</sup> by measuring the proportion of cancer-associated pathways overrepresented among genes under selection throughout the phylogeny (**Figure 3A; insets**). Many nodes within nearctic *Myotis* were enriched for cancer hallmark pathways, especially at the recent ancestors of the longest-lived species (e.g. *M. lucifugus*, *M. occultus*; **Figure 3A**). Testing the overall contribution of genes that have undergone selection in each species since the common *Myotis* ancestor, we observed significant enrichments in the representation of cancer-associated pathways only in species lineages with reductions in RICR (*M. lucifugus*, *M. occultus*, *M. evotis*, *M. thysanodes*, *M. yumanensis*; **Figure 3B**). This suggests that while genes under selection in nearctic *Myotis* frequently contribute to cancer-associated pathways, cancer resistance has only driven consistent selection in the longest-lived lineages with the greatest increases in cancer risk.

We also observed that many key genes involved in ferroptosis - specifically in iron transport, glutathione metabolism, and lipid peroxidation - were under selection at multiple instances throughout the phylogeny (**Table S3**). Many of these genes were recurrently under selection in each species' lineage, such as with ferritin (both heavy and light chains) at three distinct points in the evolutionary history of *M. yumanensis*. Genes under selection in iron transport are specifically involved in the regulation of free iron in the cell, specifically in the export & reduction of the free radical catalyst Fe<sup>2+</sup> (ferroportin, *HMOX1*) and the import, storage, and maintenance of Fe<sup>3+</sup> (ferritin and transferrin receptors 1 and 2). Additionally, we observe selective signatures in glutathione metabolism and oxidative stress response including: *SLC3A2* and *SLC7A11*, a heterodimer pair facilitating cystine import and glutamate export; glutathione synthetase; and glutathione peroxidase 3 (*GPX3*). Finally, we observed a pattern of selection in genes involved in synthesizing and maintaining key polyunsaturated fatty acids involved in ferroptosis, including *LPCAT3*, *ALOX15*, and *PRDX5*.

To test for intensified and relaxed selection in genes in long-lived or short-lived *Myotis*, we ran RELAX<sup>102</sup> on 12,438 genes present across 11 *Myotis* species, identifying 263 genes under intensified selection ( $k > 1$ ) and 101 genes under relaxed selection ( $k \leq 1$ ) after multiple testing correction ( $p_{adj} \leq 0.05$ ). Among genes of note showing significant intensified selection were *USP9X* (an X-linked ubiquitin protease associated with cancer and T cell development<sup>103,104</sup>,  $k=48.6$ ); *CDK16* (an oncogenic cyclin-dependent kinase that regulates autophagy<sup>105,106</sup>,  $k=44.9$ ); and *FGFR2* (a cell growth receptor associated with human cancers that is also a VIP<sup>107,108</sup>,  $k=26.1$ ) (**Figure S3B; Table S4**). Performing a gene set enrichment analysis for the 364 significant genes, we find a strong association among selected genes with FGF2 signaling, chromatin remodeling, and pathways associated with both retroviruses and coronaviruses, further highlighting the pleiotropic nature of selection patterns in *Myotis* (**Figure S3C; Table S4**). Finally, using RERConverge<sup>109</sup>, we investigated how genes' evolutionary rates correlated with the evolution of body size, lifespan, or the first two principal components of body size and lifespan across *Myotis*, and found a number of genes enriched in pathways associated with innate immunity, gamete production, and various metabolic processes, consistent with our other results (**Figure S3D-E; Table S4**).

The longest-lived bat in our study, *M. lucifugus*, had an overrepresentation of pathways specifically associated with DNA double-strand break (DSB) repair when looking at both lineage-wide and node-specific enrichments in positive selection using the Reactome database<sup>110</sup> (**Figure 3C; Table S3**). This includes 35 out of 65 genes in the high-fidelity Homologous Recombination Repair pathway, and 21/37 members of the Homology-Directed Repair via Single Strand Annealing (**Figure 3C; Table S3**). These results suggest that *M. lucifugus* might have an enhanced response to DNA DSBs relative to other bats. To test this hypothesis, we assessed the tolerance of *M. lucifugus* to neocarzinostatin, a potent radiomimetic agent that induces DNA

double-strand breaks (**Figure 3D**), compared to *M. evotis*, three non-*Myotis* bats (*Eidolon helvum*, *Pteropus rodrigensis*, and *Rousettus lanosus*), and humans. At low doses of neocarzinostatin, *M. lucifugus* was the only species tested showing sensitivity to neocarzinostatin after 24 hours, with a drop in viability and concomitant increase in apoptosis. At high doses, *M. lucifugus* had the highest level of apoptosis and the greatest drop in viability of all the bats tested, although all bats were more resistant to DNA damage than humans. This is consistent with other long-lived species, including elephants<sup>44,45,93</sup>, naked mole rats<sup>52</sup>, and bowhead whales<sup>48,111</sup>, where longevity and RICR are associated with an increased ability to clear out damaged cells. Together, these results support the hypothesis that *M. lucifugus* has evolved an enhanced DNA double-strand break response as predicted by genes exhibiting signatures of positive selection in this species.

## Adaptation to DNA viruses

Amongst genes under selection, a substantial portion were involved with immunity, including members of the immunoglobulin and Cluster of Differentiation gene families. These genes exhibited some of the highest evolutionary rates ( $\omega$ ) in our dataset, suggesting that they are under strong selection in *Myotis* (**Table S3; Table S4**). Because immune pathways are only one aspect of host viral adaptation<sup>112</sup>, we tested for adaptive signatures in virus-interacting proteins (VIPs) in *Myotis* and other bats. VIPs are host proteins that physically interact with viral proteins (e.g. *CD45*, **Figure 4A**), and can be proviral (contributing to viral infection, e.g. viral receptors), antiviral (protective against viral infection, e.g. interferons), or both depending on infection stage and virus type. Previous studies investigating positive selection across mammals have found an enrichment for adaptation among a set of 5,528 manually curated VIPs, defined as host proteins that have at least one experimentally verified physical interaction with a viral protein, RNA, or DNA<sup>112</sup>.

By calculating an enrichment score from the ratio of positive selection in VIPs compared to their matched control genes using BUSTED-MH<sup>113</sup>, we found that, like other mammals, *Myotis* show an enrichment for adaptation at VIPs (**Figure 4B; Table S5**). Physical host-virus interactions may not always result in fitness effects in the host. We therefore repeated our analysis using a gene set restricted to VIPs with experimental evidence of specific pro- or anti-viral effects, and thus with a stronger expectation of fitness effects. We observed an even stronger significant elevation in the ratio of positive selection in these proviral and antiviral VIPs (**Figure 4C; Table S5**), but no elevation in this ratio in other VIPs (**Figure 4D; Table S5**). This is consistent with the expectation of viral interaction as the cause of enrichment of positive selection in VIPs in bats<sup>114</sup>. We repeated this analysis using a dataset of 47 publicly-available non-*Myotis* bat genomes, and confirmed these same patterns across bats more broadly, even when excluding *Myotis* genomes (**Figure 4B** inset).

Previous work has suggested that bats may have different physiological responses to DNA and RNA viruses<sup>115</sup>. To determine if this was reflected in genomic VIP adaptation, we compared the enrichment of positive selection in VIPs that interact only with DNA viruses (DNA VIPs) to those that interact only with RNA viruses (RNA VIPs). Remarkably, we found that VIP adaptation in *Myotis* and other bats is driven by selection in DNA VIPs (**Figure 4E** and inset). This is in marked contrast to the observed pattern in RNA VIPs, which show no evidence of enrichment in adaptation (**Figure 4F** and inset). Note that this difference between DNA and RNA VIPs cannot be explained by a difference in the conservation of VIP status between the two. The vast majority of VIPs were discovered between human proteins and viruses that infect humans<sup>114</sup>, and a concern could then be that those proteins that are RNA VIPs in humans have evolved faster than DNA VIPs in bats, ultimately resulting in the more frequent loss of their VIP status in bats. We can however exclude this possibility, since DNA and RNA VIPs have very similar average dN/dS ratios (*Myotis*, 0.2 vs. 0.18 respectively; non-*Myotis* bats, 0.163 vs. 0.153 respectively).

285 In contrast to what we observe in bats, VIP adaptation in humans is driven by positive selection in RNA  
286 - and not DNA - VIPs<sup>112,116</sup>. To investigate if DNA VIP-driven adaptation in bats is exceptional among mammals,  
287 we replicated these analyses across four other large mammalian orders that are well represented among  
288 publicly-available mammalian genomes: *Primates*, *Glires*, *Eeungulata*, and *Carnivora*. We found that while other  
289 mammalian orders show a mix of adaptation enrichments in both RNA and DNA VIPs, none show an absence  
290 of genome-wide enrichment of adaptation in RNA VIPs as observed in bats (**Figure S4**). These results highlight  
291 that bats, including *Myotis*, may have faced greater selective pressures from DNA viruses than from RNA viruses,  
292 in contrast to other mammals.

## 293 Evolution of structural variation within constrained karyotypes

294 With only six known exceptions, all *Myotis* species with cytological data have a conserved karyotype (60+  
295 *Myotis* spp.:  $2n = 44^{117-121}$ ; *M. annectans*:  $2n = 46^{119}$ ; *M. laniger*:  $2n = 48^{120}$ ; *M. bechsteinii*:  $2n = 42^{122}$ ; *M.*  
296 *daubentoni*:  $2n = 42^{123}$ ; *M. davidii*:  $2n = 46^{124}$ ; *M. macrodactylus*:  $2n = 44/45^{125,126}$ ). This conserved *Myotis*  
297 karyotype, shared among species spread across six continents<sup>1,2</sup>, consists of three large and one small  
298 metacentric autosomes; 17 small telocentric autosomes; and metacentric X and Y chromosomes<sup>57,127</sup>.  
299 Consistent with this broad cytological conservation, we find large scale synteny across the Nearctic *Myotis* in  
300 this study. However, structural variants (SVs) including inversions, duplications, and translocations are relatively  
301 common within chromosomes, especially in putative centromeric regions (**Figure 5A, B**).

302 We used SyRI<sup>128</sup> to identify SVs across pairwise alignments of Nearctic *Myotis* genomes relative to the  
303 outgroup *M. myotis* and identified 6,813 - 8,013 SVs per genome. Most of these events were small, with 97 -  
304 99% of events under 10Kb. In the three large autosomes, which constitute ~30% of each genome, we cataloged  
305 an average of 509 SVs (**Table S6**). In contrast, in the small autosomes, constituting ~65% of each genome, we  
306 observed an average of 316 events, highlighting the distinct structural evolution between these chromosome  
307 types (**Table S6**). However, large ( $\geq 10$ Kb) duplications, large inverted duplications, and large inverted  
308 translocations were more common on small autosomes compared to the large autosomes (**Table S6**).

309 We also quantified the distribution of transposable elements (TEs) across chromosomes. Surprisingly,  
310 LINE elements were significantly enriched around the centromeres of all chromosomes, both metacentric and  
311 telocentric (**Figure 5B**); while this is rare in mammals, it has been described as a feature of Phyllostomid  
312 genomes<sup>129</sup>. In many cases, particularly in the 3 large metacentric chromosomes, LINE elements appear to have  
313 displaced other TEs. Rolling circle and SINE elements were particularly depleted concomitant with LINE  
314 enrichment. In contrast, SINE elements were enriched at telomeres. The concentration of segmental duplications  
315 is significantly correlated with TE density in each species (linear regression,  $p < 0.01$ ; **Figure 5B**; **Figure S5J**)  
316 highlighting the possible importance of TEs in facilitating structural evolution.

317 One particularly striking example of structural evolution we identified is a ~20-Mb block at the  
318 subtelomeric end of chromosome V15 undergoing frequent and recurrent inversions and translocations in  
319 nearctic *Myotis* (**Figure 5A**). This region spans several immune-related genes including multiple members of  
320 interleukin signaling pathways, including IL-1 and IL-36. A 10Mb portion of this block was recently identified as  
321 a potential target of recent selection by adaptive introgression<sup>69</sup>. We identified between 2-3 major (8+ kb) blocks  
322 in this region exhibiting inversions between Nearctic *Myotis*, which correspond to similarly sized regions in the  
323 outgroup *M. myotis* (**Figure 5A**; **Table S5**). Additionally, we noted a depletion of DNA transposable elements at  
324 the boundaries of each inversion (**Figure 5B**), particularly for rolling circle (RC) and SINE elements. Both of



these elements can catalyze large-scale structural rearrangements via DNA damage repair and homologous recombination, respectively<sup>130–134</sup>.

Gene duplications and losses can be drivers of evolution via dosage modification<sup>135,136</sup>, sub- and neofunctionalization<sup>137,138</sup>, regulatory network remodeling<sup>139</sup>, and other processes<sup>135</sup>. We quantified gene gains and losses across *Myotis* relative to their single-copy human orthologs. Using CAFE<sup>140</sup>, we found 38 gene families underwent significant expansions or contractions in at least one nearctic *Myotis* species (**Figure 5C**). However, gain and loss rates varied substantially across branches of the *Myotis* phylogeny. The terminal *M. auriculus* and *M. velifer* branches had ~4-fold more significant gene family expansions (37 and 35 families, respectively; **Figure 5C**) than other *Myotis* branches. In contrast, the terminal *M. californicus* and *M. yumanensis* branches had ~2-fold more significant contractions (24 and 23 families, respectively; **Figure 5C**) than other *Myotis* branches. We observe significant overrepresentation of pathways at FDR≤10% in only 4 gene sets: gene families that underwent significant expansions in *M. auriculus*, *M. velifer*, and *M. volans*; and genes that underwent significant contractions in *M. lucifugus* (**Figure S5A-H**). Many of these pathways were shared between all sets, including pathways involved in translation regulation; ROBO receptors and neuronal development; selenoprotein and selenocysteine metabolism; and influenza life cycle (**Figure S5A-H**).

Given that many of the genes in these pathways are VIPs, we used the method of Huang et al (2023)<sup>50</sup> to test if VIP genes in particular underwent significant copy number changes relative to non-VIP genes. We found that while the birth-death rate of VIP genes is similar to that of other genes ( $p = 0.071$ ), together VIP genes are significantly more likely to have undergone expansions and/or contractions on at least one branch of the *Myotis* family ( $p < 0.001$ ; **Figure S5I-J**). This suggests that there is variation in gene family birth rates across species, but that VIPs are more dynamic across the Nearctic *Myotis* as a whole than other types of genes.

To further explore the functional impact of gene duplications we ranked genes by their maximum copy number across all genomes. We found that the gene families with the highest copy numbers were concentrated in pathways associated with cancer, aging, immunity, and olfaction (**Figure 5D**). One striking case is *FBXO31*, with ~2.4x more copies on average than the next most duplicated gene in *Myotis* (20-48 copies). *FBXO31* is a SCF (SKP1-cullin-F-box) protein ligase involved in cell cycle regulation and DNA damage response, consisting of two functional domains: a F-Box domain and a CDK binding domain<sup>141</sup>, and has previously been speculated as a driver of longevity in *Myotis*<sup>96</sup>. Quantifying *FBXO31* copy number across over 500 mammals using reciprocal best-hit BLAT, we found that this gene was more highly duplicated in *Myotis* than in any other mammal genome (**Figure 5E**). Furthermore, while there were additional partial matches of non-canonical copies of *FBXO31* in non-*Myotis* species, all copies identified in *Myotis* are full-length genes with functional domains. To model the evolution of gene copy number, we used GeneRax<sup>142</sup> to reconcile the gene tree and species tree. GeneRax infers a gene family tree under scenarios of gene duplication and loss, taking into account the species tree. We found support for an original 14 duplications in the common ancestor of Nearctic *Myotis*, with subsequent gains and losses in each lineage (**Figure 5F**). These results highlight a massively expanded gene family in *Myotis* with potential consequences for the regulation of stress response and other processes.

## An actively segregating, trans-species copy number polymorphism of the antiviral factor *PKR*

Our highly contiguous genome assemblies provide a unique opportunity to understand the evolutionary and functional dynamics of structural variation in adaptation. To illustrate this, we explored the antiviral innate immune Protein Kinase R (*PKR/EIF2AK2*), an interferon-stimulated gene with adaptive duplications unique to

366 *Myotis*<sup>28</sup>. Among our Neartic *Myotis* genome assemblies we resolved the structure of the two known structural  
367 haplotypes: H1, containing a single copy of *PKR* (*PKR2*); and H2, containing two tandemly duplicated copies of  
368 *PKR* (*PKR1* and *PKR2*; **Figure 6A**). Unexpectedly, we also identified a third haplotype - H3 - with three tandem  
369 duplicates of *PKR* (*PKR1*, *PKR2*, and a third copy). While 7 out of 9 *Myotis* species carried duplicated haplotypes  
370 (H2 in 6 species, H3 in *M. californicus*), to our surprise, 5 of these cases were heterozygous for the duplicated  
371 haplotype: (i.e. H1/H2 or H1/H3; **Figure 6B**). To determine the evolutionary history of these duplicates, we used  
372 GeneRax<sup>142</sup> to construct a tree from alignments of all *PKR* gene copies across Neartic *Myotis*, using *Pipistrellus*  
373 *pygmaeus* as a non-*Myotis* outgroup (**Figure 6C**). Our results suggest that *PKR2* is the canonical copy of *PKR*,  
374 and that *PKR1* originated from a single duplication event at the root of *Myotis*. Intriguingly, we observed that in  
375 the heterozygous species, both *PKR1* and *PKR2* on the duplicated haplotype clustered with other duplicated  
376 haplotypes, resulting in species tree violations for the canonical copy, *PKR2* (**Figure 6C**). These results highlight  
377 that both the duplicated and unduplicated haplotypes have likely been segregating for over 30 million years,  
378 representing an ancient trans-species polymorphism.

379 Protein Kinase R is a stress response and innate immune factor that interacts with viral or inverted Alu  
380 repeats dsRNAs via its dsRNA binding motifs (dsRBMs), leading to PKR auto-phosphorylation and  
381 dimerization<sup>143,144</sup>. Upon activation, PKR can then phosphorylate various molecules leading to protein translation  
382 shutdown and restriction of viral replication<sup>143,144</sup>. While the independent functional impacts of PKR1 and PKR2  
383 were previously investigated<sup>28</sup>, the effects of co-expressing both copies remains unknown. This is important  
384 because their final effects may be additive, synergistic or dominant negative, providing clues into why the PKR  
385 duplication is polymorphic both within and between *Myotis* species.

386 To better understand the functional consequences of possessing one or two copies of PKR, we  
387 investigated the effect of paralog co-expression on steady state protein levels, cell viability, protein translation  
388 shutdown and antiviral restriction (**Figure 6D-G**). We used PKR-KO HeLa cells transfected with either *Myotis*  
389 *myotis* or *Myotis velifer* PKR1, PKR2, and PKR1+2. We found that the coexpression of *Myotis* Flag-PKR1 and  
390 Flag-PKR2 did not affect their protein expression levels (**Figure 6D**; **Figure S6**). Furthermore, coexpression of  
391 PKR1 and PKR2 led to a simple additive effect in their translation shutdown activity (**Figure 6E**), suggesting that  
392 neither copy is dominant negative. Using non-toxic doses of *Myotis* PKRs in the context of VSV-GFP (Vesicular  
393 stomatitis virus encoding a GFP reporter<sup>145</sup>) infections, we found that, although PKR1 and PKR2 are both  
394 antiviral<sup>28</sup>, the coexpression of PKR1 and PKR2 is not beneficial against VSV (**Figure 6F**). Finally, because  
395 duplicated haplotypes may lead to increased doses of PKR in *Myotis* cells, we tested PKR impact on cell viability.  
396 We found that at low doses none of the *Myotis* PKRs affected cell viability. However, higher doses of PKRs led  
397 to more cell toxicity, potentially resulting in a tradeoff (**Figure 6G**). Altogether, this may explain why PKR is rarely  
398 duplicated in mammals, and why both single- and duplicate haplotypes of the loci are segregating across several  
399 *Myotis* species. These genomic and functional results highlight the impact of an unfixed gene duplicate which  
400 may play a role in adaptation to viral infections.

## 401 Discussion

### 402 A functionally empowered approach to comparative genomics

403 Bats are widely known for their long lifespan, cancer resistance, and viral tolerance<sup>6,10,11,36,73,92,146-148</sup>. As  
404 highly complex and pleiotropic processes, the genes and mechanisms underlying these phenotypes can be  
405 challenging to identify. Comparative approaches to identify the genetic bases of these traits are constrained by

406 the availability of high-quality genomes, annotations, and functional resources for validation. These challenges  
407 are exacerbated in the case of rapidly-evolving phenotypes, such as host-pathogen interactions.

408 Here we outline an approach that enables functional comparative biology by generating cell lines from  
409 wing punches of wild caught bats for genome assembly, comparative genomics, and functional follow up. Cell  
410 lines are generated from minimally-invasive biopsies collected in the field thus avoiding disturbing natural  
411 populations. Given the high density of bat species concentrated at single locations world-wide<sup>149,150</sup> it is feasible  
412 to collect wing punches from a large number of individuals across a wide phylogenetic range; these wing punches  
413 can be used to generate cell lines and sequencing libraries for reference genomes in a matter of weeks. This is  
414 an important advance, not only for efforts to expand genetic resources across the tree of life<sup>151-153</sup>, but for  
415 conservation genomics. As our approach can generate genomic resources from minimal material gathered via  
416 non-lethal sampling, it is well-suited for the study of rare or endangered species for which acquiring sufficient  
417 amounts of material can be challenging.

## 418 Evolution of lifespan and cancer risk in a new phylogenetic context

419 The evolution of body size and lifespan across mammals - and the rapid evolution of lifespan in  
420 *Yinpterochiroptera* in particular - has major implications for the co-evolution of cancer risk and resistance. While  
421 models of body size evolution are well-studied in mammals<sup>7,46,75,77</sup> the evolution of lifespan is less well  
422 understood. By explicitly modeling the evolution of lifespan separately from body size, we recapitulate the extant  
423 relationship between body size and lifespan across mammals in evolutionary time. Contrary to prior work, we  
424 show that overall bats exhibit allometric lifespan scaling, comparable to other mammals. However, two bat clades  
425 - *Myotis* and *Phyllostomidae* - exhibit distinct trends with *Myotis* demonstrating an increased rate of change in  
426 lifespan given body size compared to other mammals. This altered scaling of longevity in *Myotis* has dramatic  
427 consequences for their intrinsic, per-cell cancer risk and for the evolution of tumor-suppressor genes and  
428 pathways. While cancer risk scales linearly with body size, it scales over time as a power law of 6<sup>86,89,90</sup>.  
429 Meanwhile, while mammalian body sizes span a 10<sup>6</sup> range of masses, they only span a 10<sup>2</sup> range of  
430 lifespans<sup>16,154</sup>. Unlike other systems where the evolution of cancer resistance has been driven by rapid changes  
431 in body size<sup>44-46,51,94,97</sup>, the body size of *Myotis* has not significantly changed since their common ancestor.  
432 Instead, the rapid and repeated changes in lifespan across an order of magnitude in *Myotis* lead to some of the  
433 most significant changes in intrinsic cancer risk seen across mammals.

434 We found a number of genes under selection across multiple longevity-associated pathways, consistent  
435 with the pleiotropic nature of the aging process. These include members of canonical longevity pathways such  
436 as mTOR-IGF signaling, DNA damage repair, oxidative stress, and the senescence-associated secretory  
437 phenotype. We additionally identified selection in various pathways that have likely emerged as a result of the  
438 unique biology of bats, including genes at the intersection of immunity and senescence, such as Serapin-family  
439 genes; genes in metabolic pathways including amino acid metabolism; and pervasive selection observed in the  
440 ferroptosis pathway, which sits at the intersection of bats' extreme oxidative challenges, metabolic demands,  
441 immune function, and cancer resistance. By quantifying the relative contributions of genes under selection to  
442 cancer-related pathways at each node, we found significant enrichment of these processes across the  
443 phylogeny, especially at nodes undergoing the greatest changes in lifespan and cancer risk.

444 While the implications of an increased cancer risk are clear, the implications of decreases in relative  
445 cancer risk are less so. As expected by Peto's Paradox, we observe an overrepresentation of cancer-related  
446 pathways among genes under selection at nodes experiencing high increases in relative cancer risk, consistent  
447 with patterns observed in other vertebrates<sup>46,48,51,53,76,94-97</sup>. However, we also observed an enrichment in cancer-

448 related pathway representation among genes under selection in nodes with significant decreases in cancer risk  
449 (e.g. *M. thysanodes*, *M. velifer*). This combination of low intrinsic cancer risk alongside the persistence of cancer-  
450 related adaptations, has been observed previously in sloths and armadillos<sup>76</sup>. Intriguingly, these species  
451 demonstrate some of the lowest known rates of cancer among mammals. While no reports or studies of  
452 neoplasia rates have been published in *Myotis*, the use of *in vitro* models of carcinogenesis provides a promising  
453 avenue for comparative studies of cancer resistance under controlled conditions. In agreement with our results,  
454 *in vitro* and xenograft transplant models have shown that cells of long-lived bats, including *M. lucifugus*, are more  
455 resistant to carcinogenesis than shorter-lived bats and other mammals<sup>148</sup>. Such studies provide a reliable route  
456 for the experimental validation of the evolution of cancer resistance in species where *in vivo* work would  
457 otherwise prove ethically or practically intractable.

## 458 Viral adaptation and immunity

459 The nature of viral tolerance and infectious disease adaptation in bats has major implications for  
460 understanding their role as zoonotic reservoirs and mechanisms of infectious disease adaptation. Here we focus  
461 on Virus Interacting Proteins (VIPs) that influence viral response and contain vital information about the nature  
462 of host adaptation to viruses<sup>112</sup>. By integrating comparative analyses of VIP adaptation, VIP and immune gene  
463 family expansion and contraction, and functional experiments, we show that virus adaptation in bats is mostly  
464 driven by DNA viruses, as opposed to RNA viruses; we recapitulate and expand on previous results related to  
465 positive selection in immune genes and immune gene family expansion, contraction, and loss; and demonstrate  
466 complex patterns of structural variation, including a segregating duplication of protein kinase R (PKR), a major  
467 protein involved in the antiviral innate immune system, that has functional relevance in its activity against viruses.

468 The remarkable dominance of adaptation in response to DNA viruses in bats is in contrast with viral  
469 adaptation in humans and other primates, which is driven by RNA viruses<sup>116,155</sup>; and in other mammals, in which  
470 virus adaptation is driven by a combination of DNA and RNA viruses. Most zoonoses, including those hosted by  
471 bats, are RNA viruses<sup>10</sup>, making this especially important in understanding the dynamics of emerging infectious  
472 diseases. This novel finding complements previous observations that bats are more likely than other mammals  
473 to asymptotically harbor RNA viruses, while being more susceptible themselves to other pathogens, such as  
474 fungi<sup>115</sup>. This suggests multiple, non-exclusive, possibilities. First, bats may have some other form of response  
475 to RNA viruses that sufficiently reduces the fitness effect of these viruses such that the associated VIPs did not  
476 adapt as strongly. Second, our result does not imply that bats have not adapted to RNA viruses, rather that  
477 adaptation to RNA viruses does not exceed the genomic baseline adaptation, while adaptation to DNA viruses  
478 does. Indeed, bats are known to mount adaptive immune responses to some RNA viruses and the strength of  
479 their immune response can have complex interactions with hibernation and reproduction<sup>10</sup>. It has been previously  
480 suggested that bats may rely more strongly on adaptive immunity in response to RNA viruses than to other  
481 pathogens<sup>115</sup>, though evolutionary functional analyses have also found evidence of innate immune adaptation to  
482 RNA viruses, including *RTP4* to flaviviruses<sup>156</sup> and *OAS1* to SARS-COVs<sup>157</sup>. This is consistent with our findings  
483 of positive selection and gene family expansion in adaptive immune proteins.

484 While previous work has shown associations between gene family size and certain phenotypic traits in  
485 bats<sup>36,54,158,159</sup>, confirmation of functional effects of copy number is rare. By resolving individual haplotypes in  
486 these nine *Myotis* species, we were able to confirm a single duplication event at the origin of *Myotis* *PKR1* and  
487 *PKR2*. We further demonstrate functional implications of copy number variation in Protein kinase R, as previously  
488 shown in functional evolutionary studies (eg. Jacquet et al. 2022). These results are especially interesting in the  
489 light of other studies that have found trans-species polymorphisms related to immune genes<sup>160</sup>. This further



490 illustrates the importance of high-quality genome assemblies and annotations, to distinguish copy number  
491 variation between haplotypes, as well as between functional copies and pseudogenes<sup>161</sup>.

## 492 The role of agonistic pleiotropy in driving adaptations in bats

493 Multiple hypotheses have been proposed to connect the unique physiology and ecology of bats with the  
494 evolution of remarkable adaptations such as viral infection tolerance, stress tolerance, and exceptional  
495 longevity<sup>146</sup>. Hypothesized drivers of disease resistance and longevity evolution in bats include the evolution of  
496 flight (e.g. “flight as fever” hypothesis<sup>162</sup>, though this hypothesis has recently been critiqued<sup>163</sup>, the disposable  
497 soma hypothesis<sup>164</sup>); metabolic state<sup>165</sup>; torpor<sup>6</sup>; and other adaptations to specific environments<sup>9,159,166,167</sup>.  
498 Additionally, many studies have highlighted the intersection of one or more of these traits, including a relationship  
499 between hibernation and both longevity<sup>6</sup> and disease resistance<sup>115</sup>. Our results are consistent with an *agonistic*  
500 pleiotropy hypothesis, wherein genetic adaptations for many specific traits (e.g. physiological stress to flight,  
501 hibernation, DNA virus innate immunity) may prove beneficial to other seemingly-unrelated traits (e.g. cancer  
502 resistance, cellular homeostasis, longevity).

503 Consistent with this, many of the genes and pathways highlighted in this study have been found to play  
504 vital roles across physiological traits in bats and other species. For example, two genes under selection in neartic  
505 *Myotis* - *FTH1* and *IGFN1* - have been implicated in functional studies as key hibernation genes<sup>168–170</sup>, viral  
506 interacting proteins<sup>171–174</sup>, and as pro-longevity genes<sup>175–177</sup>. Similarly, many DNA VIPs such as *BRCA1/2* and  
507 *POLG* represent core DNA maintenance genes essential for cancer resistance and longevity<sup>52,178–184</sup>; the  
508 existence of active DNA transposable elements such as *Helitron* in *Myotis* may provide another selective  
509 pressure on DNA repair genes<sup>185</sup>. Beyond individual genes, many of the overarching pathways under selection  
510 in *Myotis*, such as those associated with inflammation, senescence, and ferroptosis lie directly at the intersection  
511 of aging-related immune processes<sup>36,54,56,78,170,175,186–191</sup>. While these results suggest the possibility that traits  
512 such as cancer risk, cellular homeostasis, and antiviral response have evolved in tandem due to pleiotropic  
513 selection at overlapping points in bats’ evolutionary histories, further functional validation will be required to  
514 disentangle the functional impacts of these genetic changes and disambiguate the drivers of selection.

## 515 Acknowledgements

516 PacBio HiFi sequencing was done by the DNA Technologies and Expression Analysis Cores at the UC Davis  
517 Genome Center, supported by NIH Shared Instrumentation Grant 1S10OD010786-01. This material is based in  
518 part upon High Performance Computing (HPC) resources supported by the University of Arizona TRIF, UITS,  
519 and Research, Innovation, and Impact (RII) and maintained by the UArizona Research Technologies  
520 department. This research used the Savio computational cluster resource provided by the Berkeley Research  
521 Computing program at the University of California, Berkeley (supported by the UC Berkeley Chancellor, Vice  
522 Chancellor for Research, and Chief Information Officer). Computations were performed, in part, on the Vermont  
523 Advanced Computing Core. We thank the members of the LP2L team (CIRI) for helpful discussions.

524 MEL was funded by NSF PRFB #2010884, and a Dovetail Tree of Life Grant. JMV was funded by NSF PRFB  
525 #2109915 and NIH NIA T32AG000266. DE was funded by NIH NIGMS MIRA grant 5R35GM142677. PHS was  
526 funded by NIH NIGMS grant R35GM142916 and by the Vallee Scholars Award. LE was funded by a grant from  
527 the Agence Nationale de la Recherche (ANR, #ANR-202-CE15-0020-01 to LE) and by the CNRS. LE and DE  
528 were further funded by a grant from the Joint Call for Proposals between the CNRS and the University of Arizona

529 (International Research Center, IRC, 2021-2024). LE, DE, PHS and SP were further funded by the International  
530 Research Project (IRP) RAPIDvBAT from the CNRS, the University of Arizona and the University of California,  
531 Berkeley.

532 Image attributions for the bat photos featured in Figure 1: J. Scott Altenbach (*M. thysanodes*, *M. velifer*); Rick &  
533 Nora Bowers (*M. occultus*); U.S. National Park Service (*M. auricolus*); Frank Carey (*M. californicus*); Michael  
534 Durham (*M. evotis*); J. N. Stuart (*M. volans*); and SMBishop & the Wikimedia Foundation (*M. lucifugus*).

## 535 Author Contributions:

536 Conceptualization, J.M.V., M.E.L., D.E., P.H.S., L.E., D.F., M.B.; Methodology, J.M.V., M.E.L., D.E.,  
537 P.H.S., L.E., G.G.S.; Software, J.M.V., M.E.L., D.E., P.H.S., L.E., T.M.L.; Validation, J.M.V., M.E.L.,  
538 D.E., P.H.S., L.E., J.P.V.M.; Formal Analysis, J.M.V., M.E.L., D.E., P.H.S., L.E., S.M., A.L.C., D.M.,  
539 S.V.; Investigation, J.M.V., M.E.L., S.M., M.B., D.F., G.G.S., L.G., Z.R.H., M.H., W.K., T.M.L., A.L.C.,  
540 S.M., D.M., S.L., J.L., C.R., S.L.R.C., M.S., K.S., W.T., J.D.T., S.V., R.M., M.B., J.P.V.M., S.P., L.E.,  
541 D.E., P.H.S.; Resources, J.M.V., M.E.L., D.E., P.H.S., L.E., M.B., D.F., G.G.S., L.G., Z.R.H., M.H.,  
542 W.K., T.M.L., A.L.C., S.M., D.M., S.L., J.L., C.R., S.L.R.C., M.S., K.S., W.T., J.D.T., S.V., R.M., M.B.;  
543 Data Curation, J.M.V., M.E.L., S.M., M.B., D.F., G.G.S., L.G., Z.R.H., M.H., W.K., T.M.L., A.L.C., S.M.,  
544 D.M., S.L., J.L., C.R., S.L.R.C., M.S., K.S., W.T., J.D.T., S.V., R.M., M.B., J.P.V.M., S.P., L.E., D.E.,  
545 P.H.S.; Writing - Original Draft, J.M.V., M.E.L., D.E., P.H.S., L.E., S.M., J.L.; Writing - Review & Editing,  
546 J.M.V., M.E.L., S.M., M.B., D.F., G.G.S., L.G., Z.R.H., M.H., W.K., T.M.L., A.L.C., S.M., D.M., S.L., J.L.,  
547 C.R., S.L.R.C., M.S., K.S., W.T., J.D.T., S.V., R.M., M.B., J.P.V.M., S.P., L.E., D.E., P.H.S.;  
548 Visualization, J.M.V., M.E.L., D.E., P.H.S., L.E., S.M., A.L.C.; Supervision, J.M.V., M.E.L., D.E., P.H.S.,  
549 L.E.; Project Administration, J.M.V., M.E.L., D.E., P.H.S., L.E.; Funding Acquisition, J.M.V., M.E.L.,  
550 D.E., P.H.S., L.E.

## 551 Declaration of Interests:

552 The authors declare no competing interests.

## 553 References

- 554 1. Wilson, D.E., and Reeder, D.M. (2005). Mammal Species of the World: A Taxonomic and  
555 Geographic Reference (JHU Press).
- 556 2. Simmons, N.B., and Cirranello, A.L. Bat Species of the World: A Taxonomic and Geographic  
557 Database. <https://batnames.org/>.
- 558 3. Teeling, E.C., Hedges, S.B., and Kumar, S. (2009). Bats (Chiroptera). The timetree of life, 499–  
559 503.
- 560 4. Rietbergen, T.B., Ostende, L.W. van den H., Aase, A., Jones, M.F., Medeiros, E.D., and Simmons,  
561 N.B. (2023). The Oldest Known Bat Skeletons and Their Implications for Eocene Chiropteran  
562 Diversification. PLoS One 18, e0283505. <https://doi.org/10.1371/journal.pone.0283505>.
- 563 5. Kumar, S., Stecher, G., Suleski, M., and Hedges, S.B. (2017). TimeTree: A Resource for

- 564 Timelines, Timetrees, and Divergence Times. *Mol. Biol. Evol.* **34**, 1812–1819.  
565 <https://doi.org/10.1093/molbev/msx116>.
- 566 6. Wilkinson, G.S., and Adams, D.M. (2019). Recurrent Evolution of Extreme Longevity in Bats. *Biol.*  
567 *Lett.* **15**, 20180860. <https://doi.org/10.1098/rsbl.2018.0860>.
- 568 7. Moyers Arévalo, R.L., Amador, L.I., Almeida, F.C., and Giannini, N.P. (2020). Evolution of Body  
569 Mass in Bats: Insights from a Large Supermatrix Phylogeny. *J. Mamm. Evol.* **27**, 123–138.  
570 <https://doi.org/10.1007/s10914-018-9447-8>.
- 571 8. Datzmann, T., von Helversen, O., and Mayer, F. (2010). Evolution of Nectarivory in Phyllostomid  
572 Bats (Phyllostomidae Gray, 1825, Chiroptera: Mammalia). *BMC Evol. Biol.* **10**, 165.  
573 <https://doi.org/10.1186/1471-2148-10-165>.
- 574 9. Camacho, J., Bernal-Rivera, A., Peña, V., Morales-Sosa, P., Robb, S., Russell, J., Yi, K., Wang,  
575 Y., Tsuchiya, D., Murillo-García, O.E., et al. (2023). Sugar assimilation underlying dietary evolution  
576 of Neotropical bats. *bioRxiv*, 2023.07.02.547432. <https://doi.org/10.1101/2023.07.02.547432>.
- 577 10. Hayman, D.T.S., Bowen, R.A., Cryan, P.M., McCracken, G.F., O’Shea, T.J., Peel, A.J., Gilbert, A.,  
578 Webb, C.T., and Wood, J.L.N. (2013). Ecology of zoonotic infectious diseases in bats: current  
579 knowledge and future directions. *Zoonoses Public Health* **60**, 2–21.  
580 <https://doi.org/10.1111/zph.12000>.
- 581 11. Irving, A.T., Ahn, M., Goh, G., Anderson, D.E., and Wang, L.-F. (2021). Lessons from the host  
582 defences of bats, a unique viral reservoir. *Nature* **589**, 363–370. <https://doi.org/10.1038/s41586-020-03128-0>.  
583
- 584 12. Morales, A.E., Ruedi, M., Field, K., and Carstens, B.C. (2019). Diversification rates have no effect  
585 on the convergent evolution of foraging strategies in the most speciose genus of bats, *Myotis*.  
586 *Evolution* **73**, 2263–2280. <https://doi.org/10.1111/evo.13849>.
- 587 13. Gunnell, G.F., Smith, R., and Smith, T. (2017). 33 million year old *Myotis* (Chiroptera,  
588 *Vespertilionidae*) and the rapid global radiation of modern bats. *PLoS One* **12**, e0172621.  
589 <https://doi.org/10.1371/journal.pone.0172621>.
- 590 14. Ruedi, M., Stadelmann, B., Gager, Y., Douzery, E.J.P., Francis, C.M., Lin, L.-K., Guillén-Servent,  
591 A., and Cibois, A. (2013). Molecular Phylogenetic Reconstructions Identify East Asia as the Cradle  
592 for the Evolution of the Cosmopolitan Genus *Myotis* (Mammalia, Chiroptera). *Mol. Phylogenet.*  
593 *Evol.* **69**, 437–449. <https://doi.org/10.1016/j.ympev.2013.08.011>.
- 594 15. Tacutu, R., Craig, T., Budovsky, A., Wuttke, D., Lehmann, G., Taranukha, D., Costa, J., Fraifeld,  
595 V.E., and de Magalhães, J.P. (2013). Human Ageing Genomic Resources: Integrated Databases  
596 and Tools for the Biology and Genetics of Ageing. *Nucleic Acids Res.* **41**, D1027–D1033.  
597 <https://doi.org/10.1093/nar/gks1155>.
- 598 16. Jones, K.E., Bielby, J., Cardillo, M., Fritz, S.A., O’Dell, J., Orme, C.D.L., Safi, K., Sechrest, W.,  
599 Boakes, E.H., Carbone, C., et al. (2009). PanTHERIA: A Species-Level Database of Life History,  
600 Ecology, and Geography of Extant and Recently Extinct Mammals. *Ecology* **90**, 2648–2648.  
601 <https://doi.org/10.1890/08-1494.1>.
- 602 17. Austad, S.N. (2010). Methusaleh’s Zoo: How Nature Provides Us with Clues for Extending Human  
603 Health Span. *J. Comp. Pathol.* **142**, S10–S21. <https://doi.org/10.1016/j.jcpa.2009.10.024>.
- 604 18. Austad, S.N., and Fischer, K.E. (1991). Mammalian Aging, Metabolism, and Ecology: Evidence

- 605 from the Bats and Marsupials. *J. Gerontol.* *46*, B47–B53. <https://doi.org/10.1093/geronj/46.2.b47>.
- 606 19. Podlutzky, A.J., Khritankov, A.M., Ovodov, N.D., and Austad, S.N. (2005). A new field record for  
607 bat longevity. *J. Gerontol. A Biol. Sci. Med. Sci.* *60*, 1366–1368.  
608 <https://doi.org/10.1093/gerona/60.11.1366>.
- 609 20. Wilson, D.E., and Tyson, E.L. (1970). Longevity Records for *Artibeus Jamaicensis* and *Myotis*  
610 *Nigricans*. *J. Mammal.* *51*, 203. <https://doi.org/10.2307/1378570>.
- 611 21. Stadelmann, B., Lin, L.-K., Kunz, T.H., and Ruedi, M. (2007). Molecular Phylogeny of New World  
612 *Myotis* (Chiroptera, Vespertilionidae) Inferred from Mitochondrial and Nuclear DNA Genes.  
613 *Mol. Phylogenet. Evol.* *43*, 32–48. <https://doi.org/10.1016/j.ympev.2006.06.019>.
- 614 22. Agnarsson, I., Zambrana-Torrel, C.M., Flores-Saldana, N.P., and May-Collado, L.J. (2011). A  
615 time-calibrated species-level phylogeny of bats (Chiroptera, Mammalia). *PLoS Curr.* *3*, RRN1212.  
616 <https://doi.org/10.1371/currents.RRN1212>.
- 617 23. Seltmann, A., Troxell, S.A., Schad, J., Fritze, M., Bailey, L.D., Voigt, C.C., and Czirják, G.Á. (2022).  
618 Author Correction: Differences in acute phase response to bacterial, fungal and viral antigens in  
619 greater mouse-eared bats (*Myotis myotis*). *Sci. Rep.* *12*, 21144. <https://doi.org/10.1038/s41598-022-25685-2>.
- 620
- 621 24. Armero, A., Li, R., Bienes, K.M., Chen, X., Li, J., Xu, S., Chen, Y., Hughes, A.C., Berthet, N., and  
622 Wong, G. (2022). *Myotis fimbriatus* virome, a window to virus diversity and evolution in the genus  
623 *Myotis*. *Viruses* *14*, 1899. <https://doi.org/10.3390/v14091899>.
- 624 25. He, X., Korytář, T., Zhu, Y., Pikula, J., Bandouchova, H., Zupal, J., and Köllner, B. (2014).  
625 Establishment of *Myotis myotis* Cell Lines - Model for Investigation of Host-Pathogen Interaction in  
626 a Natural Host for Emerging Viruses. *PLoS One* *9*, e109795.  
627 <https://doi.org/10.1371/journal.pone.0109795>.
- 628 26. Hayward, J.A., Tachedjian, M., Johnson, A., Irving, A.T., Gordon, T.B., Cui, J., Nicolas, A., Smith,  
629 I., Boyd, V., Marsh, G.A., et al. (2022). Unique Evolution of Antiviral Tetherin in Bats. *J. Virol.* *96*,  
630 e0115222. <https://doi.org/10.1128/jvi.01152-22>.
- 631 27. Fernandes, A.P., Águeda-Pinto, A., Pinheiro, A., Rebelo, H., and Esteves, P.J. (2022). Evolution of  
632 TRIM5 and TRIM22 in Bats Reveals a Complex Duplication Process. *Viruses* *14*.  
633 <https://doi.org/10.3390/v14020345>.
- 634 28. Jacquet, S., Culbertson, M., Zhang, C., El Filali, A., De La Myre Mory, C., Pons, J.-B., Filippi-  
635 Codaccioni, O., Lauterbur, M.E., Ngoubangoye, B., Duhayer, J., et al. (2022). Adaptive duplication  
636 and genetic diversification of protein kinase R contribute to the specificity of bat-virus interactions.  
637 *Sci Adv* *8*, eadd7540. <https://doi.org/10.1126/sciadv.add7540>.
- 638 29. Jacquet, S., Pontier, D., and Etienne, L. (2020). Rapid Evolution of HERC6 and Duplication of a  
639 Chimeric HERC5/6 Gene in Rodents and Bats Suggest an Overlooked Role of HERCs in  
640 Mammalian Immunity. *Front. Immunol.* *11*, 605270. <https://doi.org/10.3389/fimmu.2020.605270>.
- 641 30. Chomel, B., Stuckey, M., Boulouis, H., and Aguilar Setién, Á. (2014). Bat-Related Zoonoses.  
642 *Zoonoses - Infections Affecting Humans and Animals*, 697–714. [https://doi.org/10.1007/978-94-017-9457-2\\_28](https://doi.org/10.1007/978-94-017-9457-2_28).
- 643
- 644 31. Guth, S., Mollentze, N., Renault, K., Streicker, D.G., Visher, E., Boots, M., and Brook, C.E. (2022).  
645 Bats host the most virulent-but not the most dangerous-zoonotic viruses. *Proc. Natl. Acad. Sci. U.*



- 646 S. A. 119, e2113628119. <https://doi.org/10.1073/pnas.2113628119>.
- 647 32. Williams, E.P., Spruill-Harrell, B.M., Taylor, M.K., Lee, J., Nywening, A.V., Yang, Z., Nichols, J.H.,  
648 Camp, J.V., Owen, R.D., and Jonsson, C.B. (2021). Common themes in zoonotic spillover and  
649 disease emergence: Lessons learned from bat- and rodent-borne RNA viruses. *Viruses* 13, 1509.  
650 <https://doi.org/10.3390/v13081509>.
- 651 33. Mollentze, N., and Streicker, D.G. (2020). Viral zoonotic risk is homogenous among taxonomic  
652 orders of mammalian and avian reservoir hosts. *Proc. Natl. Acad. Sci. U. S. A.* 117, 9423–9430.  
653 <https://doi.org/10.1073/pnas.1919176117>.
- 654 34. Tenthorey, J.L., Emerman, M., and Malik, H.S. (2022). Evolutionary Landscapes of Host-Virus  
655 Arms Races. *Annu. Rev. Immunol.* 40, 271–294. <https://doi.org/10.1146/annurev-immunol-072621-084422>.
- 656
- 657 35. Klunk, J., Vilgalys, T.P., Demeure, C.E., Cheng, X., Shiratori, M., Madej, J., Beau, R., Elli, D.,  
658 Patino, M.I., Redfern, R., et al. (2022). Evolution of immune genes is associated with the Black  
659 Death. *Nature* 611, 312–319. <https://doi.org/10.1038/s41586-022-05349-x>.
- 660 36. Jebb, D., Huang, Z., Pippel, M., Hughes, G.M., Lavrichenko, K., Devanna, P., Winkler, S., Jermiin,  
661 L.S., Skirmuntt, E.C., Katzourakis, A., et al. (2020). Six reference-quality genomes reveal evolution  
662 of bat adaptations. *Nature* 583, 578–584. <https://doi.org/10.1038/s41586-020-2486-3>.
- 663 37. Mynard, P., Algar, A.C., Lancaster, L.T., Bocedi, G., Fahri, F., Gubry-Rangin, C., Lupiyaningdyah,  
664 P., Nangoy, M., Osborne, O.G., Papadopulos, A.S.T., et al. (2023). Impact of phylogenetic tree  
665 completeness and mis-specification of sampling fractions on trait dependent diversification models.  
666 *Syst. Biol.* 72, 106–119. <https://doi.org/10.1093/sysbio/syad001>.
- 667 38. Garamszegi, L.Z., and Møller, A.P. (2010). Effects of sample size and intraspecific variation in  
668 phylogenetic comparative studies: a meta-analytic review. *Biol. Rev. Camb. Philos. Soc.* 85, 797–  
669 805. <https://doi.org/10.1111/j.1469-185X.2010.00126.x>.
- 670 39. Garamszegi, L.Z. ed. (2014). *Modern Phylogenetic Comparative Methods and Their Application in*  
671 *Evolutionary Biology: Concepts and Practice* (Springer) <https://doi.org/10.1007/978-3-662-43550-2>.
- 672 40. Nabhan, A.R., and Sarkar, I.N. (2012). The impact of taxon sampling on phylogenetic inference: a  
673 review of two decades of controversy. *Brief. Bioinform.* 13, 122–134.  
674 <https://doi.org/10.1093/bib/bbr014>.
- 675 41. Li, S., Vazquez, J.M., and Sudmant, P.H. (2023). The Evolution of Aging and Lifespan. *Trends*  
676 *Genet. O.* <https://doi.org/10.1016/j.tig.2023.08.005>.
- 677 42. López-Otín, C., Blasco, M.A., Partridge, L., Serrano, M., and Kroemer, G. (2013). The Hallmarks of  
678 Aging. *Cell* 153, 1194–1217. <https://doi.org/10.1016/j.cell.2013.05.039>.
- 679 43. Kolora, S.R.R., Owens, G.L., Vazquez, J.M., Stubbs, A., Chatla, K., Jainese, C., Seeto, K.,  
680 McCrea, M., Sandel, M.W., Vianna, J.A., et al. (2021). Origins and Evolution of Extreme Life Span  
681 in Pacific Ocean Rockfishes. *Science* 374, 842–847. <https://doi.org/10.1126/science.abg5332>.
- 682 44. Sulak, M., Fong, L., Mika, K., Chigurupati, S., Yon, L., Mongan, N.P., Emes, R.D., and Lynch, V.J.  
683 (2016). Correction: TP53 copy number expansion is associated with the evolution of increased  
684 body size and an enhanced DNA damage response in elephants. *Elife* 5.  
685 <https://doi.org/10.7554/eLife.24307>.

- 686 45. Vazquez, J.M., Sulak, M., Chigurupati, S., and Lynch, V.J. (2018). A Zombie LIF Gene in  
687 Elephants Is Upregulated by TP53 to Induce Apoptosis in Response to DNA Damage. *Cell Rep.*  
688 *24*, 1765–1776. <https://doi.org/10.1016/j.celrep.2018.07.042>.
- 689 46. Vazquez, J.M., and Lynch, V.J. (2021). Pervasive Duplication of Tumor Suppressors in  
690 Afrotherians during the Evolution of Large Bodies and Reduced Cancer Risk. *Elife* *10*, e65041.  
691 <https://doi.org/10.7554/eLife.65041>.
- 692 47. Davies, K.T.J., Tsagkogeorga, G., Bennett, N.C., Dávalos, L.M., Faulkes, C.G., and Rossiter, S.J.  
693 (2014). Molecular Evolution of Growth Hormone and Insulin-like Growth Factor 1 Receptors in  
694 Long-Lived, Small-Bodied Mammals. *Gene* *549*, 228–236.  
695 <https://doi.org/10.1016/j.gene.2014.07.061>.
- 696 48. Vazquez, J.M., Kraft, M., and Lynch, V.J. (2022). A CDKN2C retroduplication in Bowhead whales  
697 is associated with the evolution of extremely long lifespans and alerted cell cycle dynamics.  
698 *bioRxiv*, 2022.09.07.506958. <https://doi.org/10.1101/2022.09.07.506958>.
- 699 49. Foote, A.D., Liu, Y., Thomas, G.W.C., Vinař, T., Alföldi, J., Deng, J., Dugan, S., van Elk, C.E.,  
700 Hunter, M.E., Joshi, V., et al. (2015). Convergent evolution of the genomes of marine mammals.  
701 *Nat. Genet.* *47*, 272–275. <https://doi.org/10.1038/ng.3198>.
- 702 50. Huang, Z., Jiang, C., Gu, J., Uvizl, M., Power, S., Douglas, D., and Kacprzyk, J. (2023).  
703 Duplications of Human Longevity-Associated Genes Across Placental Mammals. *Genome Biol.*  
704 *Evol.* *15*. <https://doi.org/10.1093/gbe/evad186>.
- 705 51. Glaberman, S., Bulls, S.E., Vazquez, J.M., Chiari, Y., and Lynch, V.J. (2021). Concurrent Evolution  
706 of Antiaging Gene Duplications and Cellular Phenotypes in Long-Lived Turtles. *Genome Biol. Evol.*  
707 *13*, evab244. <https://doi.org/10.1093/gbe/evab244>.
- 708 52. MacRae, S.L., Croken, M.M., Calder, R.B., Aliper, A., Milholland, B., White, R.R., Zhavoronkov, A.,  
709 Gladyshev, V.N., Seluanov, A., Gorbunova, V., et al. (2015). DNA Repair in Species with Extreme  
710 Lifespan Differences. *Aging* *7*, 1171–1184. <https://doi.org/10.18632/aging.100866>.
- 711 53. Baines, C., Meitern, R., Kreitsberg, R., and Sepp, T. (2022). Comparative study of the evolution of  
712 cancer gene duplications across fish. *Evol. Appl.* *15*, 1834–1845.  
713 <https://doi.org/10.1111/eva.13481>.
- 714 54. Moreno Santillán, D.D., Lama, T.M., Gutierrez Guerrero, Y.T., Brown, A.M., Donat, P., Zhao, H.,  
715 Rossiter, S.J., Yohe, L.R., Potter, J.H., Teeling, E.C., et al. (2021). Large-scale genome sampling  
716 reveals unique immunity and metabolic adaptations in bats. *Mol. Ecol.* *30*, 6449–6467.  
717 <https://doi.org/10.1111/mec.16027>.
- 718 55. Scheben, A., Mendivil Ramos, O., Kramer, M., Goodwin, S., Oppenheim, S., Becker, D.J., Schatz,  
719 M.C., Simmons, N.B., Siepel, A., and McCombie, W.R. (2023). Long-Read Sequencing Reveals  
720 Rapid Evolution of Immunity- and Cancer-Related Genes in Bats. *Genome Biol. Evol.* *15*.  
721 <https://doi.org/10.1093/gbe/evad148>.
- 722 56. Tian, S., Zeng, J., Jiao, H., Zhang, D., Zhang, L., Lei, C.-Q., Rossiter, S.J., and Zhao, H. (2023).  
723 Comparative analyses of bat genomes identify distinct evolution of immunity in Old World fruit bats.  
724 *Sci Adv* *9*, eadd0141. <https://doi.org/10.1126/sciadv.add0141>.
- 725 57. Sotero-Caio, C.G., Baker, R.J., and Volleth, M. (2017). Chromosomal evolution in Chiroptera.  
726 *Genes (Basel)* *8*. <https://doi.org/10.3390/genes8100272>.

- 727 58. Nachtweide, S., and Stanke, M. (2019). Multi-Genome Annotation with AUGUSTUS. *Methods Mol.*  
728 *Biol.* 1962, 139–160. [https://doi.org/10.1007/978-1-4939-9173-0\\_8](https://doi.org/10.1007/978-1-4939-9173-0_8).
- 729 59. Lomsadze, A., Ter-Hovhannisyanyan, V., Chernoff, Y.O., and Borodovsky, M. (2005). Gene  
730 identification in novel eukaryotic genomes by self-training algorithm. *Nucleic Acids Res.* 33, 6494–  
731 6506. <https://doi.org/10.1093/nar/gki937>.
- 732 60. Shumate, A., and Salzberg, S.L. (2021). Liftoff: accurate mapping of gene annotations.  
733 *Bioinformatics*.
- 734 61. Kirilenko, B.M., Munegowda, C., Osipova, E., Jebb, D., Sharma, V., Blumer, M., Morales, A.E.,  
735 Ahmed, A.-W., Kontopoulos, D.-G., Hilgers, L., et al. (2023). Integrating gene annotation with  
736 orthology inference at scale. *Science* 380, eabn3107. <https://doi.org/10.1126/science.abn3107>.
- 737 62. Li, H. (2023). Protein-to-genome alignment with miniprot. *Bioinformatics*.
- 738 63. Simão, F.A., Waterhouse, R.M., Ioannidis, P., Kriventseva, E.V., and Zdobnov, E.M. (2015).  
739 BUSCO: assessing genome assembly and annotation completeness with single-copy orthologs.  
740 *Bioinformatics* 31, 3210–3212. <https://doi.org/10.1093/bioinformatics/btv351>.
- 741 64. Manni, M., Berkeley, M.R., Seppey, M., and Zdobnov, E.M. (2021). BUSCO: assessing genomic  
742 data quality and beyond. *Current Protocols* 1.
- 743 65. Curti, J., Fraser, D., Escalona, M., Fairbairn, C.W., Sacco, S., Sahasrabudhe, R., Nguyen, O.,  
744 Seligmann, W., Sudmant, P.H., Toffelmier, E., et al. (2023). A Genome Assembly of the Yuma  
745 Myotis Bat, *Myotis Yumanensis*. *J. Hered.*, esad053. <https://doi.org/10.1093/jhered/esad053>.
- 746 66. Amador, L.I., Moyers Arévalo, R.L., Almeida, F.C., Catalano, S.A., and Giannini, N.P. (2018). Bat  
747 Systematics in the Light of Unconstrained Analyses of a Comprehensive Molecular Supermatrix. *J.*  
748 *Mamm. Evol.* 25, 37–70. <https://doi.org/10.1007/s10914-016-9363-8>.
- 749 67. Upham, N.S., Esselstyn, J.A., and Jetz, W. (2019). Inferring the mammal tree: Species-level sets  
750 of phylogenies for questions in ecology, evolution, and conservation. *PLoS Biol.* 17, e3000494.  
751 <https://doi.org/10.1371/journal.pbio.3000494>.
- 752 68. Korstian, J.M., Paulat, N.S., Platt, R.N., Stevens, R.D., and Ray, D.A. (2022). SINE-Based  
753 Phylogenomics Reveal Extensive Introgression and Incomplete Lineage Sorting in *Myotis*. *Genes*  
754 13, 399. <https://doi.org/10.3390/genes13030399>.
- 755 69. Foley, N.M., Harris, A.J., Bredemeyer, K.R., Ruedi, M., Puechmaille, S.J., Teeling, E.C.,  
756 Criscitiello, M.F., and Murphy, W.J. (2024). Karyotypic stasis and swarming influenced the  
757 evolution of viral tolerance in a species-rich bat radiation. *Cell Genom* 4, 100482.  
758 <https://doi.org/10.1016/j.xgen.2023.100482>.
- 759 70. UniProt Consortium (2023). UniProt: The universal protein knowledgebase in 2023. *Nucleic Acids*  
760 *Res.* 51, D523–D531. <https://doi.org/10.1093/nar/gkac1052>.
- 761 71. dos Reis, M., and Yang, Z. (2011). Approximate likelihood calculation on a phylogeny for Bayesian  
762 estimation of divergence times. *Mol. Biol. Evol.* 28, 2161–2172.  
763 <https://doi.org/10.1093/molbev/msr045>.
- 764 72. Yang, Z. (2007). PAML 4: phylogenetic analysis by maximum likelihood. *Mol. Biol. Evol.* 24, 1586–  
765 1591. <https://doi.org/10.1093/molbev/msm088>.

- 766 73. Brunet-Rossinni, A.K., and Austad, S.N. (2004). Ageing studies on bats: a review. *Biogerontology*  
767 5, 211–222. <https://doi.org/10.1023/B:BGGEN.0000038022.65024.d8>.
- 768 74. Wilkinson, G.S., and South, J.M. (2002). Life History, Ecology and Longevity in Bats. *Aging Cell* 1,  
769 124–131. <https://doi.org/10.1046/j.1474-9728.2002.00020.x>.
- 770 75. Puttick, M.N., and Thomas, G.H. (2015). Fossils and living taxa agree on patterns of body mass  
771 evolution: a case study with Afrotheria. *Proc. Biol. Sci.* 282, 20152023.  
772 <https://doi.org/10.1098/rspb.2015.2023>.
- 773 76. Vazquez, J.M., Pena, M.T., Muhammad, B., Kraft, M., Adams, L.B., and Lynch, V.J. (2022).  
774 Parallel Evolution of Reduced Cancer Risk and Tumor Suppressor Duplications in Xenarthra. *Elife*  
775 11, e82558. <https://doi.org/10.7554/eLife.82558>.
- 776 77. Slater, G.J., Goldbogen, J.A., and Pyenson, N.D. (2017). Independent evolution of baleen whale  
777 gigantism linked to Plio-Pleistocene ocean dynamics. *Proc. Biol. Sci.* 284.  
778 <https://doi.org/10.1098/rspb.2017.0546>.
- 779 78. Ricklefs, R.E. (2010). Life-history connections to rates of aging in terrestrial vertebrates. *Proc. Natl.*  
780 *Acad. Sci. U. S. A.* 107, 10314–10319. <https://doi.org/10.1073/pnas.1005862107>.
- 781 79. Tillquist, R.C., Shoemaker, L.G., Knight, K.B., and Clauset, A. (2016). The evolution of primate  
782 body size: Left-skewness, maximum size, and Cope’s Rule. *bioRxiv*, 092866.  
783 <https://doi.org/10.1101/092866>.
- 784 80. Kuparinen, A., Yeung, E., and Hutchings, J.A. (2023). Correlation between body size and  
785 longevity: New analysis and data covering six taxonomic classes of vertebrates. *Acta Oecol.*  
786 (Montrouge) 119, 103917. <https://doi.org/10.1016/j.actao.2023.103917>.
- 787 81. Montgomery, S.H., Geisler, J.H., McGowen, M.R., Fox, C., Marino, L., and Gatesy, J. (2013). The  
788 evolutionary history of cetacean brain and body size: Cetacean brain evolution. *Evolution* 67,  
789 3339–3353. <https://doi.org/10.1111/evo.12197>.
- 790 82. Pyenson, N.D., and Sponberg, S.N. (2011). Reconstructing body size in extinct crown Cetacea  
791 (neoceti) using allometry, phylogenetic methods and tests from the fossil record. *J. Mamm. Evol.*  
792 18, 269–288. <https://doi.org/10.1007/s10914-011-9170-1>.
- 793 83. Delsuc, F., Gibb, G.C., Kuch, M., Billet, G., Hautier, L., Southon, J., Rouillard, J.-M., Fernicola,  
794 J.C., Vizcaíno, S.F., MacPhee, R.D.E., et al. (2016). The phylogenetic affinities of the extinct  
795 glyptodonts. *Curr. Biol.* 26, R155–R156. <https://doi.org/10.1016/j.cub.2016.01.039>.
- 796 84. Argot, C. (2008). Changing Views in Paleontology: The Story of a Giant (Megatherium, Xenarthra).  
797 In *Mammalian Evolutionary Morphology Vertebrate Paleobiology and Paleoanthropology Series.*,  
798 E. J. Sargis and M. Dagosto, eds. (Springer Netherlands), pp. 37–50. [https://doi.org/10.1007/978-](https://doi.org/10.1007/978-1-4020-6997-0_3)  
799 [1-4020-6997-0\\_3](https://doi.org/10.1007/978-1-4020-6997-0_3).
- 800 85. Raj Pant, S., Goswami, A., and Finarelli, J.A. (2014). Complex body size trends in the evolution of  
801 sloths (Xenarthra: Pilosa). *BMC Evol. Biol.* 14, 184. <https://doi.org/10.1186/s12862-014-0184-1>.
- 802 86. Armitage, P. (1985). Multistage Models of Carcinogenesis. *Environ. Health Perspect.* 63, 195–201.  
803 <https://doi.org/10.1289/ehp.8563195>.
- 804 87. Armitage, P., and Doll, R. (2004). The Age Distribution of Cancer and a Multi-Stage Theory of  
805 Carcinogenesis. *Br. J. Cancer* 91, 6602297. <https://doi.org/10.1038/sj.bjc.6602297>.



- 806 88. Peto, R., Roe, F.J., Lee, P.N., Levy, L., and Clack, J. (1975). Cancer and ageing in mice and men.  
807 Br. J. Cancer 32, 411–426. <https://doi.org/10.1038/bjc.1975.242>.
- 808 89. Peto, R. (2015). Quantitative Implications of the Approximate Irrelevance of Mammalian Body Size  
809 and Lifespan to Lifelong Cancer Risk. Philos. Trans. R. Soc. Lond. B Biol. Sci. 370, 20150198.  
810 <https://doi.org/10.1098/rstb.2015.0198>.
- 811 90. Nunnery, L. (2018). Size Matters: Height, Cell Number and a Person's Risk of Cancer. Proc. R.  
812 Soc. B 285, 20181743. <https://doi.org/10.1098/rspb.2018.1743>.
- 813 91. Caulin, A.F., and Maley, C.C. (2011). Peto's Paradox: evolution's prescription for cancer  
814 prevention. Trends Ecol. Evol. 26, 175–182. <https://doi.org/10.1016/j.tree.2011.01.002>.
- 815 92. Vincze, O., Colchero, F., Lemaître, J.-F., Conde, D.A., Pavard, S., Bieuville, M., Urrutia, A.O.,  
816 Ujvari, B., Boddy, A.M., Maley, C.C., et al. (2022). Cancer risk across mammals. Nature 601, 263–  
817 267. <https://doi.org/10.1038/s41586-021-04224-5>.
- 818 93. Abegglen, L.M., Caulin, A.F., Chan, A., Lee, K., Robinson, R., Campbell, M.S., Kiso, W.K., Schmitt,  
819 D.L., Waddell, P.J., Bhaskara, S., et al. (2015). Potential Mechanisms for Cancer Resistance in  
820 Elephants and Comparative Cellular Response to DNA Damage in Humans. JAMA 314, 1850–  
821 1860. <https://doi.org/10.1001/jama.2015.13134>.
- 822 94. Tollis, M., Robbins, J., Webb, A., Kuderna, L.F.K., Caulin, A.F., Garcia, J.D., Bérubé, M.,  
823 Pourmand, N., Marquès-Bonet, T., O'Connell, M., et al. (2019). Return to the sea, get huge, beat  
824 cancer: An analysis of cetacean genomes including an assembly for the humpback whale  
825 (*Megaptera novaeangliae*). Mol. Biol. Evol. 36, 1746–1763.  
826 <https://doi.org/10.1093/molbev/msz099>.
- 827 95. Tollis, M., Schneider-Utaka, A.K., and Maley, C.C. (2020). The evolution of human cancer gene  
828 duplications across mammals. Mol. Biol. Evol. 37, 2875–2886.  
829 <https://doi.org/10.1093/molbev/msaa125>.
- 830 96. Caulin, A.F., Graham, T.A., Wang, L.-S., and Maley, C.C. (2015). Solutions to Peto's paradox  
831 revealed by mathematical modelling and cross-species cancer gene analysis. Philos. Trans. R.  
832 Soc. Lond. B Biol. Sci. 370, 20140222. <https://doi.org/10.1098/rstb.2014.0222>.
- 833 97. Nair, N.U., Cheng, K., Naddaf, L., Sharon, E., Pal, L.R., Rajagopal, P.S., Unterman, I., Aldape, K.,  
834 Hannenhalli, S., Day, C.-P., et al. (2022). Cross-species identification of cancer resistance-  
835 associated genes that may mediate human cancer risk. Sci. Adv. 8, eabj7176.  
836 <https://doi.org/10.1126/sciadv.abj7176>.
- 837 98. Smith, M.D., Wertheim, J.O., Weaver, S., Murrell, B., Scheffler, K., and Kosakovsky Pond, S.L.  
838 (2015). Less is more: an adaptive branch-site random effects model for efficient detection of  
839 episodic diversifying selection. Mol. Biol. Evol. 32, 1342–1353.  
840 <https://doi.org/10.1093/molbev/msv022>.
- 841 99. Hanahan, D., and Weinberg, R.A. (2011). Hallmarks of Cancer: The Next Generation. Cell 144,  
842 646–674. <https://doi.org/10.1016/j.cell.2011.02.013>.
- 843 100. Hanahan, D., and Weinberg, R.A. (2000). The Hallmarks of Cancer. Cell 100, 57–70.  
844 [https://doi.org/10.1016/S0092-8674\(00\)81683-9](https://doi.org/10.1016/S0092-8674(00)81683-9).
- 845 101. Hanahan, D. (2022). Hallmarks of Cancer: New Dimensions. Cancer Discov. 12, 31–46.  
846 <https://doi.org/10.1158/2159-8290.CD-21-1059>.

- 847 102. Wertheim, J.O., Murrell, B., Smith, M.D., Kosakovsky Pond, S.L., and Scheffler, K. (2015). RELAX:  
848 detecting relaxed selection in a phylogenetic framework. *Mol. Biol. Evol.* 32, 820–832.  
849 <https://doi.org/10.1093/molbev/msu400>.
- 850 103. Wang, A., Zhu, F., Liang, R., Li, D., and Li, B. (2019). Regulation of T cell differentiation and  
851 function by ubiquitin-specific proteases. *Cell. Immunol.* 340, 103922.  
852 <https://doi.org/10.1016/j.cellimm.2019.103922>.
- 853 104. Meng, Y., Hong, C., Yang, S., Qin, Z., Yang, L., and Huang, Y. (2023). Roles of USP9X in cellular  
854 functions and tumorigenesis (Review). *Oncol. Lett.* 26, 506. <https://doi.org/10.3892/ol.2023.14093>.
- 855 105. Dohmen, M., Krieg, S., Agalaridis, G., Zhu, X., Shehata, S.N., Pfeifferberger, E., Amelang, J.,  
856 Bütepage, M., Buerova, E., Pfaff, C.M., et al. (2020). AMPK-dependent activation of the Cyclin  
857 Y/CDK16 complex controls autophagy. *Nat. Commun.* 11, 1032. [https://doi.org/10.1038/s41467-](https://doi.org/10.1038/s41467-020-14812-0)  
858 [020-14812-0](https://doi.org/10.1038/s41467-020-14812-0).
- 859 106. Wang, X., Liu, R., Li, S., Xia, W., Guo, H., Yao, W., Liang, X., Lu, Y., and Zhang, H. (2023). The  
860 roles, molecular interactions, and therapeutic value of CDK16 in human cancers. *Biomed.*  
861 *Pharmacother.* 164, 114929. <https://doi.org/10.1016/j.biopha.2023.114929>.
- 862 107. Katoh, Y., and Katoh, M. (2009). FGFR2-related pathogenesis and FGFR2-targeted therapeutics  
863 (Review). *Int. J. Mol. Med.* 23, 307–311. [https://doi.org/10.3892/ijmm\\_00000132](https://doi.org/10.3892/ijmm_00000132).
- 864 108. Wang, K., Lai, C., Li, T., Wang, C., Wang, W., Ni, B., Bai, C., Zhang, S., Han, L., Gu, H., et al.  
865 (2018). Basic fibroblast growth factor protects against influenza A virus-induced acute lung injury  
866 by recruiting neutrophils. *J. Mol. Cell Biol.* 10, 573–585. <https://doi.org/10.1093/jmcb/mjx047>.
- 867 109. Kowalczyk, A., Meyer, W.K., Partha, R., Mao, W., Clark, N.L., and Chikina, M. (2019).  
868 RERconverge: an R package for associating evolutionary rates with convergent traits.  
869 *Bioinformatics* 35, 4815–4817. <https://doi.org/10.1093/bioinformatics/btz468>.
- 870 110. Milacic, M., Beavers, D., Conley, P., Gong, C., Gillespie, M., Griss, J., Haw, R., Jassal, B.,  
871 Matthews, L., May, B., et al. (2024). The reactome pathway knowledgebase 2024. *Nucleic Acids*  
872 *Res.* 52, D672–D678. <https://doi.org/10.1093/nar/gkad1025>.
- 873 111. Firsanov, D., Zacher, M., Tian, X., Zhao, Y., George, J.C., Sformo, T.L., Tomblin, G., Biashad,  
874 S.A., Gilman, A., Hamilton, N., et al. (2023). DNA repair and anti-cancer mechanisms in the  
875 longest-living mammal: the bowhead whale. *bioRxiv*, 2023.05.07.539748.  
876 <https://doi.org/10.1101/2023.05.07.539748>.
- 877 112. Enard, D., Cai, L., Gwennap, C., and Petrov, D.A. (2016). Viruses are a dominant driver of protein  
878 adaptation in mammals. *Elife* 5. <https://doi.org/10.7554/eLife.12469>.
- 879 113. Murrell, B., Weaver, S., Smith, M.D., Wertheim, J.O., Murrell, S., Aylward, A., Eren, K., Pollner, T.,  
880 Martin, D.P., Smith, D.M., et al. (2015). Gene-wide identification of episodic selection. *Mol. Biol.*  
881 *Evol.* 32, 1365–1371. <https://doi.org/10.1093/molbev/msv035>.
- 882 114. Souilmi, Y., Lauterbur, M.E., Tobler, R., Huber, C.D., Johar, A.S., Moradi, S.V., Johnston, W.A.,  
883 Krogan, N.J., Alexandrov, K., and Enard, D. (2021). An ancient viral epidemic involving host  
884 coronavirus interacting genes more than 20,000 years ago in East Asia. *Curr. Biol.* 31, 3704.  
885 <https://doi.org/10.1016/j.cub.2021.07.052>.
- 886 115. Brook, C.E., and Dobson, A.P. (2015). Bats as “special” reservoirs for emerging zoonotic  
887 pathogens. *Trends Microbiol.* 23, 172–180. <https://doi.org/10.1016/j.tim.2014.12.004>.

- 888 116. Enard, D., and Petrov, D.A. (2018). Evidence that RNA Viruses Drove Adaptive Introgression  
889 between Neanderthals and Modern Humans. *Cell* 175, 360–371.e13.  
890 <https://doi.org/10.1016/j.cell.2018.08.034>.
- 891 117. Volleth, M. (2012). Variations on a theme: Karyotype comparison in Eurasian *Myotis* species and  
892 implications for phylogeny. *Vespertilio* 16, 329–350.
- 893 118. McBee, K. (1986). Standard karyology of nine species of vespertilionid bats (Chiroptera:  
894 Vespertilionidae) from Thailand. *Annals of Carnegie Museum* 55, 95–116.
- 895 119. Bickham, J.W., McBee, K., and Schlitter, D.A. (1986). Chromosomal variation among seven  
896 species of *Myotis* (Chiroptera: Vespertilionidae). *J. Mammal.* 67, 746–750.  
897 <https://doi.org/10.2307/1381139>.
- 898 120. Zhang, W.D. (1984). A study on karyotype of *Myotis chinensis* and *M. laniger* Peter. *J Anhui*  
899 *Normal Univ* 7, 42–47.
- 900 121. Zima, J. (1985). Synopsis of karyotypes of vespertilionid bats (Mammalia: Chiroptera). *Acta Univ.*  
901 *Carol. Biol* 1981, 311–329.
- 902 122. Karataş, A., Sözen, M., Özkurt, Ş., and Matur, F. (2007). Karyology of three bat species of the  
903 genus *Myotis* (*M. myotis*, *M. bechsteinii*, *M. brandtii*) (Chiroptera: Vespertilionidae) from Turkey.  
904 *Zool. Middle East* 40, 5–9. <https://doi.org/10.1080/09397140.2007.10638198>.
- 905 123. Bovey, R. (1949). Chromosomes of Chiroptera and Insectivora.
- 906 124. Yi, W.U., and Harada, M. (2006). Karyology of seven species of bats (Mammalia: Chiroptera) from  
907 Guangdong, China. *Shou Lei Xue Bao* 26, 403.
- 908 125. Yoshitaka Obara, Takafumi Tomiyasu, and Kazuo Saitoh (1976). CHROMOSOME STUDIES IN  
909 THE JAPANESE VESPERTILIONID BATS: I. KARYOTYPIC VARIATIONS IN *MYOTIS*  
910 *MACRODACTYLUS TEMMINCK*. *Jpn. J. Genet.* 51, 201–206.
- 911 126. Vujošević, M., Rajičić, M., and Blagojević, J. (2018). B Chromosomes in Populations of Mammals  
912 Revisited. *Genes* 9. <https://doi.org/10.3390/genes9100487>.
- 913 127. O'Brien, S.J., Menninger, J.C., and Nash, W.G. (2006). *Atlas of Mammalian Chromosomes* (John  
914 Wiley & Sons).
- 915 128. Goel, M., Sun, H., Jiao, W.-B., and Schneeberger, K. (2019). SyRI: finding genomic  
916 rearrangements and local sequence differences from whole-genome assemblies. *Genome Biol.* 20,  
917 277. <https://doi.org/10.1186/s13059-019-1911-0>.
- 918 129. de Sotero-Caio, C.G., Cabral-de-Mello, D.C., Calixto, M. da S., Valente, G.T., Martins, C., Loreto,  
919 V., de Souza, M.J., and Santos, N. (2017). Centromeric enrichment of LINE-1 retrotransposons  
920 and its significance for the chromosome evolution of Phyllostomid bats. *Chromosome Res.* 25,  
921 313–325. <https://doi.org/10.1007/s10577-017-9565-9>.
- 922 130. Kosek, D., Grabundzija, I., Lei, H., Bilic, I., Wang, H., Jin, Y., Peaslee, G.F., Hickman, A.B., and  
923 Dyda, F. (2021). The large bat Helitron DNA transposase forms a compact monomeric assembly  
924 that buries and protects its covalently bound 5'-transposon end. *Mol. Cell* 81, 4271–4286.e4.  
925 <https://doi.org/10.1016/j.molcel.2021.07.028>.
- 926 131. Ducani, C., Bernardinelli, G., and Högberg, B. (2014). Rolling circle replication requires single-

- 927 stranded DNA binding protein to avoid termination and production of double-stranded DNA.  
928 *Nucleic Acids Res.* *42*, 10596–10604. <https://doi.org/10.1093/nar/gku737>.
- 929 132. Thomas, J., Phillips, C.D., Baker, R.J., and Pritham, E.J. (2014). Rolling-circle transposons  
930 catalyze genomic innovation in a mammalian lineage. *Genome Biol. Evol.* *6*, 2595–2610.  
931 <https://doi.org/10.1093/gbe/evu204>.
- 932 133. Balachandran, P., Walawalkar, I.A., Flores, J.I., Dayton, J.N., Audano, P.A., and Beck, C.R.  
933 (2022). Transposable element-mediated rearrangements are prevalent in human genomes. *Nat.*  
934 *Commun.* *13*, 7115. <https://doi.org/10.1038/s41467-022-34810-8>.
- 935 134. Ait Saada, A., Guo, W., Costa, A.B., Yang, J., Wang, J., and Lobachev, K.S. (2023). Widely  
936 spaced and divergent inverted repeats become a potent source of chromosomal rearrangements in  
937 long single-stranded DNA regions. *Nucleic Acids Res.* *51*, 3722–3734.  
938 <https://doi.org/10.1093/nar/gkad153>.
- 939 135. Kondrashov, F.A. (2011). Gene Dosage and Duplication. In *Evolution after Gene Duplication*, K.  
940 Dittmar and D. Liberles, eds. (John Wiley & Sons), pp. 57–76.
- 941 136. Kondrashov, F.A., Rogozin, I.B., Wolf, Y.I., and Koonin, E.V. (2002). Selection in the evolution of  
942 gene duplications. *Genome Biol.* *3*, RESEARCH0008. [https://doi.org/10.1186/gb-2002-3-2-](https://doi.org/10.1186/gb-2002-3-2-research0008)  
943 [research0008](https://doi.org/10.1186/gb-2002-3-2-research0008).
- 944 137. Rastogi, S., and Liberles, D.A. (2005). Subfunctionalization of duplicated genes as a transition  
945 state to neofunctionalization. *BMC Evol. Biol.* *5*, 28. <https://doi.org/10.1186/1471-2148-5-28>.
- 946 138. Assis, R., and Bachtrog, D. (2013). Neofunctionalization of young duplicate genes in *Drosophila*.  
947 *Proc. Natl. Acad. Sci. U. S. A.* *110*, 17409–17414. <https://doi.org/10.1073/pnas.1313759110>.
- 948 139. Tirosh, I., and Barkai, N. (2007). Comparative analysis indicates regulatory neofunctionalization of  
949 yeast duplicates. *Genome Biol.* *8*, R50. <https://doi.org/10.1186/gb-2007-8-4-r50>.
- 950 140. Mendes, F.K., Vanderpool, D., Fulton, B., and Hahn, M.W. (2021). CAFE 5 models variation in  
951 evolutionary rates among gene families. *Bioinformatics* *36*, 5516–5518.  
952 <https://doi.org/10.1093/bioinformatics/btaa1022>.
- 953 141. Duan, S., Moro, L., Qu, R., Simoneschi, D., Cho, H., Jiang, S., Zhao, H., Chang, Q., de Stanchina,  
954 E., Arbini, A.A., et al. (2021). Loss of FBXO31-mediated degradation of DUSP6 dysregulates ERK  
955 and PI3K-AKT signaling and promotes prostate tumorigenesis. *Cell Rep.* *37*, 109870.  
956 <https://doi.org/10.1016/j.celrep.2021.109870>.
- 957 142. Morel, B., Kozlov, A.M., Stamatakis, A., and Szöllösi, G.J. (2020). GeneRax: A Tool for Species-  
958 Tree-Aware Maximum Likelihood-Based Gene Family Tree Inference under Gene Duplication,  
959 Transfer, and Loss. *Mol. Biol. Evol.* *37*, 2763–2774. <https://doi.org/10.1093/molbev/msaa141>.
- 960 143. Kaufman, R.J. (1999). Double-stranded RNA-activated protein kinase mediates virus-induced  
961 apoptosis: a new role for an old actor. *Proc. Natl. Acad. Sci. U. S. A.* *96*, 11693–11695.  
962 <https://doi.org/10.1073/pnas.96.21.11693>.
- 963 144. García, M.A., Gil, J., Ventoso, I., Guerra, S., Domingo, E., Rivas, C., and Esteban, M. (2006).  
964 Impact of protein kinase PKR in cell biology: from antiviral to antiproliferative action. *Microbiol. Mol.*  
965 *Biol. Rev.* *70*, 1032–1060. <https://doi.org/10.1128/MMBR.00027-06>.
- 966 145. Ostertag, D., Hoblitzell-Ostertag, T.M., and Perrault, J. (2007). Overproduction of double-stranded



- 967 RNA in vesicular stomatitis virus-infected cells activates a constitutive cell-type-specific antiviral  
968 response. *J. Virol.* *81*, 503–513. <https://doi.org/10.1128/JVI.01218-06>.
- 969 146. Lagunas-Rangel, F.A. (2020). Why do bats live so long?—Possible molecular mechanisms.  
970 *Biogerontology* *21*, 1–11. <https://doi.org/10.1007/s10522-019-09840-3>.
- 971 147. Chionh, Y.T., Cui, J., Koh, J., Mendenhall, I.H., Ng, J.H.J., Low, D., Itahana, K., Irving, A.T., and  
972 Wang, L.-F. (2019). High basal heat-shock protein expression in bats confers resistance to cellular  
973 heat/oxidative stress. *Cell Stress Chaperones* *24*, 835–849. <https://doi.org/10.1007/s12192-019-01013-y>.
- 974
- 975 148. Hua, R., Ma, Y.-S., Yang, L., Hao, J.-J., Hua, Q.-Y., Shi, L.-Y., Yao, X.-Q., Zhi, H.-Y., and Liu, Z.  
976 (2024). Experimental evidence for cancer resistance in a bat species. *Nat. Commun.* *15*, 1401.  
977 <https://doi.org/10.1038/s41467-024-45767-1>.
- 978 149. Peixoto, F.P., Braga, P.H.P., and Mendes, P. (2018). A synthesis of ecological and evolutionary  
979 determinants of bat diversity across spatial scales. *BMC Ecol.* *18*, 18.  
980 <https://doi.org/10.1186/s12898-018-0174-z>.
- 981 150. USGS (2022). North American Bat Ranges.  
982 [http://dds.cr.usgs.gov/pub/data/nationalatlas/bat000p010g\\_nt00373.tar.gz](http://dds.cr.usgs.gov/pub/data/nationalatlas/bat000p010g_nt00373.tar.gz)  
983 [http://dds.cr.usgs.gov/pub/data/nationalatlas/bat000p010g\\_nt00373.tar.gz](http://dds.cr.usgs.gov/pub/data/nationalatlas/bat000p010g_nt00373.tar.gz).
- 984 151. Rhie, A., McCarthy, S.A., Fedrigo, O., Damas, J., Formenti, G., Koren, S., Uliano-Silva, M., Chow,  
985 W., Fungtammasan, A., Kim, J., et al. (2021). Towards complete and error-free genome  
986 assemblies of all vertebrate species. *Nature* *592*, 737–746. <https://doi.org/10.1038/s41586-021-03451-0>.
- 987
- 988 152. The Darwin Tree of Life Project Consortium (2022). Sequence Locally, Think Globally: The Darwin  
989 Tree of Life Project. *Proceedings of the National Academy of Sciences* *119*, e2115642118.  
990 <https://doi.org/10.1073/pnas.2115642118>.
- 991 153. Lewin, H.A., Richards, S., Lieberman Aiden, E., Allende, M.L., Archibald, J.M., Bálint, M., Barker,  
992 K.B., Baumgartner, B., Belov, K., Bertorelle, G., et al. (2022). The Earth BioGenome Project 2020:  
993 Starting the Clock. *Proceedings of the National Academy of Sciences* *119*, e2115635118.  
994 <https://doi.org/10.1073/pnas.2115635118>.
- 995 154. Tacutu, R., Thornton, D., Johnson, E., Budovsky, A., Barardo, D., Craig, T., Diana, E., Lehmann,  
996 G., Toren, D., Wang, J., et al. (2018). Human Ageing Genomic Resources: new and updated  
997 databases. *Nucleic Acids Res.* *46*, D1083–D1090. <https://doi.org/10.1093/nar/gkx1042>.
- 998 155. Enard, D., and Petrov, D.A. (2020). Ancient RNA virus epidemics through the lens of recent  
999 adaptation in human genomes. *Philos. Trans. R. Soc. Lond. B Biol. Sci.* *375*, 20190575.  
000 <https://doi.org/10.1098/rstb.2019.0575>.
- 001 156. Boys, I.N., Xu, E., Mar, K.B., De La Cruz-Rivera, P.C., Eitson, J.L., Moon, B., and Schoggins, J.W.  
002 (2020). RTP4 is a potent IFN-inducible anti-flavivirus effector engaged in a host-virus arms race in  
003 bats and other mammals. *Cell Host Microbe* *28*, 712–723.e9.  
004 <https://doi.org/10.1016/j.chom.2020.09.014>.
- 005 157. Lytras, S., Wickenhagen, A., Sugrue, E., Stewart, D.G., Swingler, S., Sims, A., Jackson Ireland, H.,  
006 Davies, E.L., Ludlam, E.M., Li, Z., et al. (2023). Resurrection of 2'-5'-oligoadenylate synthetase 1  
007 (OAS1) from the ancestor of modern horseshoe bats blocks SARS-CoV-2 replication. *PLoS Biol.*  
008 *21*, e3002398. <https://doi.org/10.1371/journal.pbio.3002398>.

- 009 158. Tsagkogeorga, G., Müller, S., Dessimoz, C., and Rossiter, S.J. (2017). Comparative genomics  
010 reveals contraction in olfactory receptor genes in bats. *Sci. Rep.* 7, 259.  
011 <https://doi.org/10.1038/s41598-017-00132-9>.
- 012 159. Gutiérrez-Guerrero, Y.T., Ibarra-Laclette, E., Martínez Del Río, C., Barrera-Redondo, J., Rebollar,  
013 E.A., Ortega, J., León-Paniagua, L., Urrutia, A., Aguirre-Planter, E., and Eguiarte, L.E. (2020).  
014 Genomic consequences of dietary diversification and parallel evolution due to nectarivory in leaf-  
015 nosed bats. *Gigascience* 9. <https://doi.org/10.1093/gigascience/giaa059>.
- 016 160. Xie, S.S., Huang, C.H., Reid, M.E., Blancher, A., and Blumenfeld, O.O. (1997). The glycophorin A  
017 gene family in gorillas: structure, expression, and comparison with the human and chimpanzee  
018 homologues. *Biochem. Genet.* 35, 59–76. <https://doi.org/10.1023/a:1022212630370>.
- 019 161. Gustavsson, E.K., Sethi, S., Gao, Y., Brenton, J.W., García-Ruiz, S., Zhang, D., Garza, R.,  
020 Reynolds, R.H., Evans, J.R., Chen, Z., et al. (2024). The annotation of GBA1 has been concealed  
021 by its protein-coding pseudogene GBAP1. *Sci. Adv.* 10, eadk1296.  
022 <https://doi.org/10.1126/sciadv.adk1296>.
- 023 162. O’Shea, T.J., Cryan, P.M., Cunningham, A.A., Fooks, A.R., Hayman, D.T.S., Luis, A.D., Peel, A.J.,  
024 Plowright, R.K., and Wood, J.L.N. (2014). Bat flight and zoonotic viruses. *Emerg. Infect. Dis.* 20,  
025 741–745. <https://doi.org/10.3201/eid2005.130539>.
- 026 163. Levesque, D.L., Boyles, J.G., Downs, C.J., and Breit, A.M. (2021). High Body Temperature is an  
027 Unlikely Cause of High Viral Tolerance in Bats. *J. Wildl. Dis.* 57, 238–241.  
028 <https://doi.org/10.7589/JWD-D-20-00079>.
- 029 164. Kirkwood, T.B.L. (2017). The disposable soma theory. The evolution of senescence in the tree of  
030 life, 23–39.
- 031 165. Toshkova, N., Zhelyzkova, V., Reyes-Ruiz, A., Haerens, E., de Castro Deus, M., Lacombe, R.V.,  
032 Lecerf, M., Gonzalez, G., Jouvenet, N., Planchais, C., et al. (2024). Temperature sensitivity of bat  
033 antibodies links metabolic state of bats with antigen-recognition diversity. *Nat. Commun.* 15, 5878.  
034 <https://doi.org/10.1038/s41467-024-50316-x>.
- 035 166. Mandl, J.N., Schneider, C., Schneider, D.S., and Baker, M.L. (2018). Going to bat(s) for studies of  
036 disease tolerance. *Front. Immunol.* 9, 2112. <https://doi.org/10.3389/fimmu.2018.02112>.
- 037 167. Pei, G., Balkema-Buschmann, A., and Dorhoi, A. (2024). Disease tolerance as immune defense  
038 strategy in bats: One size fits all? *PLoS Pathog.* 20, e1012471.  
039 <https://doi.org/10.1371/journal.ppat.1012471>.
- 040 168. Vermillion, K.L., Anderson, K.J., Hampton, M., and Andrews, M.T. (2015). Gene expression  
041 changes controlling distinct adaptations in the heart and skeletal muscle of a hibernating mammal.  
042 *Physiol. Genomics* 47, 58–74. <https://doi.org/10.1152/physiolgenomics.00108.2014>.
- 043 169. Lam, B., Kajderowicz, K.M., Keys, H.R., Roessler, J.M., Frenkel, E.M., Kirkland, A., Bisht, P., El-  
044 Brolosy, M.A., Jaenisch, R., Bell, G.W., et al. (2024). Multi-species genome-wide CRISPR screens  
045 identify GPX4 as a conserved suppressor of cold-induced cell death. *bioRxiv.org*,  
046 2024.07.25.605098. <https://doi.org/10.1101/2024.07.25.605098>.
- 047 170. Sone, M., and Yamaguchi, Y. (2024). Cold resistance of mammalian hibernators ~ a matter of  
048 ferroptosis? *Front. Physiol.* 15, 1377986. <https://doi.org/10.3389/fphys.2024.1377986>.
- 049 171. Kaelber, J.T., Demogines, A., Harbison, C.E., Allison, A.B., Goodman, L.B., Ortega, A.N., Sawyer,

- 050 S.L., and Parrish, C.R. (2012). Evolutionary reconstructions of the transferrin receptor of Caniforms  
051 supports canine parvovirus being a re-emerged and not a novel pathogen in dogs. *PLoS Pathog.*  
052 *8*, e1002666. <https://doi.org/10.1371/journal.ppat.1002666>.
- 053 172. Demogines, A., Abraham, J., Choe, H., Farzan, M., and Sawyer, S.L. (2013). Dual host-virus arms  
054 races shape an essential housekeeping protein. *PLoS Biol.* *11*, e1001571.  
055 <https://doi.org/10.1371/journal.pbio.1001571>.
- 056 173. Kerr, S.A., Jackson, E.L., Lungu, O.I., Meyer, A.G., Demogines, A., Ellington, A.D., Georgiou, G.,  
057 Wilke, C.O., and Sawyer, S.L. (2015). Computational and functional analysis of the virus-receptor  
058 interface reveals host range trade-offs in New World arenaviruses. *J. Virol.* *89*, 11643–11653.  
059 <https://doi.org/10.1128/JVI.01408-15>.
- 060 174. Kaur, H., Kalayjian, R., Wu, K., Tassiopoulos, K., Palella, F., Taiwo, B., Bush, W., Hileman, C.,  
061 Bedimo, R., Koletar, S., et al. (2022). Associations of L-Ferritin and Tim-1 with frailty measures in  
062 people with HIV: a cross-sectional and longitudinal study. *Lancet Healthy Longev.* *3*, S5.  
063 [https://doi.org/10.1016/s2666-7568\(22\)00066-6](https://doi.org/10.1016/s2666-7568(22)00066-6).
- 064 175. Kim, J., Jo, Y., Cho, D., and Ryu, D. (2022). L-threonine promotes healthspan by expediting  
065 ferritin-dependent ferroptosis inhibition in *C. elegans*. *Nat. Commun.* *13*, 6554.  
066 <https://doi.org/10.1038/s41467-022-34265-x>.
- 067 176. Daghlas, I., and Gill, D. (2021). Genetically predicted iron status and life expectancy. *Clin. Nutr.* *40*,  
068 2456–2459. <https://doi.org/10.1016/j.clnu.2020.06.025>.
- 069 177. Perez, K., Ciotlos, S., McGirr, J., Limbad, C., Doi, R., Nederveen, J.P., Nilsson, M.I., Winer, D.A.,  
070 Evans, W., Tarnopolsky, M., et al. (2022). Single nuclei profiling identifies cell specific markers of  
071 skeletal muscle aging, frailty, and senescence. *Aging (Albany NY)* *14*, 9393–9422.  
072 <https://doi.org/10.18632/aging.204435>.
- 073 178. Trifunovic, A., Wredenberg, A., Falkenberg, M., Spelbrink, J.N., Rovio, A.T., Bruder, C.E.,  
074 Bohlooly-Y, M., Gidlöf, S., Oldfors, A., Wibom, R., et al. (2004). Premature ageing in mice  
075 expressing defective mitochondrial DNA polymerase. *Nature* *429*, 417–423.  
076 <https://doi.org/10.1038/nature02517>.
- 077 179. Van Goethem, G., Dermaut, B., Löfgren, A., Martin, J.J., and Van Broeckhoven, C. (2001).  
078 Mutation of POLG is associated with progressive external ophthalmoplegia characterized by  
079 mtDNA deletions. *Nat. Genet.* *28*, 211–212. <https://doi.org/10.1038/90034>.
- 080 180. Cao, L., Li, W., Kim, S., Brodie, S.G., and Deng, C.-X. (2003). Senescence, aging, and malignant  
081 transformation mediated by p53 in mice lacking the Brca1 full-length isoform. *Genes Dev.* *17*, 201–  
082 213. <https://doi.org/10.1101/gad.1050003>.
- 083 181. Vijg, J., Perls, T., Franceschi, C., and van Orsouw, N.J. (2001). BRCA1 gene sequence variation in  
084 centenarians. *Ann. N. Y. Acad. Sci.* *928*, 85–96. <https://doi.org/10.1111/j.1749-6632.2001.tb05639.x>.
- 086 182. Fearon, E.R. (1997). Human cancer syndromes: clues to the origin and nature of cancer. *Science*  
087 *278*, 1043–1050. <https://doi.org/10.1126/science.278.5340.1043>.
- 088 183. Donoho, G., Brenneman, M.A., Cui, T.X., Donoviel, D., Vogel, H., Goodwin, E.H., Chen, D.J., and  
089 Hastay, P. (2003). Deletion of Brca2 exon 27 causes hypersensitivity to DNA crosslinks,  
090 chromosomal instability, and reduced life span in mice. *Genes Chromosomes Cancer* *36*, 317–  
091 331. <https://doi.org/10.1002/gcc.10148>.

- 092 184. Wooster, R., Bignell, G., Lancaster, J., Swift, S., Seal, S., Mangion, J., Collins, N., Gregory, S.,  
093 Gumbs, C., and Micklem, G. (1995). Identification of the breast cancer susceptibility gene BRCA2.  
094 *Nature* 378, 789–792. <https://doi.org/10.1038/378789a0>.
- 095 185. Ray, D.A., Feschotte, C., Pagan, H.J.T., Smith, J.D., Pritham, E.J., Arensburger, P., Atkinson,  
096 P.W., and Craig, N.L. (2008). Multiple Waves of Recent DNA Transposon Activity in the Bat,  
097 *Myotis Lucifugus*. *Genome Res.* 18, 717–728. <https://doi.org/10.1101/gr.071886.107>.
- 098 186. Sotgia, S., Zinellu, A., Mangoni, A.A., Serra, R., Pintus, G., Caruso, C., Deiana, L., and Carru, C.  
099 (2017). Cellular immune activation in Sardinian middle-aged, older adults and centenarians. *Exp.*  
100 *Gerontol.* 99, 133–137. <https://doi.org/10.1016/j.exger.2017.10.005>.
- 101 187. Lee, K.-A., Flores, R.R., Jang, I.H., Saathoff, A., and Robbins, P.D. (2022). Immune senescence,  
102 immunosenescence and aging. *Front. Aging* 3, 900028. <https://doi.org/10.3389/fragi.2022.900028>.
- 103 188. Yousefzadeh, M.J., Flores, R.R., Zhu, Y., Schmiechen, Z.C., Brooks, R.W., Trussoni, C.E., Cui, Y.,  
104 Angelini, L., Lee, K.-A., McGowan, S.J., et al. (2021). An aged immune system drives senescence  
105 and ageing of solid organs. *Nature* 594, 100–105. <https://doi.org/10.1038/s41586-021-03547-7>.
- 106 189. Lee, C.-S., Chang, C.-H., Chen, C.-Y., Shih, C.-Y., Peng, J.-K., Huang, H.-L., Chen, P.-Y., Huang,  
107 T.-L., Chen, C.-Y., and Tsai, J.-S. (2022). Upregulation of cluster of differentiation 36 mRNA  
108 expression in peripheral blood mononuclear cells correlates with frailty severity in older adults. *J.*  
109 *Cachexia Sarcopenia Muscle* 13, 1948–1955. <https://doi.org/10.1002/jcsm.13003>.
- 110 190. Kimmel, J.C., Yi, N., Roy, M., Hendrickson, D.G., and Kelley, D.R. (2021). Differentiation reveals  
111 latent features of aging and an energy barrier in murine myogenesis. *Cell Rep.* 35, 109046.  
112 <https://doi.org/10.1016/j.celrep.2021.109046>.
- 113 191. Tian, Y., Lu, J., Hao, X., Li, H., Zhang, G., Liu, X., Li, X., Zhao, C., Kuang, W., Chen, D., et al.  
114 (2020). FTH1 inhibits ferroptosis through ferritinophagy in the 6-OHDA model of Parkinson's  
115 disease. *Neurotherapeutics* 17, 1796–1812. <https://doi.org/10.1007/s13311-020-00929-z>.
- 116 192. Jonathan Sleeman, Center Director, USGS National Wildlife Health Center (2020). NWHC  
117 Operations During the COVID-19 Pandemic and Information About Coronaviruses in Wildlife.
- 118 193. White-Nose Syndrome Disease Management Working Group National White-Nose Syndrome  
119 Decontamination Protocol.
- 120 194. Dudchenko, O., Batra, S.S., Omer, A.D., Nyquist, S.K., Hoeger, M., Durand, N.C., Shamim, M.S.,  
121 Machol, I., Lander, E.S., Aiden, A.P., et al. (2017). De novo assembly of the *Aedes aegypti*  
122 genome using Hi-C yields chromosome-length scaffolds. *Science* 356, 92–95.  
123 <https://doi.org/10.1126/science.aal3327>.
- 124 195. Lindblad-Toh, K., Garber, M., Zuk, O., Lin, M.F., Parker, B.J., Washietl, S., Kheradpour, P., Ernst,  
125 J., Jordan, G., Mauceli, E., et al. (2011). A high-resolution map of human evolutionary constraint  
126 using 29 mammals. *Nature* 478, 476–482. <https://doi.org/10.1038/nature10530>.
- 127 196. Bolger, A.M., Lohse, M., and Usadel, B. (2014). Trimmomatic: a flexible trimmer for Illumina  
128 sequence data. *Bioinformatics* 30, 2114–2120. <https://doi.org/10.1093/bioinformatics/btu170>.
- 129 197. Cheng, H., Concepcion, G.T., Feng, X., Zhang, H., and Li, H. (2021). Haplotype-resolved de novo  
130 assembly using phased assembly graphs with hifiasm. *Nat. Methods* 18, 170–175.  
131 <https://doi.org/10.1038/s41592-020-01056-5>.



- 132 198. Cheng, H., Jarvis, E.D., Fedrigo, O., Koepfli, K.-P., Urban, L., Gemmell, N.J., and Li, H. (2022).  
133 Haplotype-resolved assembly of diploid genomes without parental data. *Nat. Biotechnol.* *40*, 1332–  
134 1335. <https://doi.org/10.1038/s41587-022-01261-x>.
- 135 199. Zhou, C., McCarthy, S.A., and Durbin, R. (2023). YaHS: yet another Hi-C scaffolding tool.  
136 *Bioinformatics* *39*. <https://doi.org/10.1093/bioinformatics/btac808>.
- 137 200. Li, H., and Durbin, R. (2009). Fast and accurate short read alignment with Burrows-Wheeler  
138 transform. *Bioinformatics* *25*, 1754–1760. <https://doi.org/10.1093/bioinformatics/btp324>.
- 139 201. Li, H., and Durbin, R. (2010). Fast and accurate long-read alignment with Burrows-Wheeler  
140 transform. *Bioinformatics* *26*, 589–595. <https://doi.org/10.1093/bioinformatics/btp698>.
- 141 202. Open2C, Abdennur, N., Fudenberg, G., Flyamer, I.M., Galitsyna, A.A., Goloborodko, A., Imakaev,  
142 M., and Venev, S.V. (2024). Pairtools: From sequencing data to chromosome contacts. *PLoS*  
143 *Comput. Biol.* *20*, e1012164. <https://doi.org/10.1371/journal.pcbi.1012164>.
- 144 203. Danecek, P., Bonfield, J.K., Liddle, J., Marshall, J., Ohan, V., Pollard, M.O., Whitwham, A., Keane,  
145 T., McCarthy, S.A., Davies, R.M., et al. (2021). Twelve years of SAMtools and BCFtools.  
146 *Gigascience* *10*. <https://doi.org/10.1093/gigascience/giab008>.
- 147 204. Harry, E. (2022). PretextView (Paired REad TEXTure Viewer): A desktop application for viewing  
148 pretext contact maps.
- 149 205. Rapid curation GitLab. <https://gitlab.com/wtsi-grit/rapid-curation>.
- 150 206. Uliano-Silva, M., Ferreira, J.G.R.N., Krasheninnikova, K., Darwin Tree of Life Consortium,  
151 Formenti, G., Abueg, L., Torrance, J., Myers, E.W., Durbin, R., Blaxter, M., et al. (2023). MitoHiFi:  
152 a python pipeline for mitochondrial genome assembly from PacBio high fidelity reads. *BMC*  
153 *Bioinformatics* *24*, 288. <https://doi.org/10.1186/s12859-023-05385-y>.
- 154 207. Palmer, J.M., and Stajich, J.E. (2023). funannotate: Eukaryotic Genome Annotation Pipeline  
155 (Github).
- 156 208. Smit, A.F.A., Hubley, R., and Green, P. (2015). RepeatMasker Open-4.0. 2013--2015. Preprint at  
157 Seattle, USA.
- 158 209. Zoonomia Consortium (2020). A comparative genomics multitool for scientific discovery and  
159 conservation. *Nature* *587*, 240–245. <https://doi.org/10.1038/s41586-020-2876-6>.
- 160 210. Flynn, J.M., Hubley, R., Goubert, C., Rosen, J., Clark, A.G., Feschotte, C., and Smit, A.F. (2020).  
161 RepeatModeler2 for automated genomic discovery of transposable element families. *Proc. Natl.*  
162 *Acad. Sci. U. S. A.* *117*, 9451–9457. <https://doi.org/10.1073/pnas.1921046117>.
- 163 211. Išerić, H., Alkan, C., Hach, F., and Numanagić, I. (2022). Fast characterization of segmental  
164 duplication structure in multiple genome assemblies. *Algorithms Mol. Biol.*
- 165 212. Brown, M., González De la Rosa, P.M., and Mark, B. (2023). A Telomere Identification Toolkit  
166 <https://doi.org/10.5281/zenodo.10091385>.
- 167 213. Li, H. (2021). New strategies to improve minimap2 alignment accuracy. *Bioinformatics*.
- 168 214. Goel, M., and Schneeberger, K. (2022). plotsr: visualizing structural similarities and  
169 rearrangements between multiple genomes. *Bioinformatics* *38*, 2922–2926.  
170 <https://doi.org/10.1093/bioinformatics/btac196>.

- 171 215. Palmer, J.M., and Stajich, J. (2020). Funannotate v1.8.1: Eukaryotic genome annotation (Zenodo)  
172 <https://doi.org/10.5281/ZENODO.4054262>.
- 173 216. Leinonen, R., Diez, F.G., Binns, D., Fleischmann, W., Lopez, R., and Apweiler, R. (2004). UniProt  
174 archive. *Bioinformatics* 20, 3236–3237. <https://doi.org/10.1093/bioinformatics/bth191>.
- 175 217. Haas, B.J., Papanicolaou, A., Yassour, M., Grabherr, M., Blood, P.D., Bowden, J., and Others  
176 (2013). De novo transcript sequence reconstruction from RNA Seq: reference generation and  
177 analysis with Trinity. *Nat Protol.* 2013; 8 (8): 1494--512. Preprint.
- 178 218. Korf, I. (2004). Gene finding in novel genomes. *BMC Bioinformatics* 5, 59.  
179 <https://doi.org/10.1186/1471-2105-5-59>.
- 180 219. Majoros, W.H., Pertea, M., and Salzberg, S.L. (2004). TigrScan and GlimmerHMM: two open  
181 source ab initio eukaryotic gene-finders. *Bioinformatics* 20, 2878–2879.  
182 <https://doi.org/10.1093/bioinformatics/bth315>.
- 183 220. Stanke, M., Keller, O., Gunduz, I., Hayes, A., Waack, S., and Morgenstern, B. (2006).  
184 AUGUSTUS: ab initio prediction of alternative transcripts. *Nucleic Acids Res.* 34, W435–W439.  
185 <https://doi.org/10.1093/nar/gkl200>.
- 186 221. Haas, B.J., Salzberg, S.L., Zhu, W., Pertea, M., and Allen, J.E. (2008). Automated eukaryotic gene  
187 structure annotation using EVIDENCEModeler and the Program to Assemble Spliced Alignments.  
188 *Genome Biol.*
- 189 222. Quintaje, S.B., and Orchard, S. (2008). The annotation of both human and mouse kinomes in  
190 UniProtKB/Swiss-Prot: one small step in manual annotation, one giant leap for full comprehension  
191 of genomes. *Mol. Cell. Proteomics.*
- 192 223. Buchfink, B., Reuter, K., and Drost, H.-G. (2021). Sensitive protein alignments at tree-of-life scale  
193 using DIAMOND. *Nat. Methods* 18, 366–368. <https://doi.org/10.1038/s41592-021-01101-x>.
- 194 224. Emms, D.M., and Kelly, S. (2019). OrthoFinder: phylogenetic orthology inference for comparative  
195 genomics. *Genome Biol.* 20, 238. <https://doi.org/10.1186/s13059-019-1832-y>.
- 196 225. Ranwez, V., Douzery, E.J.P., Cambon, C., Chantret, N., and Delsuc, F. (2018). MACSE v2: Toolkit  
197 for the Alignment of Coding Sequences Accounting for Frameshifts and Stop Codons. *Mol. Biol.*  
198 *Evol.* 35, 2582–2584. <https://doi.org/10.1093/molbev/msy159>.
- 199 226. Whelan, S., Irisarri, I., and Burki, F. (2018). PREQUAL: detecting non-homologous characters in  
200 sets of unaligned homologous sequences. *Bioinformatics* 34, 3929–3930.  
201 <https://doi.org/10.1093/bioinformatics/bty448>.
- 202 227. Bowman, J., Silva, N., Schüefftan, E., Almeida, J.M., Brattig-Correia, R., Oliveira, R.A.,  
203 Tüttelmann, F., Enard, D., Navarro-Costa, P., and Lynch, V.J. (2023). Pervasive relaxed selection  
204 on spermatogenesis genes coincident with the evolution of polygyny in gorillas. *bioRxiv*,  
205 2023.10.27.564379. <https://doi.org/10.1101/2023.10.27.564379>.
- 206 228. Scornavacca, C., Belkhir, K., Lopez, J., Dernas, R., Delsuc, F., Douzery, E.J.P., and Ranwez, V.  
207 (2019). OrthoMaM v10: Scaling-Up Orthologous Coding Sequence and Exon Alignments with More  
208 than One Hundred Mammalian Genomes. *Mol. Biol. Evol.* 36, 861–862.  
209 <https://doi.org/10.1093/molbev/msz015>.
- 210 229. Cunningham, F., Allen, J.E., Allen, J., Alvarez-Jarreta, J., Amode, M.R., Armean, I.M., Austine-

- 211 Orimoloye, O., Azov, A.G., Barnes, I., Bennett, R., et al. (2022). Ensembl 2022. *Nucleic Acids Res.*  
212 50, D988–D995. <https://doi.org/10.1093/nar/gkab1049>.
- 213 230. Minh, B.Q., Schmidt, H.A., Chernomor, O., Schrempf, D., Woodhams, M.D., von Haeseler, A., and  
214 Lanfear, R. (2020). IQ-TREE 2: New Models and Efficient Methods for Phylogenetic Inference in  
215 the Genomic Era. *Mol. Biol. Evol.* 37, 1530–1534. <https://doi.org/10.1093/molbev/msaa015>.
- 216 231. Dos Reis, M., and Yang, Z. (2019). Bayesian Molecular Clock Dating Using Genome-Scale  
217 Datasets. *Methods Mol. Biol.* 1910, 309–330. [https://doi.org/10.1007/978-1-4939-9074-0\\_10](https://doi.org/10.1007/978-1-4939-9074-0_10).
- 218 232. Phillips, M.J. (2016). Geomolecular dating and the origin of placental mammals. *Syst. Biol.* 65,  
219 546–557. <https://doi.org/10.1093/sysbio/syv115>.
- 220 233. Gunnell, G.F., and Simmons, N.B. (2005). Fossil evidence and the origin of bats. *J. Mamm. Evol.*  
221 12, 209–246. <https://doi.org/10.1007/s10914-005-6945-2>.
- 222 234. Eiting, T.P., and Gunnell, G.F. (2009). Global Completeness of the Bat Fossil Record. *J. Mamm.*  
223 *Evol.* 16, 151–173. <https://doi.org/10.1007/s10914-009-9118-x>.
- 224 235. Storch, G., Sigé, B., and Habersetzer, J. (2002). *Tachypteron franzeni* n. gen., n. sp., earliest  
225 emballonurid bat from the Middle Eocene of Messel (Mammalia, Chiroptera). *Palaontol. Z.* 76,  
226 189–199. <https://doi.org/10.1007/bf02989856>.
- 227 236. Ravel, A., Marivaux, L., Tabuce, R., Ben Haj Ali, M., Essid, E.L.M., and Vianey-Liaud, M. (2012). A  
228 new large philisid (Mammalia, Chiroptera, Vespertilionoidea) from the late Early Eocene of  
229 Chambi, Tunisia: LARGE BAT FROM CHAMBI. *Palaeontology* 55, 1035–1041.  
230 <https://doi.org/10.1111/j.1475-4983.2012.01160.x>.
- 231 237. Lim, B.K. (2009). Review of the origins and biogeography of bats in South America. *Chiroptera*  
232 *Neotropical* 15, 391–410.
- 233 238. Morgan, G.S., and Czaplewski, N.J. (2003). A New Bat (Chiroptera: Natalidae) from the Early  
234 Miocene of Florida, with Comments on Natalid Phylogeny. *J Mammal* 84, 729–752.  
235 [https://doi.org/10.1644/1545-1542\(2003\)084<0729:ANBCNF>2.0.CO;2](https://doi.org/10.1644/1545-1542(2003)084<0729:ANBCNF>2.0.CO;2).
- 236 239. Foley, N.M., Mason, V.C., Harris, A.J., Bredemeyer, K.R., Damas, J., Lewin, H.A., Eizirik, E.,  
237 Gatesy, J., Karlsson, E.K., Lindblad-Toh, K., et al. (2023). A genomic timescale for placental  
238 mammal evolution. *Science* 380, eabl8189. <https://doi.org/10.1126/science.abl8189>.
- 239 240. Elliot, M.G., and Mooers, A.Ø. (2014). Inferring ancestral states without assuming neutrality or  
240 gradualism using a stable model of continuous character evolution. *BMC Evol. Biol.* 14, 226.  
241 <https://doi.org/10.1186/s12862-014-0226-8>.
- 242 241. Kosakovsky Pond, S.L., Poon, A.F.Y., Velazquez, R., Weaver, S., Hepler, N.L., Murrell, B., Shank,  
243 S.D., Magalis, B.R., Bouvier, D., Nekrutenko, A., et al. (2020). HyPhy 2.5-A customizable platform  
244 for evolutionary hypothesis testing using PHYlogenies. *Mol. Biol. Evol.* 37, 295–299.  
245 <https://doi.org/10.1093/molbev/msz197>.
- 246 242. Lucaci, A.G., Zehr, J.D., Enard, D., Thornton, J.W., and Kosakovsky Pond, S.L. (2023).  
247 Evolutionary Shortcuts via Multinucleotide Substitutions and Their Impact on Natural Selection  
248 Analyses. *Mol. Biol. Evol.* 40. <https://doi.org/10.1093/molbev/msad150>.
- 249 243. Wu, N., Nguyen, X.-N., Wang, L., Appourchaux, R., Zhang, C., Panthu, B., Gruffat, H., Journo, C.,  
250 Alais, S., Qin, J., et al. (2019). The interferon stimulated gene 20 protein (ISG20) is an innate

- 251 defense antiviral factor that discriminates self versus non-self translation. *PLoS Pathog.* 15.  
252 <https://doi.org/10.1371/journal.ppat.1008093>.
- 253 244. GTEX Consortium (2020). The GTEX Consortium atlas of genetic regulatory effects across human  
254 tissues. *Science* 369, 1318–1330. <https://doi.org/10.1126/science.aaz1776>.
- 255 245. Luisi, P., Alvarez-Ponce, D., Pybus, M., Fares, M.A., Bertranpetit, J., and Laayouni, H. (2015).  
256 Recent positive selection has acted on genes encoding proteins with more interactions within the  
257 whole human interactome. *Genome Biol. Evol.* 7, 1141–1154. <https://doi.org/10.1093/gbe/evv055>.
- 258 246. Gene Ontology Consortium (2021). The Gene Ontology resource: enriching a GOld mine. *Nucleic  
259 Acids Res.* 49, D325–D334. <https://doi.org/10.1093/nar/gkaa1113>.
- 260 247. Eisenberg, E., and Levanon, E.Y. (2013). Human housekeeping genes, revisited. *Trends Genet.*  
261 29, 569–574. <https://doi.org/10.1016/j.tig.2013.05.010>.
- 262 248. Kosakovsky Pond, S.L., Murrell, B., Fourment, M., Frost, S.D.W., Delpont, W., and Scheffler, K.  
263 (2011). A random effects branch-site model for detecting episodic diversifying selection. *Mol. Biol.  
264 Evol.* 28, 3033–3043. <https://doi.org/10.1093/molbev/msr125>.
- 265 249. Quinlan, A.R. (2014). BEDTools: The Swiss-Army Tool for Genome Feature Analysis. *Curr. Protoc.  
266 Bioinformatics* 47, 11.12.1–34. <https://doi.org/10.1002/0471250953.bi1112s47>.
- 267 250. Dainat, J. AGAT: Another Gff Analysis Toolkit to handle annotations in any GTF/GFF format  
268 <https://doi.org/10.5281/zenodo.3552717>.
- 269 251. Legrand, A., Dahoui, C., De La Myre Mory, C., Noy, K., Guiguettaz, L., Versapuech, M., Loyer, C.,  
270 Pillon, M., Wcislo, M., Guéguen, L., et al. (2024). SAMD9L acts as an antiviral factor against HIV-1  
271 and primate lentiviruses by restricting viral and cellular translation. *PLoS Biol.* 22, e3002696.  
272 <https://doi.org/10.1371/journal.pbio.3002696>.
- 273 252. Gene Ontology Consortium, Aleksander, S.A., Balhoff, J., Carbon, S., Cherry, J.M., Drabkin, H.J.,  
274 Ebert, D., Feuermann, M., Gaudet, P., Harris, N.L., et al. (2023). The Gene Ontology  
275 knowledgebase in 2023. *Genetics* 224, iyad031. <https://doi.org/10.1093/genetics/iyad031>.
- 276 253. Ashburner, M., Ball, C.A., Blake, J.A., Botstein, D., Butler, H., Cherry, J.M., Davis, A.P., Dolinski,  
277 K., Dwight, S.S., Eppig, J.T., et al. (2000). Gene ontology: tool for the unification of biology. The  
278 Gene Ontology Consortium. *Nat. Genet.* 25, 25–29. <https://doi.org/10.1038/75556>.
- 279 254. Kanehisa, M., and Goto, S. (2000). KEGG: kyoto encyclopedia of genes and genomes. *Nucleic  
280 Acids Res.* 28, 27–30. <https://doi.org/10.1093/nar/28.1.27>.
- 281 255. Kowalczyk, A., Partha, R., Clark, N.L., and Chikina, M. (2020). Pan-mammalian analysis of  
282 molecular constraints underlying extended lifespan. *Elife* 9. <https://doi.org/10.7554/eLife.51089>.

## 283 Materials and Methods

### 284 Data availability

285 All sequencing data and genomes generated in this study are available on NCBI under Bioprojects  
286 PRJNA973719 and PRJNA1035541. Annotations generated in this study are available at



287 <https://github.com/docmanny/myotis-gene-annotations>. All other code is available at  
288 <https://github.com/sudmantlab/MyotisGenomeAssembly>.

## 289 Sample collection and cell line derivation

290 All bats sampled for this study were wild caught under scientific collection permits for California and  
291 Arizona (see Supplemental Table 1). Bats were sampled using standard mist-netting procedures, including  
292 taking standard body measurements, following USGS recommendations for White-Nose Syndrome and COVID-  
293 19 prevention<sup>192,193</sup>.

294 For *M. lucifugus*, the donor individual was field-caught in California and transported to the Genetics  
295 Laboratory of the California Department of Fish and Wildlife, where they were euthanized via isoflurane. The  
296 *M. velifer* individual was caught in Arizona and euthanized in the field via isoflurane. For both *M. lucifugus* and  
297 *M. velifer*, tissues were collected and preserved via flash-freezing in liquid nitrogen.

298 For *M. volans*, *M. occultus*, *M. auriculus*, and *M. californicus*, two 3-mm wing punch biopsies were taken  
299 from the left and right plagiopatagium of each donor individual and placed in a live cell collection media consisting  
300 of DMEM/F12 (Gibco) supplemented with 15mM HEPES (Gibco), 20% FBS (Gibco), and 0.2% Primocin  
301 (Invivogen) [yohe2019; curty2023; capel2023]. Wing punches were then brought back to a cell culture  
302 facility in Berkeley, where they were used to generate cell lines as previously described[yohe2019;  
303 curty2023; capel2023]. Additional cell lines for *M. lucifugus*, *M. velifer*, *M. yumanensis*, *M. evotis*, and *M.*  
304 *thysanodes* were similarly collected and generated.

305 Cell lines for the *M. evotis* and *M. thysanodes* genomes were generously provided by Richard Miller. Cell  
306 lines for functional work in *Rousettus langosus*, *Pteropus rodrigenis*, and *Eidolon helvum* were provided by the  
307 San Diego Frozen Zoo.

## 308 Sequencing and assembly

309 For 6 genomes (*M. evotis*, *M. thysanodes*, *M. volans*, *M. occultus*, *M. auriculus*, and *M. californicus*) DNA  
310 was extracted from primary cell lines expanded from 3M cells at Passage 2-4 to approximately 40M cells per  
311 line using a Circulomics BigDNA CCB kit following the UHMW protocol for cells. DNA from *M. lucifugus* was  
312 extracted from flash-frozen tissue by the Genetics Lab of the California Department of Fish and Wildlife. PacBio  
313 HiFi libraries were generated and sequenced on a Sequel II (PacBio) by the Functional Genomics Core at the  
314 University of California, Berkeley. For cell-line-derived genomes, Hi-C libraries for these genomes were  
315 generated from 1M cells at Passage 3 using the OmniC for Illumina kit (Dovetail genomics); libraries were  
316 submitted for quality control and sequencing on the Illumina NovaSeq platform (Novogene). For the *M. velifer*  
317 genomes, DNA was extracted from flash-frozen tissues, and all DNA extraction, library prep, and sequencing  
318 was completed by Dovetail Genomics following standard protocols. For *M. lucifugus*, a previously published Hi-  
319 C dataset from 4 pooled individuals was used for scaffolding<sup>194,195</sup>.

320 The PacBio reads were processed using SMRTTools (v6.0.0-1, PacBio) to generate the circular  
321 consensus sequences using the settings --minPasses=3 --minRQ=0.99. Hi-C reads were processed using  
322 trimmomatic<sup>196</sup> (v0.35-6) to remove adapter sequences and low-quality bases using the settings  
323 ILLUMINACLIP:data/trimmomatic-adapters/TruSeq3-PE-2.fa:2:40:15 SLIDINGWINDOW:5:20. To generate the  
324 primary contig assemblies, we used hifiasm<sup>197,198</sup> (v0.14-hd174df1\_0) in Hi-C mode, providing both the CCS

reads and the trimmed Hi-C reads as input, and purging duplicates using the -l2 option. For our reference genomes, we proceeded with the primary contig assembly (\*.asm.hic.p\_ctg.gfa).

All reference genomes were scaffolded with YAHS<sup>199</sup> (v1.1a.1s) and the Hi-C datasets. Dovetail Omni-C data were processed and mapped to the genome following the manufacturer's instructions using bwa<sup>200,201</sup> (v0.7.17-h5bf99c6\_8), pairtools<sup>202</sup> (v0.3.0-py37hb9c2fc3\_5), and samtools<sup>203</sup> (v1.12-h9aed4be\_1). YAHS was run using both default settings as well as with --no-contig-ec; after comparing the outputs, we proceeded with the --no-contig-ec version for our final assemblies.

To finalize the assemblies, we performed manual curation using PreTextView<sup>204</sup> and the Rapid Curation toolkit<sup>205</sup> (version ff964069). The X chromosomes were identified based on size, synteny across genomes, and half-coverage observed in XY genomes; putative Y chromosomes were similarly identified in XY genomes. Mitochondrial genomes were identified and removed from the final assembly by running mitohifi<sup>206</sup> (v3.0) in contig mode on the assembly and removing all scaffolds identified as mitogenomes. The consensus mitogenome from mitohifi was designated as the representative mitogenome for the assembly after manual curation. Finally, to eliminate spurious duplicates, we used FunAnnotate<sup>207</sup> (v1.8.15) and the “clean” function to identify and remove any remaining scaffolds with 90% identical to a larger scaffold.

## Identification and annotation of repetitive elements

We used RepeatMasker<sup>208</sup> (version 4.0.7-open) to annotate repetitive elements in our genomes. We first ran RepeatMasker using a curated database of transposable elements from 249 mammalian species<sup>36,209</sup> (David Ray, pers. comm.) and the settings “-engine ncbi -s -noisy -xsmall” followed by a second run using RepeatModeler<sup>210</sup> and RepeatMasker to identify *de novo* repeats missing from the curated database. All repeats were then soft-masked in all genomes. To assess the repeat landscape, we calculated the summary of divergence from the repeat alignments and created the repeat landscape using auxiliary RepeatMasker scripts (calcDivergenceFromAlign.pl & createRepeatLandscape.pl).

## Structural variation

To understand the distribution of structural variants, including segmental duplication events, we used SyRI (Synteny and Rearrangement Identifier<sup>128</sup>) and BISER (Brisk Inference of Segmental duplication Evolutionary stRucture<sup>211</sup>). We first masked telomere regions using TIDK (Telomere Identification toolKit<sup>212</sup>), and mapped the primary 22 scaffolds of the nearctic *Myotis* genomes to each other with minimap2<sup>213</sup>. The scaffold corresponding to the X chromosome was omitted because there is no corresponding scaffold in the *M. yumanensis* assembly. To verify homologous chromosomes and fix strand orientation, we used *fixchr* from the SyRI package and manually renamed scaffolds accordingly, then re-mapped with minimap2. We ran SyRI on the resulting files and plotted the results with plotsr<sup>214</sup>. We ran BISER on the primary 22 scaffolds of the nearctic *Myotis* genomes with -keep-contigs and default settings to generate bed files with the inferred segmental duplication regions.

## RNA-seq

To assist our annotation efforts, we generated mRNA-seq for 7 of the species sequenced *de novo* in this study. For *M. velifer*, samples of heart, brain, kidneys, lungs, pancreas, and testis collected from the donor individual were provided to Dovetail Genomics (CA, USA) for mRNA-seq library preparation and sequencing. Using the same cell lines used for the genomes of *M. occultus*, *M. thysanodes*, *M. evotis*, *M. volans*, *M. auriculus*, and *M. californicus*, we generated rRNA-depleted total RNA-seq libraries using the NEBNext rRNA Depletion Kit v2 and Ultra II Directional RNA Library Prep Kits. RNA and libraries were quality controlled on an Agilent Bioanalyzer using the RNA 6000 Nano and DNA High Sensitivity assays, respectively. Samples were sequenced on to 100M 150PE reads per sample using the Novoseq platform (Novogene). For *M. lucifugus*, we used the following published RNA-seq data on NCBI SRA generated using poly-A selection and paired-end sequencing: SRR6793287, SRR6793288, SRR6793289, SRR6793290, SRR6793291, SRR6793292, SRR6793293, SRR6793294, SRR6793295, SRR6793296, SRR6793297, SRR6793298, SRR6793299, SRR6793300, SRR6793301, SRR7064951, SRR10512805, SRR10512806, SRR10512807, SRR10512808, SRR10512809, SRR10512818, SRR10512829, SRR10512840, SRR10512845, SRR10512846, SRR10512847, SRR10512848, SRR10512849, SRR10512850, SRR10512851, SRR10512852, SRR10083333, SRR10083334, SRR10083335, SRR10083336, SRR10083337, SRR10083338, SRR10083339, SRR10083340, SRR10083351, SRR10083352, SRR1916825, SRR1916826, SRR1916827, SRR1916830, SRR1916832, SRR1916834, SRR1916836, SRR1916839, SRR1916841, SRR1916842, SRR18761564, SRR18761566, SRR18761568, SRR18761571, SRR18761573, SRR18761563, SRR18761565, SRR18761567, SRR18761569, SRR18761570, SRR18761572, SRR18761574, SRR1270869, SRR1270914, SRR1270919, SRR1270921, SRR1270922, SRR1270923, SRR4249979, SRR4249988, SRR5676382, SRR5676383, SRR5676395, SRR5676396, SRR5676402, SRR1869462, and SRR1013468.

## Gene annotation and alignment

### Gene predictions

To create optimal gene annotations, we combined *ab initio* gene predictions; orthology inferences; and transcriptomic evidence for a total-evidence dataset facilitated using FunAnnotate<sup>207,215</sup> with manual interventions. To generate high-quality orthology-based evidence, we downloaded the UNIPARC database<sup>216</sup> of genes present in all Chiropteran genomes and mapped these proteins to our genomes using miniprot<sup>62</sup> (v 0.6-r194-dirty). We assembled our transcriptome data into transcripts using TRINITY<sup>217</sup> (v 2.13.2), and mapped these transcripts to our genomes using minimap2<sup>213</sup> (v 2.24).

Next, we ran BUSCO<sup>63,64</sup> (version 5.4.3) using the “eutheria\_odb10” database and AUGUSTUS<sup>58</sup> to identify BUSCO orthologs in our genomes. GFFs describing the gene structure of single-copy BUSCO orthologs was then used by FunAnnotate to train SNAP<sup>218</sup> and GlimmerHMM<sup>219</sup> (v 3.0.4) prior to gene prediction. GeneMark-ES<sup>59</sup> (v 4.72) was run using its self-trained model. AUGUSTUS<sup>220</sup> (v 3.4) was run using a previously-generated model jointly trained on 6 high-quality bat genome assemblies<sup>36</sup> and supplemented with protein and transcriptome hints generated by FunAnnotate from the UNIPARC and Trinity datasets.

To leverage high-quality annotations from other genomes, we used TOGA<sup>61</sup> (version 1.0.1) to generate gene annotations for each of our species, using inference from hg38 annotations. TOGA outputs a table of genes (“reg” genes) associated with the projected transcripts from the reference genomes, and a BED file describing the CDS structure of these projected transcripts. To generate a final GFF file summarizing these data, we converted the original BED file to a GFF file using [program]; removed the erroneous “Gene” level attributes; and

400 added in new “Gene” entries describing the TOGA-designated genes, modifying the “Parent” attributes of the  
401 mRNAs to refer to the correct parent gene. Transcript projections that were not associated with a TOGA gene  
402 designation were then dropped.

403 Finally, we used LiftOff<sup>60</sup> (v1.6.3) to lift over annotations from the *Myotis myotis* genome  
404 (mMyoMyo1.0\_primary<sup>36</sup>). Using BUSCO and manual curation, we assessed both the original GenBank  
405 (GCF\_014108235.1) and NCBI RefSeq (GCA\_014108235.1) annotations, and selected the NCBI RefSeq  
406 annotation, as it had slightly improved BUSCO scoring and less erroneous intron-exon junctions at select genes.  
407 We removed all non-protein-coding genes from the initial GFF file, then ran LiftOff using the settings “ -  
408 exclude\_partial -polish -cdfs”.

409 We evaluated each line of evidence by assessing their completeness using BUSCO and comparing the  
410 completeness score to the total number of predicted genes. We found that SNAP and GLIMMERHMM performed  
411 the poorest for gene annotations, with both the lowest BUSCO scores and the highest number of low-quality  
412 predictions. The miniprot-UniParc and TOGA-hg38 datasets generated the highest quality gene prediction  
413 datasets, with near-complete BUSCO scores and reduced low-quality protein predictions.

## 414 Gene prediction curation

415 We used EvidenceModeler<sup>221</sup> (version 2.0) to generate an initial consensus gene set using only the best  
416 lines of evidence (AUGUSTUS, weight 2; high quality AUGUSTUS, weight 5; TOGA-hg38, weight 12; miniprot-  
417 UniParc, weight 5; and LiftOff-mMyoMyo1, weight 5) with hints from protein orthology (miniprot-UniParc, weight  
418 6) and RNA-seq (TRINITY, weight 5) for alternative splicing. By default, EvidenceModeler does not consider  
419 genes that are located within intronic regions of other genes. To restore these genes, we intersected the  
420 EvidenceModeler consensus gene GFF with the TOGA-hg38 GFF to identify which genes were present in  
421 intronic regions and omitted from EvidenceModeler; these genes were then added back to the EvidenceModeler  
422 gene set.

423 To eliminate remaining spurious predictions, we cross-referenced our gene annotations against the  
424 SwissProt<sup>222</sup> database using DIAMOND<sup>223</sup> (v. 2.1.4) with settings “--ultra-sensitive --outfmt 6 qseqid bitscore  
425 sseqid pident length mismatch gapopen qlen qstart qend slen sstart send ppos evaluate --max-target-seqs 1 --  
426 evaluate 1e-10”. We kept all genes that matched a protein on SwissProt with at least 80% identity, matched over  
427 50% of the target sequence, and coded for at least 50 amino acids. Of the remaining genes, we kept them only  
428 if they contained both a start and stop codon with no internal stop codons.

429 Finally, we further curated our annotations by putting the EVM and TOGA gene predictions in competition  
430 with each other when they both annotated the same locus, but with different overlapping or neighboring  
431 annotations. In such cases, one of the gene annotations is likely closer to the truth. To determine which, we  
432 compared EVM and TOGA gene models with their closest human gene BLAST hits. Only proteins with a BLAST  
433 match to a human Ensembl v99 annotation with the lowest E-values below 0.001 were considered. These human  
434 homologs were used as a reference for curation as they are well-defined and characterized. We observed that  
435 occasionally, either the EVM or TOGA model predicted a transcript much longer than their human closest  
436 homolog. Closer inspection revealed that such cases represent artifactual mergers of neighboring genes during  
437 the annotation process, clearly visible from the fact that they map to two distinct human homologs in succession.  
438 Such cases were resolved by choosing the annotations (between EVM and TOGA) that were not affected by the  
439 artificial merger. We further observed a specific class of mergers between neighboring, segmentally duplicated



440 genes, with the resulting annotations representing chimeric mixes of exons from the duplicates. In such cases  
441 we selected the annotations that clearly stayed within the boundaries of the separate duplicates, as identified by  
442 mapping to the closest human homolog. For the remaining annotations where both TOGA and EVM both mapped  
443 to a single human homolog throughout their entire length, we selected the most complete annotation that was  
444 closest in length to the human homolog.

## 445 Orthologous Gene Alignments

446 Phylogeny and selection analyses described in this manuscript rely on high-quality alignments of bat  
447 orthologous coding sequences. To first find and align orthologous *Myotis* genes to the greatest extent possible,  
448 we first complemented the gene annotations described above with likely missing annotations that could still be  
449 found through BLAT homology searches. Missing gene annotations are always expected in non-model species  
450 genomes and reflect a feature of annotation pipelines in general, not an artifactual issue. For example if the first  
451 coding exon of a gene falls into a small local assembly gap, the lack of a start codon may prevent the trigger of  
452 a CDS annotation, or may lead to the clearly incomplete CDS being subsequently filtered out. Similarly,  
453 erroneous indels representing sequencing errors may interrupt coding reading frames. Genes with missing  
454 annotations can still be detected in assemblies through classic BLAST or BLAT homology searches, and then  
455 aligned with their annotated orthologs from other species. To align orthologous *Myotis* genes from ten species  
456 (those sequenced here plus *Myotis myotis* and *M. yumanensis*), we first decided to use *Myotis velifer* as the  
457 *Myotis* species of reference, since the RNA-seq data we used was generated with *M. velifer* tissues.

458 We first looked for missing homologs of *M. velifer* genes in the other *Myotis* genomes by blatting *M. velifer*  
459 CDS to the other *Myotis* assemblies (BLAT command line including non-default options -q=dnax -t=dnax -fine)  
460 to find matches outside of already annotated genomic segments. When multiple velifer CDS matched to the  
461 same locus with multiple overlapping homologous BLAT matches, we selected the match with the highest  
462 number of identical nucleotides. The remaining matching BLAT sequences were further considered if they  
463 spanned at least 50% of the velifer CDS, and included 100 codons or more. BLAT matches including stop codons  
464 were removed. This process added 1,837 putative CDS to consider for orthologous alignments for *M. auriculus*,  
465 1,785 for *M. californicus*, 1,796 for *M. evotis*, 1,505 for *M. lucifugus*, 3,234 for *M. myotis*, 1,826 for *M. occultus*,  
466 1,822 for *M. thysanodes*, 1,800 for *M. volans* and 1,729 for *M. yumanensis*. The correct reading frames for these  
467 putative CDS were then determined by aligning to the velifer CDS that generated the initial match with MACSE  
468 v2. MACSE has the crucial advantage over other aligners of being able to repair broken reading frames due to  
469 sequencing indel errors or erroneous gene annotations. At this stage, we restricted any further analysis to those  
470 velifer CDS with human homologs (BLASTP E-value<0.001 with at least one human canonical protein-coding  
471 gene from Ensembl). One-to-one orthologs with the 23,030 remaining velifer CDS in other *Myotis* species were  
472 then determined using Orthofinder v2.5.4<sup>224</sup>. The sequences of each group of ortholog were then aligned with  
473 MACSE v2<sup>225</sup> with default settings. The resulting CDS with potentially repaired reading frames were then  
474 checked with PREQUAL<sup>226</sup> to exclude sequencing errors and erroneous inclusion of non-homologous segments  
475 in annotations. The remaining parts of orthologous sequences that passed PREQUAL filtering were then aligned  
476 again using MACSE v2 with default settings. The first round of alignment with MACSE ensures that we do not  
477 remove portions of CDS that look like they have no homology and would thus be removed by PREQUAL, just  
478 because of frameshifts that are easy to repair first with MACSE. The second round of MACSE is to align the  
479 remaining codons once PREQUAL has removed erroneous portions of CDS that could have otherwise disturbed  
480 the alignment process. We further masked (i.e. replaced with indels) codons near indels with putative alignment  
481 errors as described in Bowman et al.<sup>227</sup>. Of the 23,030 initial *M. velifer* CDSs, this process resulted in 21,756  
482 alignments with at least one ortholog in another *Myotis* species.

483 We also aligned pan-Chiroptera orthologs from 47 non-*Myotis* genomes publicly available on NCBI at the  
484 time of analysis, to test the generality of our observations to all bats. We used the same strategy described  
485 above to complement *Myotis* gene annotations with BLAT matches, but this time blatting velifer CDS on non-  
486 *Myotis* assemblies (with `-q=dnax -t=dnax -fine` again) to find all the potential orthologs in the non-*Myotis*  
487 assemblies. We previously found that because BLAT represents a first filter to include only portions of  
488 homologous CDS with good local similarity, using BLAT matches results in higher quality alignments of orthologs  
489 than using existing gene annotations of disparate qualities that too often include non-homologous portions of  
490 introns among other issues<sup>227,228</sup>. As before with only *Myotis* species, we recovered putative one-to-one orthologs  
491 with Orthofinder. This process resulted in the alignment (as previously described with two rounds of MACSE and  
492 PREQUAL in the middle) of 19,009 orthologous CDS with at least one non-*Myotis* orthologous CDS.

493 To test whether the patterns of virus-driven adaptation observed in bats are unique across mammals, we  
494 also prepared four more datasets of 70 primate orthologous CDS alignments, 138 euungulate alignments, 127  
495 glires alignments, and 82 carnivora alignments (see supplementary files XY for the species and their respective  
496 assemblies used). We used the same pipeline as the one used to align 47 pan-chiroptera species as described  
497 above, except that instead of starting from velifer CDS, we started from human Ensembl v109<sup>229</sup> CDS (the  
498 longest isoform available in each case) for primates, *Mus musculus* Ensembl v109 longest CDS for glires, *Canis  
499 familiaris* Ensembl v109 longest CDS for carnivores, and *Bos taurus* Ensembl v109 longest CDS for euungulates  
500 . These species were chosen for the very high quality of their gene annotations.

## 501 Gene Trees & Phylogeny

502 A phylogeny of all 536 mammals in our alignments was generated using IQTREE<sup>230</sup> (version 2.3.1) using  
503 all gene alignments with the settings “-B 1000 -m GTR+F3x4+R6.” To generate gene trees, we first filtered our  
504 gene alignments to exclude alignments with over 50% gaps in the sequence and less than 4 species. With the  
505 remaining alignments, we used IQTREE to find the best-fitting substitution model and tree using settings “--wbt  
506 --bnni --alrt 1000 -B 1000 --safe”. The best substitution models for each gene were saved as a NEXUS file. To  
507 generate the phylogeny of bats, we first concatenated all gene alignments using `catfasta2phymI`  
508 (<https://github.com/nylander/catfasta2phymI>) to concatenate our individual gene alignments into species-level  
509 alignments, filling in missing species in each sub-alignment with gap symbols to preserve the alignment structure.  
510 Furthermore, we generated a partition file describing the region of each gene sub-alignment within the  
511 concatenated alignment.

## 512 Time-calibration of 59 bat genomes

513 Using our codon alignments of 59 bat genomes, we generated a time-calibrated phylogeny using  
514 *mcmctree*<sup>231</sup> and PAML<sup>72</sup> (v. 4.10.0) using an approximate likelihood method. Using the pan-bat codon  
515 alignments and our phylogeny as input, with fossil calibrations based on previously published work<sup>4,36,232–239</sup>, we  
516 ran *mcmctree* twice to generate the Hessian matrix and confirm convergence. This was followed by 10  
517 independent chains using the “out.BV” file from the first run. Finally, the output files of all 10 chains were  
518 combined to compute final divergence time estimates (see Table S2).

## 519 Ancestral Body Size, Lifespan, and Cancer Risk reconstruction

520 To explore how body size and lifespan have evolved over time in mammals, we used a super-phylogeny  
521 of mammal species<sup>67</sup> subsampled to only contain species with extant body size and lifespan data collected from  
522 AnAge<sup>15</sup> and PanTHERIA<sup>16</sup>. Ancestral body sizes and lifespans were simulated separately using StableTraits<sup>240</sup>.

523 To estimate ancestral longevity quotients (AncLQs), we followed the method of Austad and Fisher<sup>18</sup> and  
524 used a linear model of lifespan given body size trained on non-flying mammals to predict the lifespans at each  
525 ancestral node given median estimates of body size. AncLQs were then estimated from the ratio of observed  
526 lifespan versus predicted lifespan for each node.

527 Relative Incidence of Cancer Risk (RICR) was calculated across our mammalian phylogeny following the  
528 method of Vazquez and Lynch (2021)<sup>46</sup>. The cancer risk  $K$  at a given node was calculated using the log of the  
529 median predicted body size and lifespan. An organism's lifetime risk of cancer  $K$  is proportional to  $Dt^6$ , where  $D$   
530 is the body size and  $T$  is the maximum lifespan. RICR is then calculated as the  $\log_2$  ratio of the cancer risk  
531 between a node and its direct ancestor.

## 532 Selection Scans & Evolutionary Rates

### 533 aBSREL

534 To conservatively test for branch-specific selection, we used aBSREL<sup>98,241</sup> (version 2.5.48) to test for  
535 selection at each branch within the Nearctic *Myotis* clade for 15,734 gene alignments spanning 536 mammals.  
536 These genes were identified as 1:1 orthologs across the full alignment, with no more than 50% sequence gaps  
537 and at least 4 species present in the alignment. We defined genes under selection as those with an FDR-  
538 corrected p-value of less than 0.05; genes were specifically identified as under positive selection if  $\omega > 1$ .

### 539 BUSTED

540 To quantify the total amount of positive selection across the *Myotis* tree or the different species trees  
541 used in this manuscript, we used an improved version of the BUSTED<sup>113,241</sup> test called BUSTED-MH. The original  
542 BUSTED test estimates for a given gene the proportion of codons that have evolved under positive selection,  
543 with  $dN/dS > 1$ , summed over all the branches of a given tree, regardless of the branch and regardless of the  
544 codons in a multi-species alignment. The version of BUSTED we used, BUSTED-MH, includes two crucial  
545 improvements over the original BUSTED that make it much less likely to generate false positive inferences of  
546 positive selection, albeit at the cost of becoming a very conservative test. First, BUSTED-MH takes synonymous  
547 substitution rate variation into account, which prevents mistaking cases where  $dN/dS$  is greater than one just  
548 because  $dS$  is low, with cases where  $dN/dS$  is greater than one because positive selection actually increased  
549  $dN$ . Second, BUSTED-MH takes complex substitutions that simultaneously involve more than one nucleotide  
550 into account in its likelihood models. This prevents attributing positive selection to cases where  $dN/dS$  is greater  
551 than one where instead a complex substitution changed multiple amino acids in a single event. BUSTED-MH  
552 has been shown to strongly reduce the rate of false positives that typically plague  $dN/dS$ -based tests of positive  
553 selection<sup>242</sup>.

We applied BUSTED-MH to 19,646 *Myotis* orthologous CDS alignments with at least five orthologs. These orthologs are cases where the Orthofinder gene trees coincide with the species tree. This effectively removes issues regarding whether we should use the gene or the species tree, at the cost of removing 2,110 genes from the *Myotis* selection analysis. Similarly, we applied BUSTED-MH to 17,469 non-*Myotis* bat alignments with at least five orthologs. This includes a subset of 14,091 alignments with orthologs in two thirds of the non-*Myotis* bat species that we specifically used to show that patterns of virus-driven adaptation are representative of all, and not just a limited subset of bats. We also tested 17,890 primate alignments with at least five orthologs with BUSTED-MH, as well as 19,311 glires, 18,000 carnivora and 18,504 ungulate alignments.

## RERConverge

Between-species life history diversity may be undergirded by significant evolutionary rate shifts in important genes, where evolutionary change across the gene tree correlates either positively or negatively with changes in a particular life history trait across the trait tree. In *Myotis*, we were interested specifically in testing whether or not longevity-related metrics could be correlated with evolutionary rate shifts for particular genes, and if, among those, we could identify types of genes (gene ontologies) that were enriched.

To answer this question, we used RERconverge<sup>109</sup>, an R package which uses gene trees to compute relative evolutionary rates (RERs), then tests for correlations between RERs and trait changes between species. 40 bat genomes were aligned to produce MSAs, which were then split into three groups to be tested independently: all bats (n=59), non-*Myotis* bats (n=29), and *Myotis* (n=11). Gene trees were constructed under the GTR+G model with the same topology as determined in our phylogenetic analysis, across all 39 available bat species. After concatenating the gene trees, RERs were calculated in RERconverge. Trait correlation analysis was performed by regressing these RERs against 4 distinct trait axes. Two of the axes were maximum longevity and size, which were obtained from AnAge<sup>154</sup> and PanTHERIA<sup>16</sup>; an additional two axes were obtained by plotting species along the first 2 principal components of size and maximum longevity. Since size generally correlates with longevity, even within *Myotis*, PCA allows us to describe species using orthogonal trait axes that roughly correspond to size-independent longevity and longevity-independent size. Using a Wilcoxon rank-sum test, we then tested for enrichment in correlation significance amongst different gene sets.

## RELAX

The evolution of life history diversity across a clade may also manifest in differential selection regimes across relevant genes or types of genes. Specifically, the evolution of a particular life history may be driven by either relaxation or intensification of selection in different genes. In *Myotis*, we were again interested in whether we could identify genes and gene sets related to increased longevity within the clade.

RELAX<sup>102</sup> is used to identify genes under either relaxation or intensification of selection across groups of species within a clade using MSAs and a labeled species tree. MSAs for 11 available *Myotis* species across ~19,000 shared genes were fit using the BS-REL framework to a branch-site model, using the species tree determined from our phylogenetic analysis. 4 longer-lived species, *Myotis lucifugus*, *M. occultus*, *M. evotis*, and *M. myotis* were set as the foreground class with the remaining species set as the background class. RELAX then used these branch classes to estimate a distribution of  $\omega$  (dN/dS) for each branch class, constrained by the relaxation factor  $k$ . An LRT is performed for  $k \neq 1$  against  $k = 1$ , with  $k > 1$  implying relaxation of selection and  $k < 1$  implying intensification of selection. The results from this test were then used to perform a Wilcoxon rank-sum test to identify enrichment in the significance of the  $k$ -parameter amongst different gene sets.



## 594 VIPs

595 To determine if *Myotis* and other bats are enriched for adaptation at Virus Interacting Proteins (VIPs), we  
596 conducted a test comparing levels of adaptation, inferred by BUSTED, in sets of VIP genes compared to matched  
597 control genes. Sets of control genes were resampled in a bootstrap procedure  
598 ([https://github.com/DavidPierreEnard/Gene\\_Set\\_Enrichment\\_Pipeline](https://github.com/DavidPierreEnard/Gene_Set_Enrichment_Pipeline)) to generate 95% confidence intervals for  
599 sets of genes at progressively smaller BUSTED p-value thresholds<sup>112,114,116,155</sup>. When VIPs are subject to greater  
600 levels of positive selection than expected relative to the sets of matched control genes, we expect a pattern in  
601 which the high p-value thresholds show weaker enrichment but smaller confidence intervals, because more  
602 genes are used in these calculations. As the p-value threshold gets smaller, the signal of enrichment is expected  
603 to get stronger but at the expense of larger confidence intervals.

604

605 We generated five sets of VIP genes: A set of all VIP genes with aligned orthologs from at least five  
606 species in the tested clade (Nearctic *Myotis* or pan-Chiroptera without *Myotis*); a set of VIP genes with known  
607 pro- and/or anti-viral activity; a set of VIP genes with no known pro- and/or anti-viral activity; a set of VIP genes  
608 that interact only with DNA viruses; and a set of VIP genes that interact only with RNA viruses. Because both  
609 the number of species and genes included, as well as their level of homology, influences the power of these  
610 tests we also tested the influence of the stringency of gene choice by generating a separate set of genes for the  
611 pan-Chiroptera analyses that included only genes with aligned orthologs in at least two thirds of the non-*Myotis*  
612 species. Analyses using this more limited set of genes show the same result in terms of enrichment of adaptation  
613 in VIP genes and comparing DNA VIPs and RNA VIPs, showing that the observed patterns are valid across bats  
614 regardless of the stringency of homology.

615

616 The bootstrap procedure matches a tested gene set of interest such as VIPs with sets of control genes  
617 (non-VIPs when testing VIPs) that have the same average values as the set of interest for multiple potential  
618 confounding factors that could explain differences in adaptation instead of interactions with viruses. For example,  
619 if the level of gene mRNA expression has an influence on the rate of adaptation, we then need to match VIPs  
620 with control sets of non-VIPs that collectively have the same average expression as VIPs. For each group of  
621 tested VIPs we build 1,000 control sets with randomly sampled non-VIPs according to a matching procedure  
622 described in Enard & Petrov 2020<sup>155,243</sup>. We match the 27 following factors between VIPs and non-VIPs, for all  
623 tested groups of species:

- 624 ● the length of the aligned CDS.
- 625 ● the overall CDS GC content in each orthologous alignment.
- 626 ● the GC content at aligned codons' position 1, 2 and 3 separately.
- 627 ● the number of species with a one-to-one ortholog out of all the species included in an alignment, where  
628 species with no ortholog are represented by gaps the whole length of the alignment.
- 629 ● the number of species with an ortholog at least 90% of the length of the species of reference (*Myotis*  
630 *velifer* in bats, human in primates, etc; see above).
- 631 ● the overall proportion of each orthologous alignment made of indels.
- 632 ● the three synonymous rates of evolution estimated by the likelihood model of HYPHY Busted.
- 633 ● the proportions of codons that fall in the three latter synonymous rates.
- 634 ● average human mRNA expression in 53 GTEx v7 tissues<sup>244</sup>, in  $\log_2$  of Transcripts Per Million (TPM).

- 635 • lymphocyte human mRNA expression from GTEx v7, in  $\log_2$  of TPM.
- 636 • testis human mRNA expression from GTEx v7, in  $\log_2$  of TPM.
- 637 • mRNA expression in  $\log_2$  of TPM for six separate *Myotis velifer* tissues: heart, brain, kidneys, lungs,  
638 pancreas, and testis.
- 639 • the number in  $\log_2$  of protein-protein interactions (PPIs) in the human protein interaction network<sup>245</sup>.
- 640 • the proportion of genes that are immune genes according to Gene Ontology annotations of the  
641 closest human homolog including Gene Ontology terms GO:0002376 (immune system process),  
642 GO:0006952 (defense response), and/or GO:0006955 (immune response) as of summer 2021<sup>246</sup>.
- 643 • the proportion of housekeeping genes defined as genes with stable expression across many human  
644 tissues, listed in Eisenberg & Levanon<sup>247</sup>.
- 645 • the overall dN/dS ratio estimated by Busted for the orthologous CDS alignments.

646 We match the overall dN/dS between VIPs and control non-VIPs to account for an important issue  
647 of dN/dS tests: dN/dS-based tests tend to lose statistical power to detect positive selection in CDS  
648 alignments with higher selective constraint<sup>248</sup>. The amount of positively selected sites being equal,  
649 positive selection tests based on dN/dS tend to have lower statistical power and tend to generate more  
650 false negative results when the rest of the coding sequence is more highly constrained. VIPs tend to be  
651 much more strongly constrained than non-VIPs<sup>112</sup>, which gives a strong, unfair statistical disadvantage  
652 to VIPs when testing positive selection with BUSTED or other HYPHY tests. We limit this issue by  
653 matching VIPs and control non-VIPs for dN/dS. Thus, VIPs have an excess of adaptation compared to  
654 non-VIPs when they have a balance of the same total amount of non-synonymous changes more tilted  
655 towards advantageous rather than neutral amino acid changes. In this case non-VIPs still have less  
656 constraint (more neutral changes) than VIPs, and thus still more power to detect positive selection, but  
657 not to an extent as severe and unfair as if we did not match the overall dN/dS<sup>112</sup>. In the case where VIPs  
658 do not have an excess of adaptation, then they have the same balance of advantageous and neutral  
659 amino acid changes resulting in the same overall dN/dS. This is the case of RNA VIPs in bats in this  
660 study; this internal negative control shows that the matching of dN/dS works as intended.

## 661 Gene Duplications

662 To quantify patterns of gene duplication and loss, we quantified the copy number of genes with human  
663 orthologs from our gene annotations for each nearctic *Myotis* genome. To calculate per-gene expansion and  
664 loss rates and their statistical significance, we ran CAFE<sup>140</sup> v5 on the previously described set of copy number  
665 counts using our time-calibrated species tree pruned to include only the nine nearctic *Myotis* species. *M. myotis*  
666 was excluded because of its lower quality assembly. We ran CAFE on the subset of genes with two or more  
667 copies in at least one species using a Poisson distribution for the root frequency ( $-p$ ), first generating an error  
668 model to correct for genome assembly and annotation error ( $-e$ ). We compared the base model (each gene  
669 family belongs to the same evolutionary rate category) to gamma models (each gene family can belong to one  
670 of  $k$  evolutionary rate categories) with different values of  $k$ . A final gamma model with  $k=9$  was chosen to balance  
671 model log likelihood with the number of gene families for which the optimizer failed. The model was run three  
672 separate times to ensure convergence.

673 To understand if genes in these pathways have higher birth rates or are more likely to have significant  
674 changes in gene copy number than expected relative to other genes, we compared the gene copy birth rate  $\lambda$   
675 and number of genes that have significantly expanded or contracted in copy number on at least one branch  
676 within our nearctic *Myotis* phylogeny. Following Huang et al.<sup>50</sup>, we tested if VIP genes in particular underwent

677 significant copy number changes or had significantly different birth/death rates than non-VIP genes. For each  
678 category of VIP genes (all VIPs, DNA VIPs, DNA only VIPs, RNA VIPs, and RNA only VIPs), we generated 100  
679 bootstrap sets of control non-VIP genes with the same number of genes as the corresponding VIP gene set. We  
680 ran CAFE on each set of VIP genes and the corresponding control non-VIP genes to infer per-gene birth-death  
681 rates and per-gene, per-branch expansion/loss events.

## 682 Assessment of DNA Double-Strand Break Tolerance

683 We assessed each species' tolerance to DNA double strand breaks using a by measuring viability,  
684 cytotoxicity, and apoptosis across a range of doses of Neocarzinostatin, a radiomimetic drug. We measured dose  
685 response curves in wing-derived primary dermal fibroblasts across 5 bat species (*Myotis lucifugus*, n=8; *Myotis*  
686 *evotis*, n=3; *Rousettus langosus*, n=2; *Eidolon helvum*, n=2; *Pteropus rodrigensis*, n=2) using the multiplexed  
687 ApoTox-Glo assay (Promega). Using 96-well plates, two individuals and 11 doses were assessed simultaneously  
688 with four technical replicates. Results were normalized to treatment controls for each individual in R as previously  
689 described<sup>44,45,48,51</sup>.

## 690 Mapping PKR exons

691 We further validated the annotations for the PKR locus by re-aligning the primary *M. velifer* coding  
692 sequence back to the nine nearctic *Myotis* reference genomes, as well as a non-*Myotis* outgroup, *Pipistrellus*  
693 *pygmaeus*, and the genome haplotypes for each of these species. Because the presence of two copies makes  
694 this task challenging for most aligners, we independently aligned the *M. velifer* reference PKR sequence to  
695 sequential sections of each genome in 50kb search regions surrounding the known loci in each genome. This  
696 alignment search was conducted for 5 regions upstream (250 kb) and 5 regions downstream (250 kb) of the  
697 known loci. In species with two known copies, the location of each copy was included in a separate search  
698 region. This was to prevent erroneous merging or loss of exons. These regions were retrieved using bedtools  
699 getfasta<sup>249</sup> and alignment was performed using minimap2<sup>62</sup>. Minimap2 settings were optimized to retain secondary  
700 alignments (-p 0 -n 1 -outsc=0.0 -outc=0.0) and find known exons with accurate boundaries (-J 18 -F 21 -O 15  
701 -L 10). The resulting gff file was converted to bed format using AGAT<sup>250</sup>, sequences retrieved with bedtools  
702 getfasta, and a custom script used to remove identical duplicates. Finally, all sequences were aligned with  
703 MACSE v2.07<sup>225</sup>. We used BISER<sup>128,211</sup> to confirm the presence of segmental duplications in these regions.

## 704 PKR cell lines and vectors

705 All PKR experiments were performed using HeLa PKR-KO cells (kindly provided by A. Geballe, Fred  
706 Hutchinson Cancer Center, Seattle WA) that were plated either at densities of 5x10<sup>4</sup> cells/mL in 24-well plates  
707 or at 1x10<sup>5</sup> cells/mL in 12-well plates. The cells were maintained at 37°C with 5% CO<sub>2</sub> and cultured in DMEM  
708 supplemented with 5% fetal bovine serum (FBS), 1% penicillin/ streptomycin mix and 1 µg/mL puromycin (Sigma-  
709 Aldrich). All transfections were performed 24 hours after seeding, using 3 µL of TransIT-LT1 Transfection  
710 Reagent (Mirus Bio) per 1 µg of DNA and Opti-MEM media. We used previously-generated pSG5-FLAGx2  
711 vectors encoding either *M. myotis* PKR-1 (GenBank OP006550), *M. myotis* PKR-2 (GenBank OP006559), *M.*  
712 *velifer* PKR-1 (GenBank OP006558), or *M. velifer* PKR-2 (GenBank OP006557)<sup>28</sup>. Plasmids encoding the  
713 interferon-stimulated gene ISG20<sup>243</sup> and a constitutively active variant of the sterile alpha motif domain-  
714 containing protein 9-like SAMD9L-F886Lfs\*11 (here, SAMD9L<sup>251</sup>) were used as controls in viral infections and  
715 cell translation experiments, respectively.

716

## 717 Western blot

718 We assessed for the steady state protein expression of *M. myotis* Flag-PKR<sub>s</sub> after transfection of 350  
719 ng and 700 ng of DNA plasmids encoding either PKR1 alone, PKR2 alone, or both PKR1 and PKR2 (175 ng of  
720 each and 350 ng of each, respectively). Briefly, cells were re-suspended and lysed in ice-cold RIPA buffer (50  
721 mM Tris pH8, 150 mM NaCl, 2 mM EDTA, 0.5% NP40) with protease inhibitor cocktail (Roche) and sonicated.  
722 20  $\mu$ L of the clarified fraction was denatured with 5  $\mu$ L of 6x Laemmli buffer at 95°C for 5 min and loaded into 4-  
723 20% BioRad Criterion TGX Stain-Free precast gel. The wet transfer into a PVDF membrane was executed  
724 overnight at 4°C. The membranes were blocked in a 1xTBS-T buffer (Tris HCl 50 mM pH8, NaCl 30 mM, 0.05%  
725 of Tween 20) containing 10 % powder milk, and were incubated for 1h. The membranes were incubated with  
726 primary mouse anti-Flag (Sigma F3165) and anti-Tubulin (Sigma T5168) antibodies and secondary anti-Mouse  
727 IgG-Peroxidase conjugated (Sigma A9044). Detection was made using the Chemidoc Imagina System (BioRad)  
728 with SuperSignal West Pico Chemiluminescent Substrate (ThermoFisher Scientific).

## 729 Cell viability assay

730 HeLa PKR-KO cells were transfected 24h after plating in 96 well plates, with 100 or 200 ng of pSG5  
731 plasmid: empty or coding for *M. myotis* or *M. velifer* PKR1, PKR2 or PKR1+2 equal mix (50%-50%). 24 hours  
732 post-transfection, positive control cells were treated with an apoptosis-inducing drug, Etoposide, at different  
733 doses (250, 200 or 100  $\mu$ M). 48 hours post transfection, cells were harvested and lysed to quantify luminescent  
734 signal according to CellTiter-Glo® Luminescent Cell Viability Assay (Promega) kit protocol.

735

## 736 VSV infection

737 Cells were transfected 24 h after plating with 350 ng of pSG5 plasmid: empty, or encoding *M. myotis* or  
738 *M. velifer* PKR1, PKR2, or equal input of PKR1 and PKR2 (175 ng per plasmid), or a plasmid encoding interferon-  
739 stimulated exonuclease gene 20 (ISG20), due to its known antiviral activity against VSV as positive control<sup>243</sup>.  
740 Cells were infected 24 h post transfection with replicative VSV-GFP virus<sup>145</sup> at a MOI of 3. Cells were fixed with  
741 4% paraformaldehyde 16-18 hours post infection. VSV infection was quantified by measuring the percentage of  
742 GFP positive cell populations with BD FACSCanto II Flow Cytometer (SFR BioSciences). Fold change results  
743 were normalized to the empty pSG5 condition across at least three independent experiments.

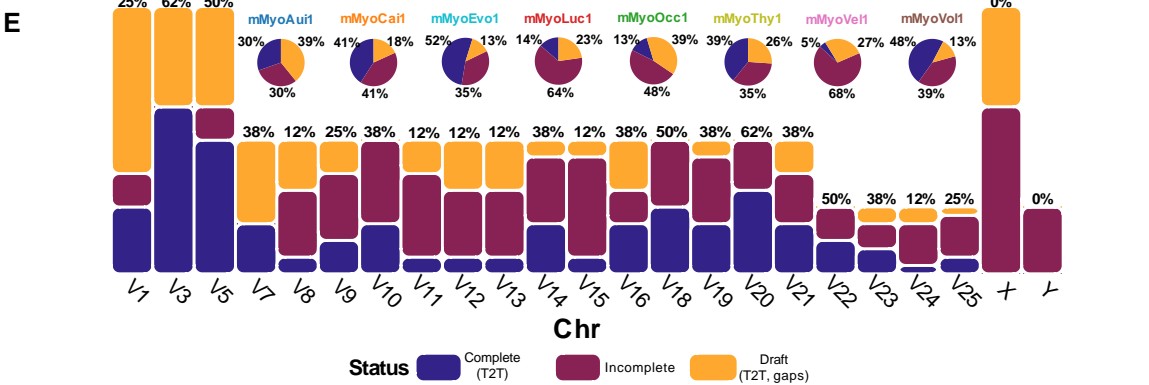
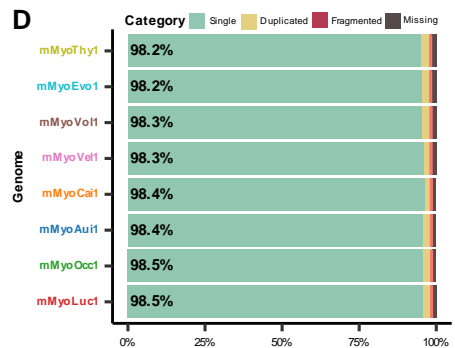
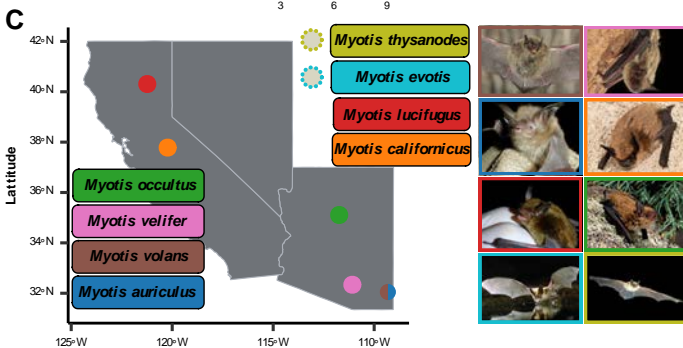
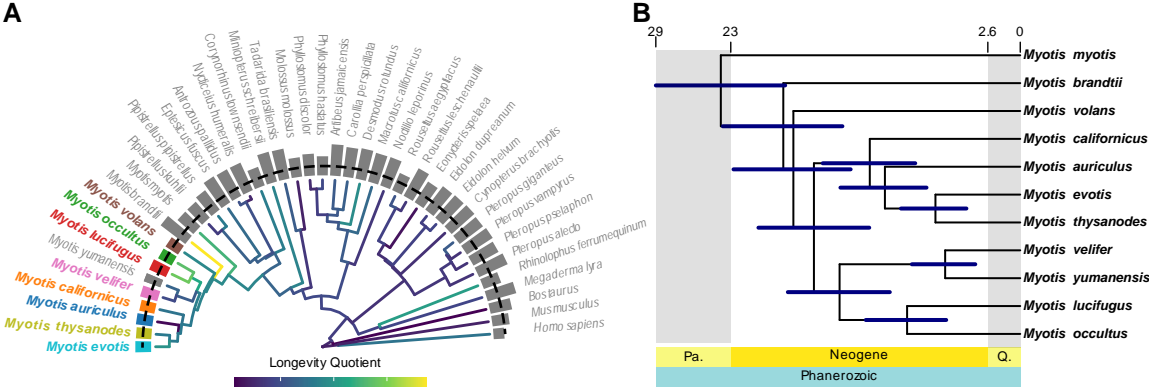
## 744 Luciferase reporter assays

745 Luciferase reporter assays were carried out to investigate whether the two PKR paralogs have  
746 synergistic, additive or dominant negative effect in translation shutdown. Transfection was performed as  
747 previously described with additional 50 ng of FFLuc firefly luciferase reporter plasmid per well. Sterile alpha motif  
748 domain-containing proteins 9L (SAMMD9L gain-of-function mutant) was used as a positive control of translational  
749 repression<sup>251</sup>. 24 h post transfection, cells were briefly washed with PBS, lysed by a 5x reporter lysis buffer  
750 (Promega) and incubated overnight at -20°C. Cells were then collected and 100  $\mu$ l of the luciferase substrate  
751 (Promega) was added to 20  $\mu$ l of the lysis supernatant. Alternatively, cells were lysed using BrightGlow Lysis  
752 Reagent (Promega E2620). The relative luminescence units (RLUs) were immediately quantified with LUMIstar

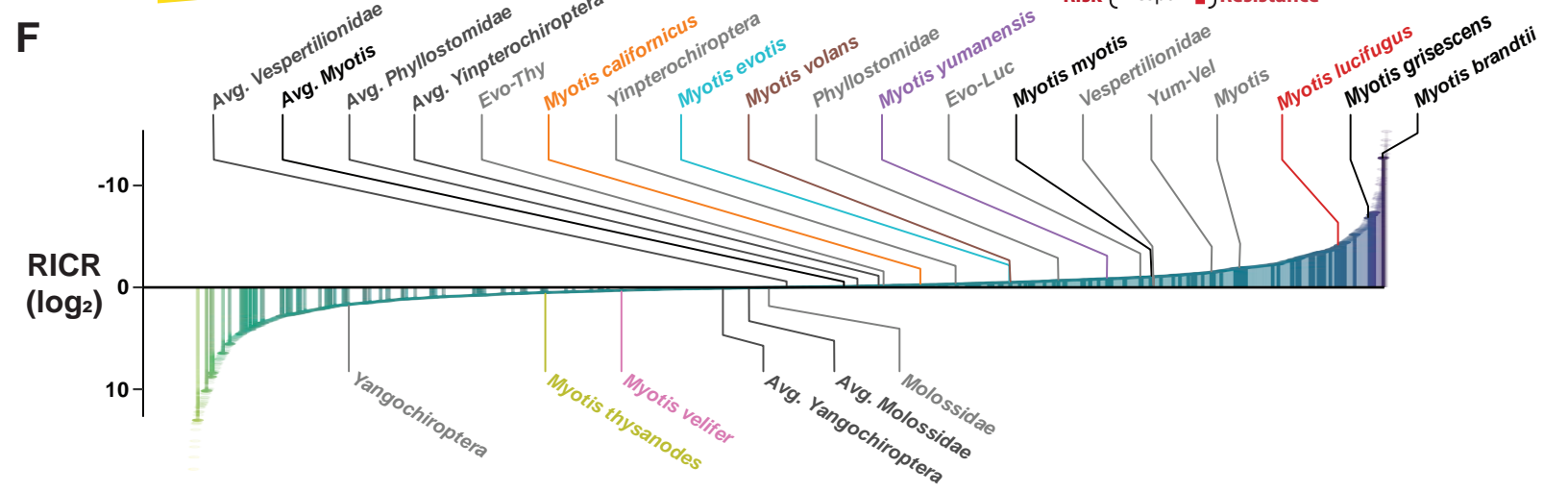
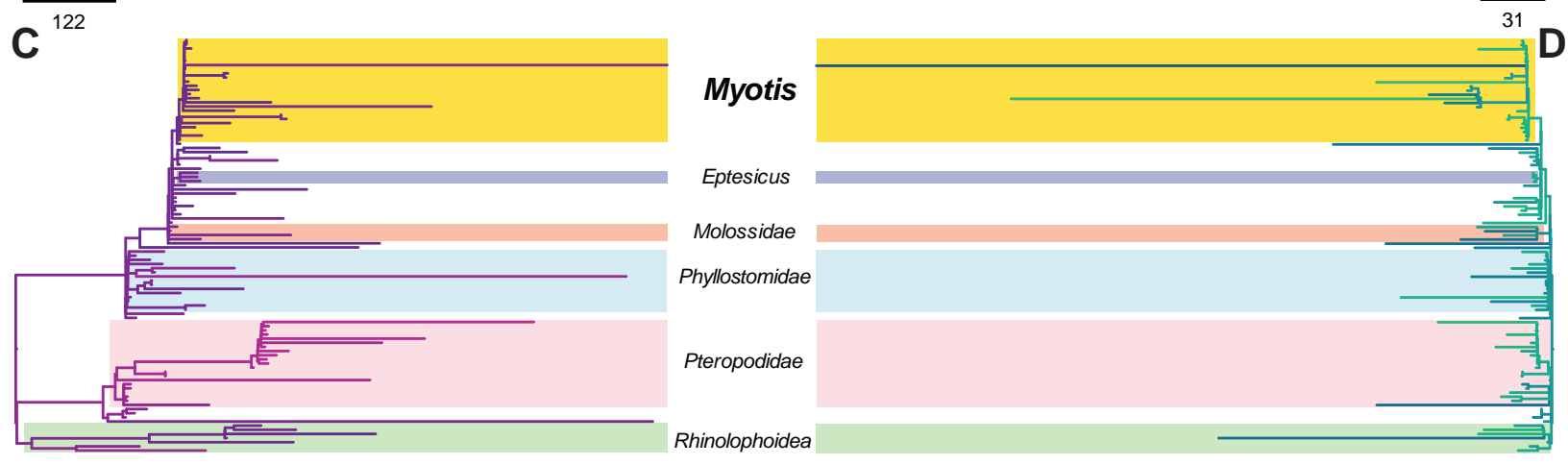
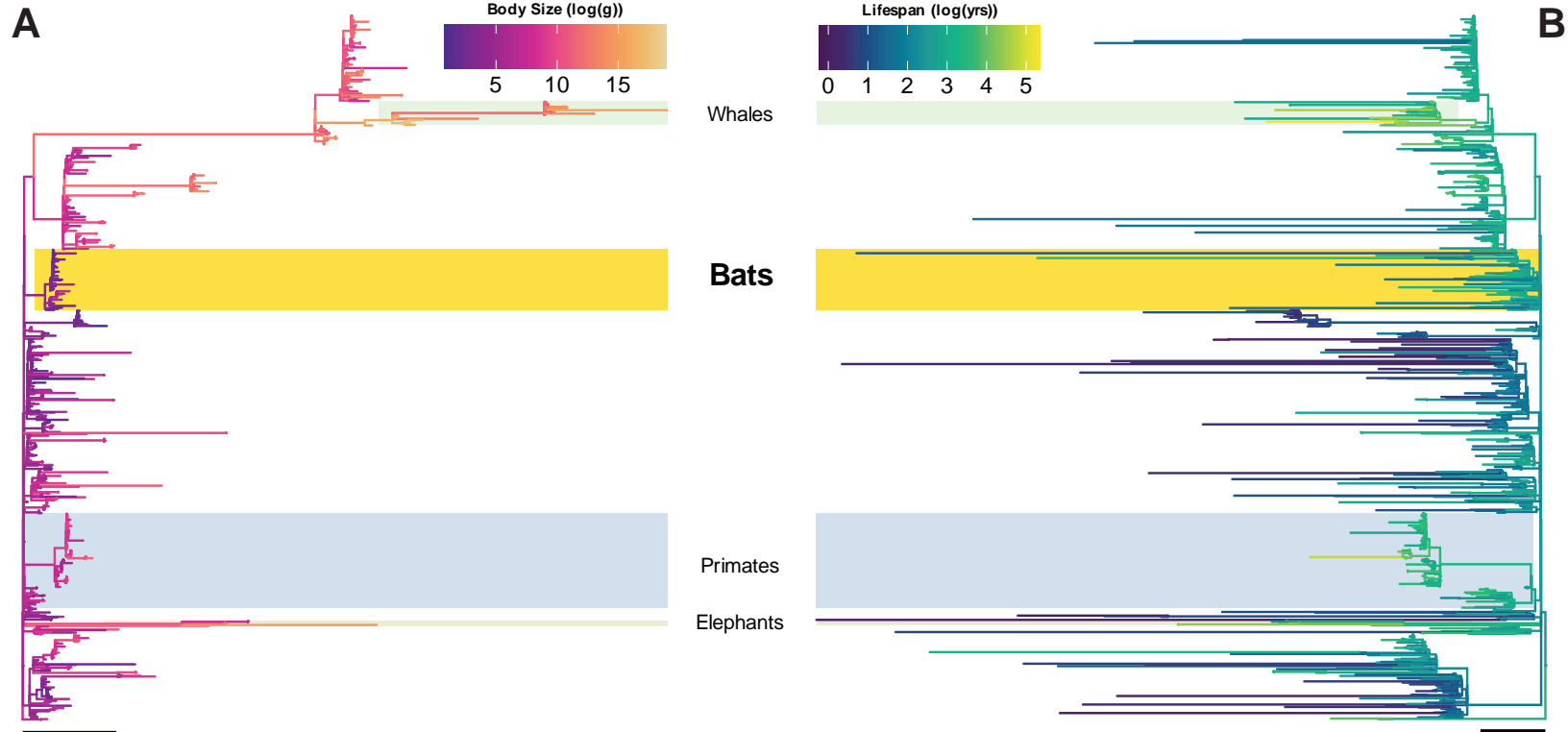


753 Omega microplate reader optima (BMG Labtech). All luciferase assays were conducted in technical duplicates  
754 in at least five independent experiments. Fold change results were normalized to the empty pSG5 condition  
755 within each independent experiment.

## 756 **Figures**

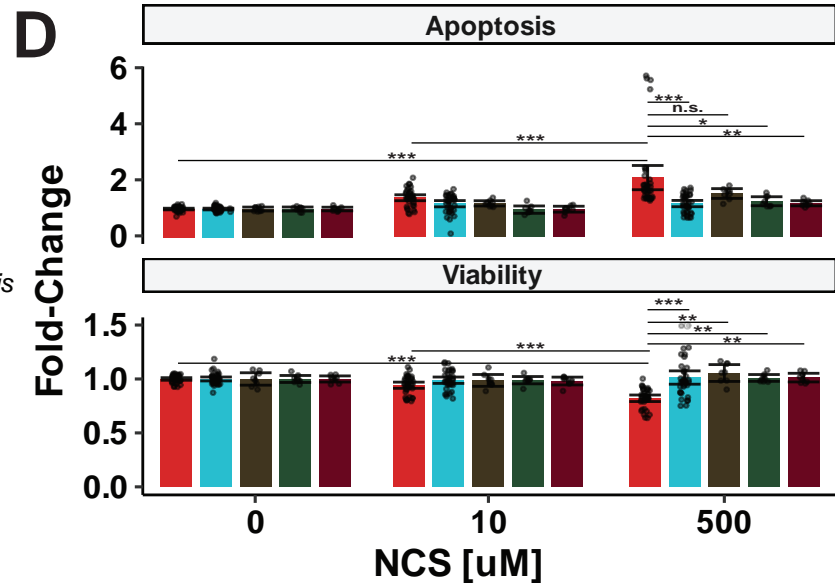
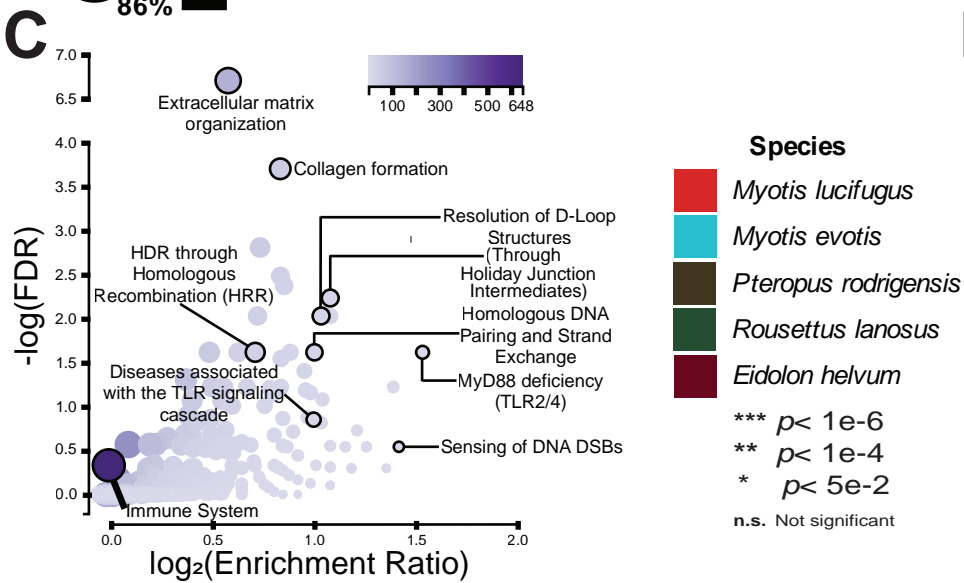
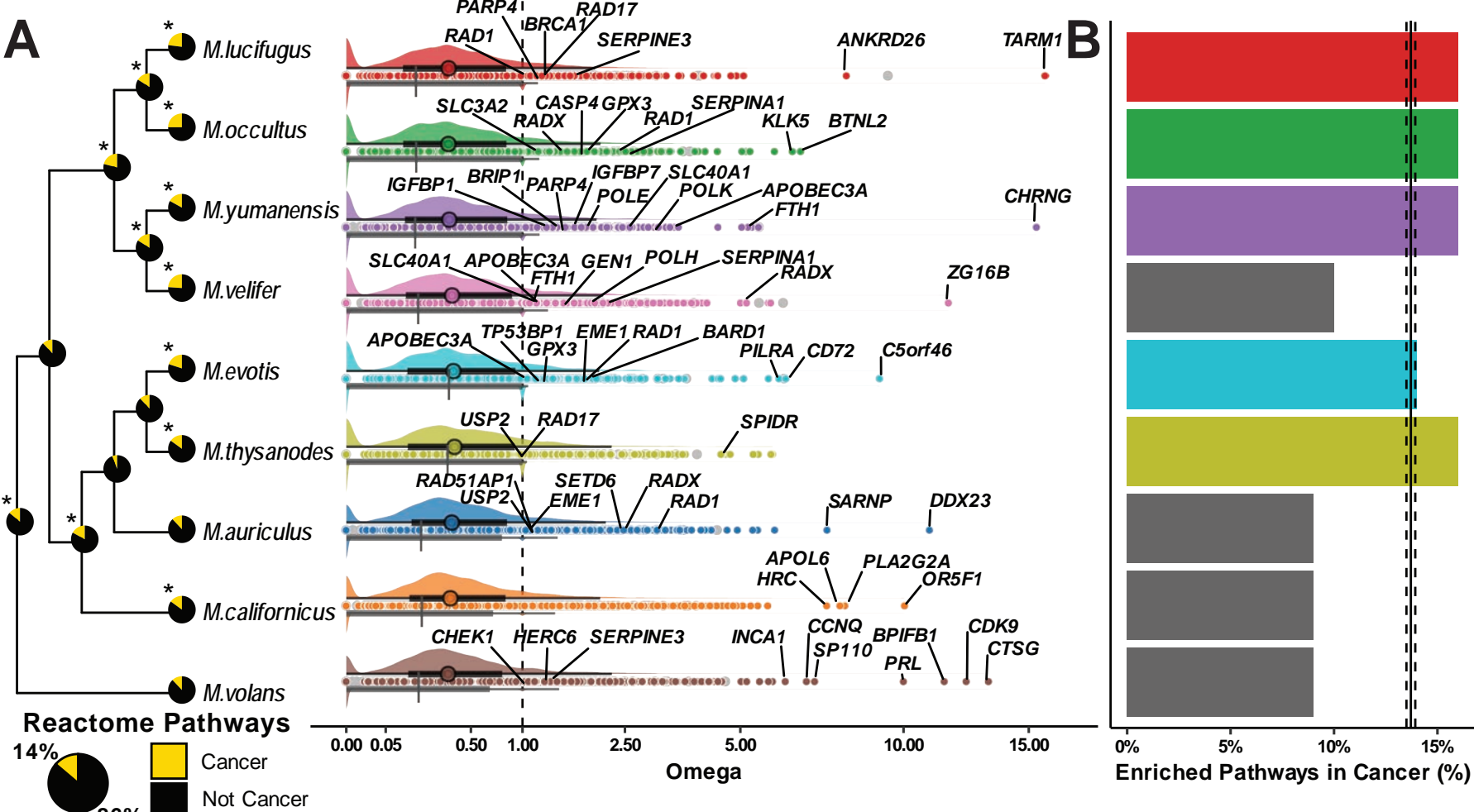


757 **Figure 1:** 8 near-complete reference assemblies for North American (Nearctic) *Myotis*. **A)** Phylogeny of 38 bat  
758 genomes with 3 outgroup species: cow (*bosTau9*), mouse (*mm39*); and human (*T2T-CHM13v2.0*). Bars at the tips  
759 of the phylogeny indicate the AuNG score of each genome (lower values equal more contiguous genomes); the  
760 dotted line represents the AuNG score for complete (T2T) genome assemblies as represented by T2T-CHM13v2.0.  
761 **B)** The time-calibrated phylogeny of 9 Nearctic and two representative Palaeartic *Myotis* species based on  
762 orthologous codon alignments. Blue bars represent age uncertainties. **C)** Map of capture sites with representative  
763 images (see “Acknowledgements” for attributions) for the individuals and species sequenced in this study; cell lines  
764 for *M. evotis* and *M. thysanodes* were provided by Richard Miller and were not collected for this study. **D)** BUSCO  
765 (v5, odb10\_mammalia) scores for annotations generated for the 8 new *Myotis* genomes. **E)** Ideogram bar plot  
766 indicating completion status of each chromosome in assembly. Pie graphs indicate completion status of all  
767 chromosomes in assembly. All chromosomes were positively identified based on size, synteny, and homology to  
768 human chromosomes<sup>57</sup>. “Complete (T2T)” status indicates that a chromosome is fully assembled telomere-to-  
769 telomere without gaps; “Draft (T2T, gaps)” status indicates that a chromosome is fully scaffolded with both  
770 telomeres, but has one or more gaps in the assembly; “Incomplete” status indicates that a chromosome was  
771 positively identified, but was not scaffolded from telomere to telomere (only contains one telomere).

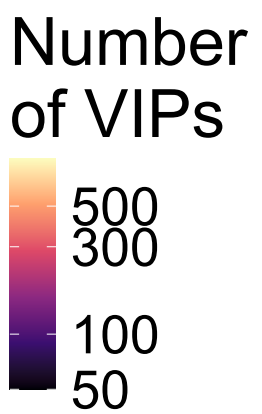
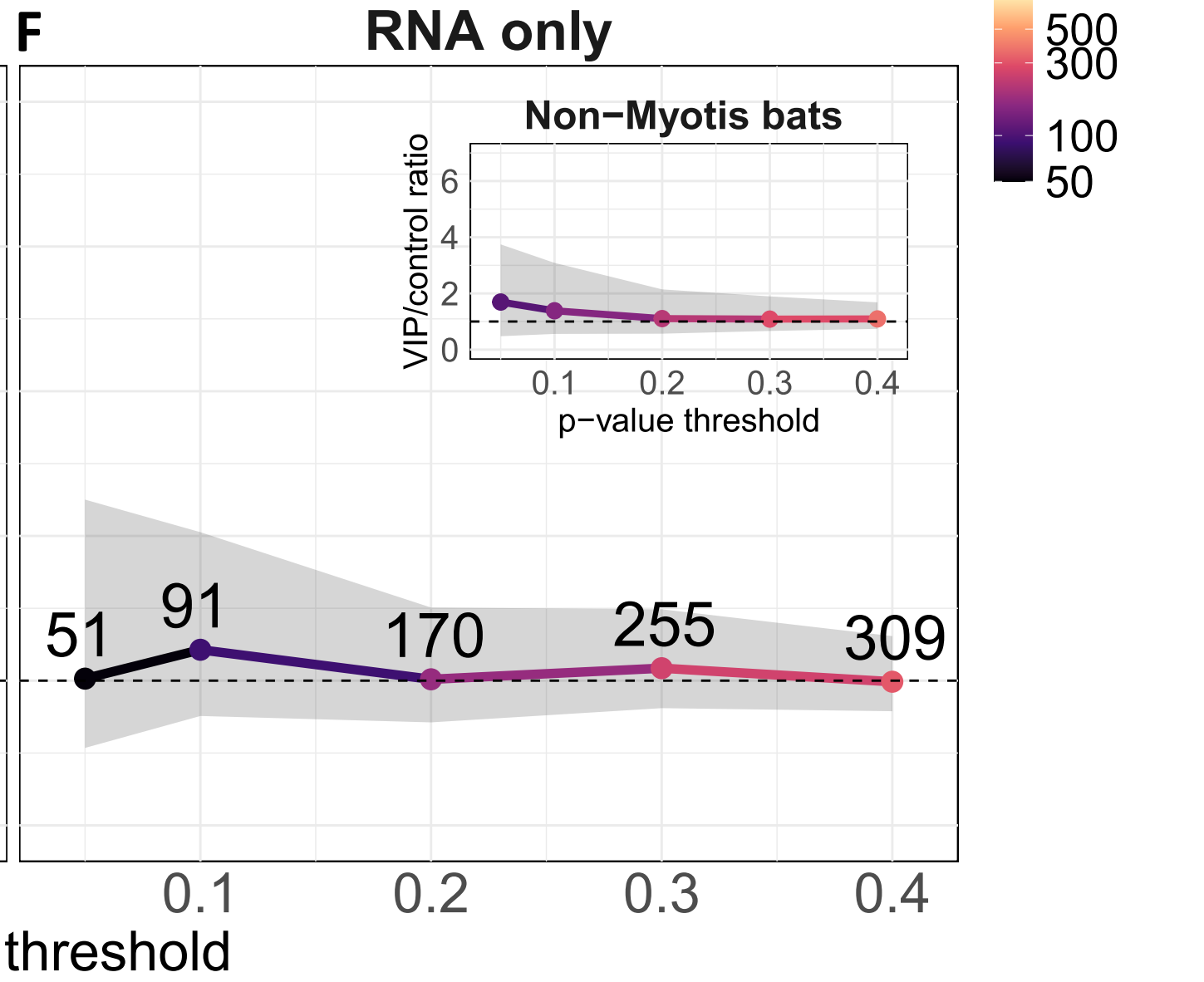
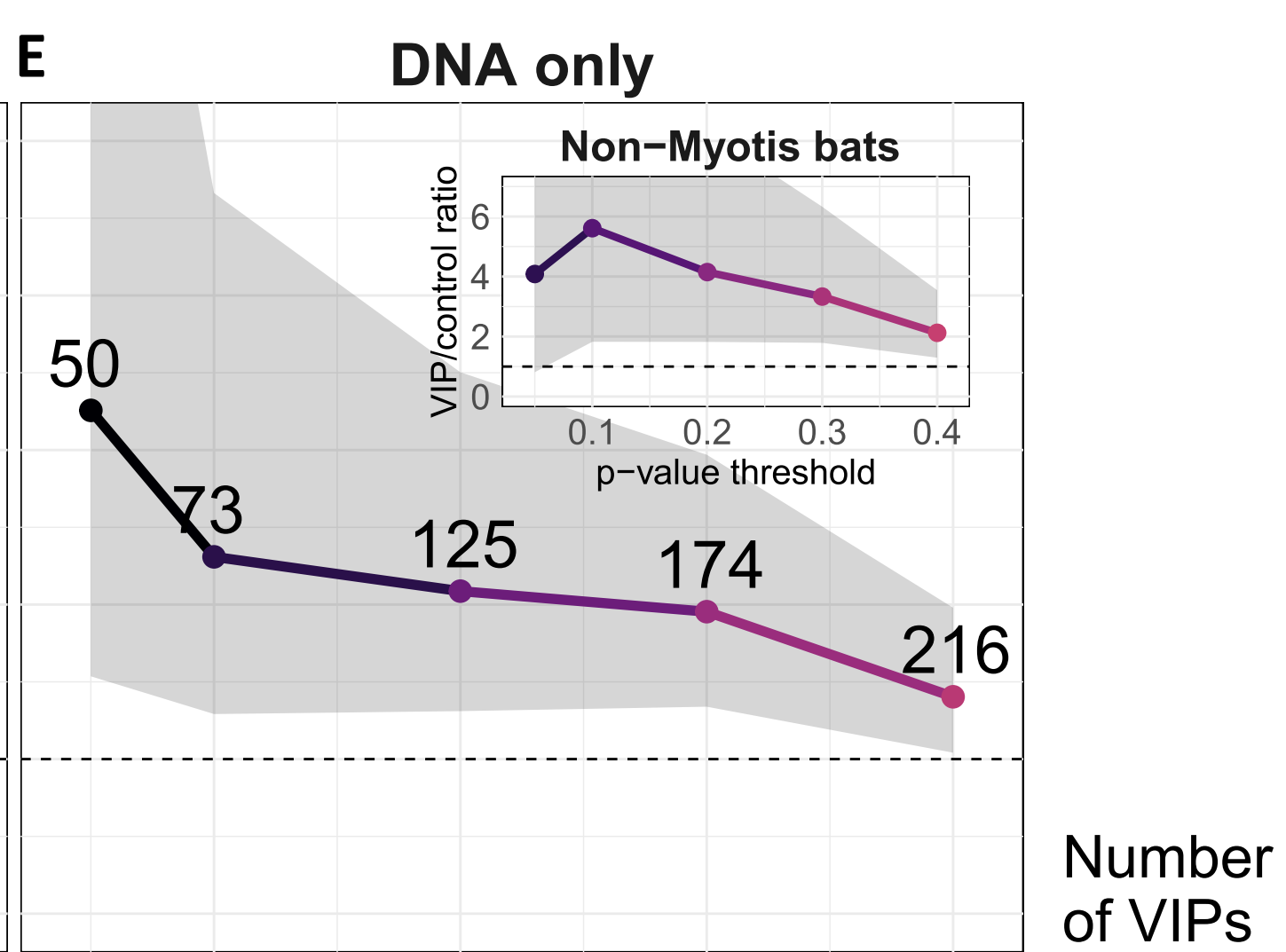
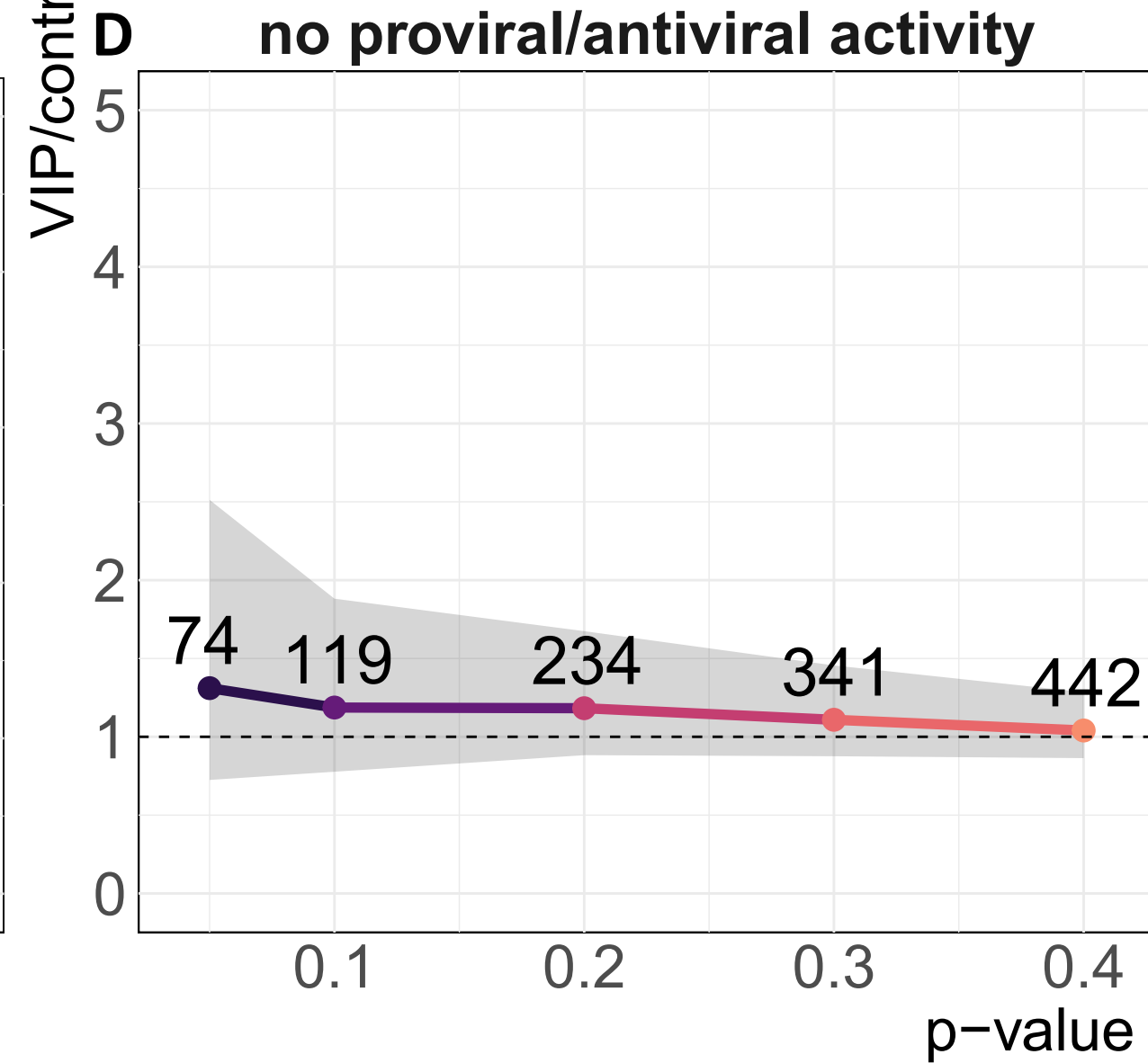
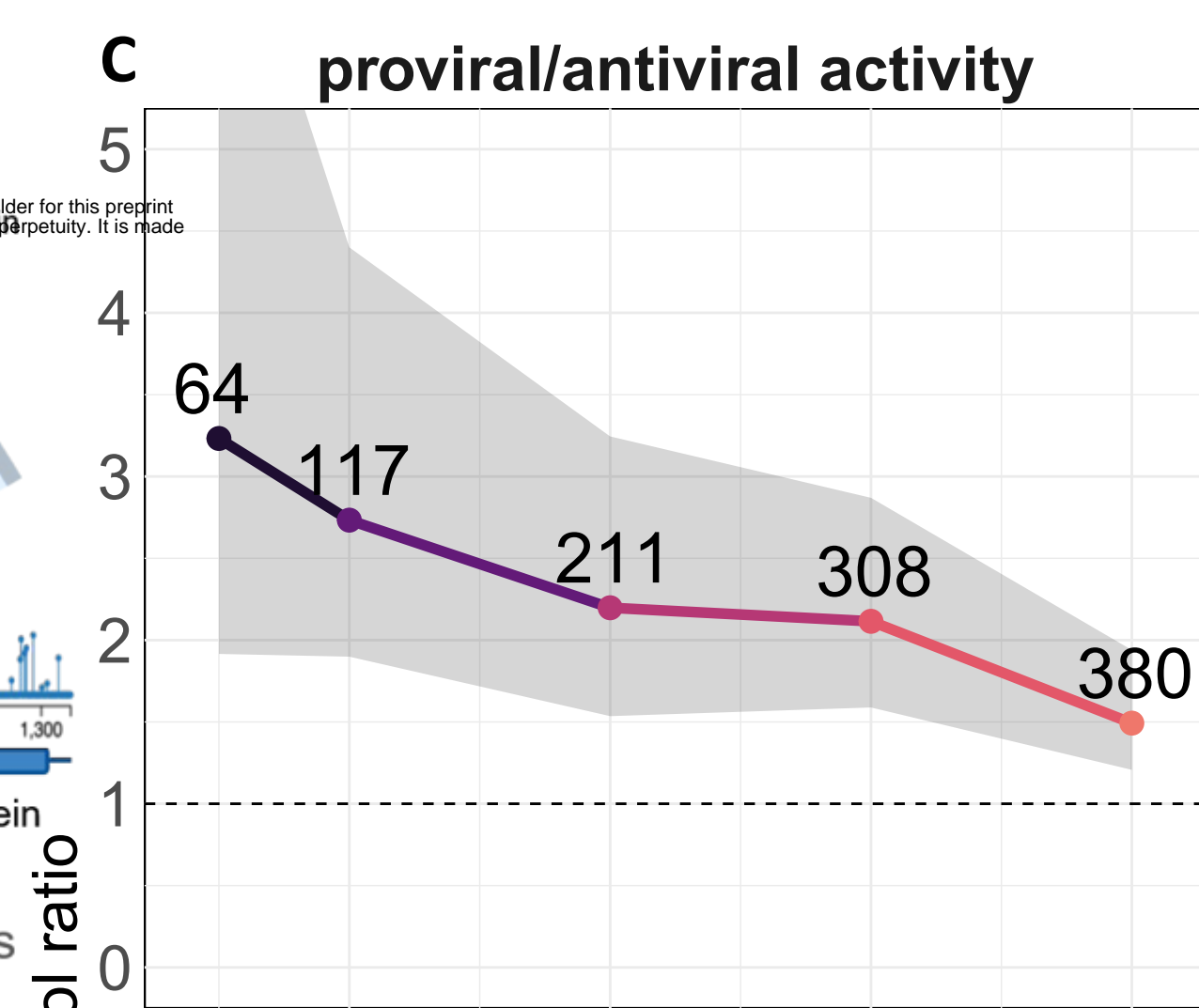
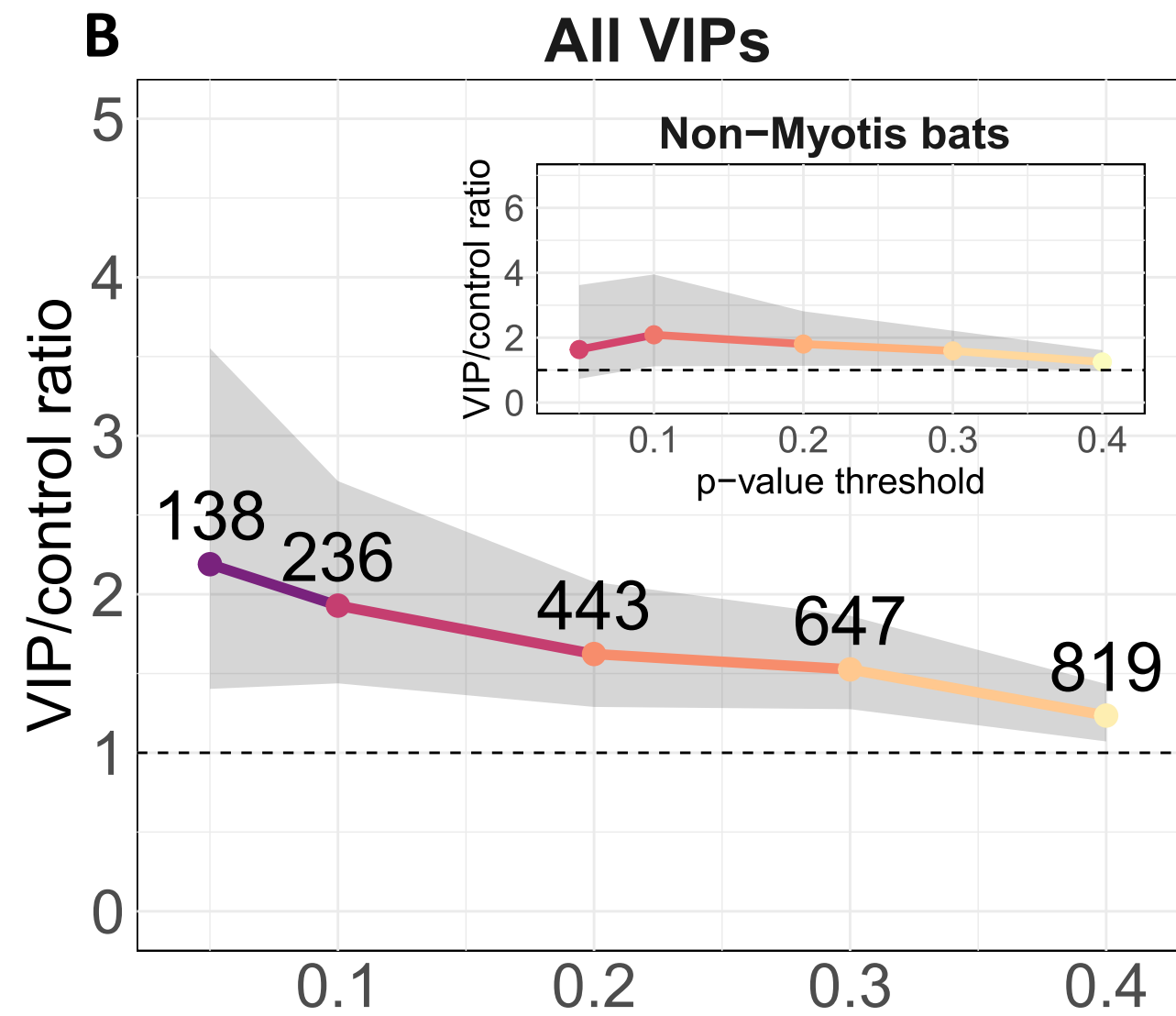
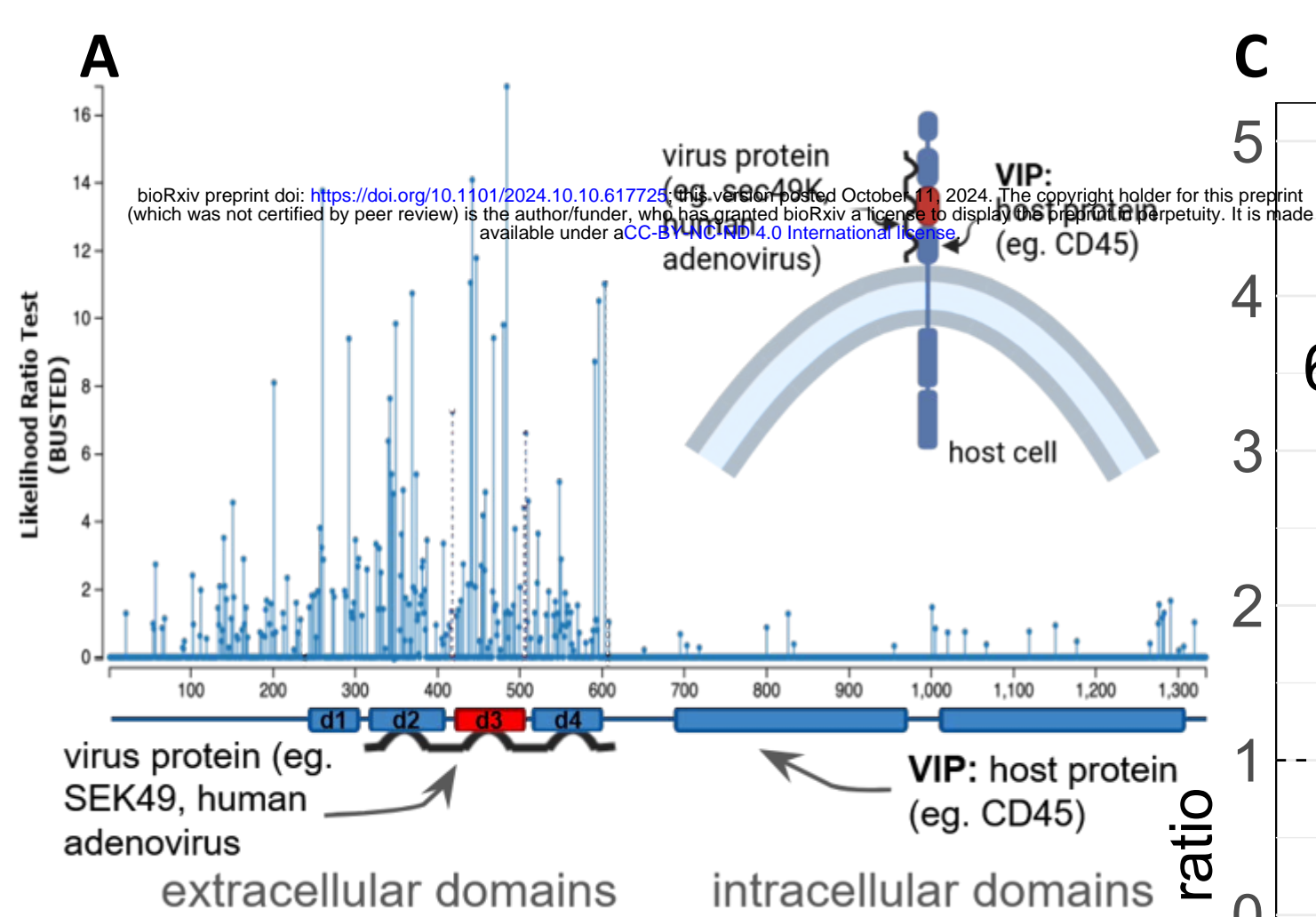




772 **Figure 2:** Evolution of body size, lifespan, and cancer risk in bats and mammals. **A, B)** Cophylo plot of the evolution  
773 of body size (**A**) and lifespan (**B**) across *Eutheria*. **C, D)** Cophylo plot of the evolution of body size (**C**) and lifespan  
774 (**D**) in bats. Branch lengths in **A-D** are scaled proportional to the rate of change of the trait over time, and tree scales  
775 are shown below their respective phylogenies. **E)** Diagram illustrating the relationship between changes in body  
776 size and lifespan with changes in cancer risk and resistance. Changes in either body size or lifespan are directly  
777 proportional to changes in theoretical cancer risk; to resolve Peto's Paradox and normalize cancer risk across  
778 mammals<sup>89,92</sup>, changes in theoretical cancer risk must be inversely proportional to changes of the intrinsic cancer  
779 risk per cell, implying increased cancer resistance. **F)** Reduced Intrinsic Cancer Risk (RICR) for every node in  
780 *Eutheria*, ranked from greatest reduction in cancer risk to greatest increase in cancer risk. RICR relative to the most  
781 recent ancestor of select nodes are highlighted, as well as the average RICR across for all nodes within select  
782 clades.

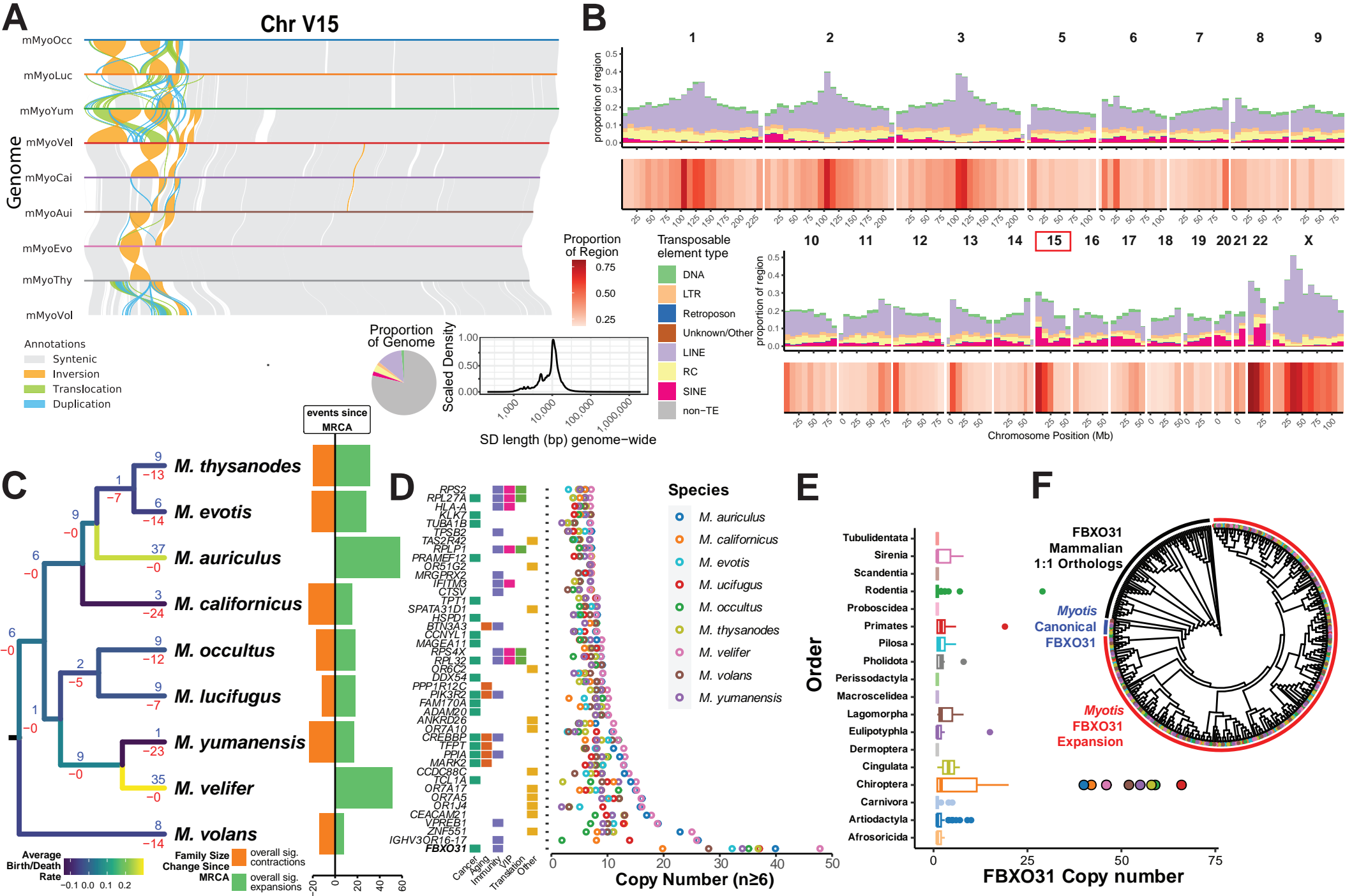


783 **Figure 3:** Selection in Nearctic *Myotis* is enriched for pleiotropic cancer resistance pathways. **A) Left:** phylogeny of  
784 Nearctic *Myotis*; **Right:** raincloud plot of omega values for all genes in each species since its most recent ancestor.  
785 The distribution of omega ( $\omega$ ) values for significant ( $p \leq 0.05$  after multiple testing correction) genes and all genes is  
786 shown in color above the line. The 95% confidence interval and median for significant  $\omega$ 's are represented by the  
787 black bar and circle, respectively; the overall 95% confidence interval and median are shown in grey below.  
788 Individual genes'  $\omega$ 's are represented by colored points. Individual genes' omega values and grey, respectively.  
789 **Left inset:** Proportion of cancer-associated Reactome pathways among the top 100 pathways overrepresented  
790 among genes under selection at each node. Below, pie chart indicates expected proportion of pathways out of 100  
791 that are cancer-associated after 1000 random samples. Nodes with proportions greater than the expected value  
792 with  $p \leq 0.05$  using Fisher's exact test are indicated with an asterisk. **B)** Proportion of cancer-associated Reactome  
793 pathways among the top 100 pathways overrepresented among genes under selection across all nodes in a  
794 species' evolutionary history. **C)** Volcano plot of overrepresented pathways in Reactome among the union set of  
795 genes under selection across all nodes in the evolutionary history for *M. lucifugus*. **D)** Viability and Apoptosis fold-  
796 change in 5 bat species in response to different doses of neocarzinostatin, a potent inducer of DNA double-strand  
797 breaks. Points represent individual replicates normalized to each species' control, while bars represent mean  $\pm$  95%  
798 confidence intervals.

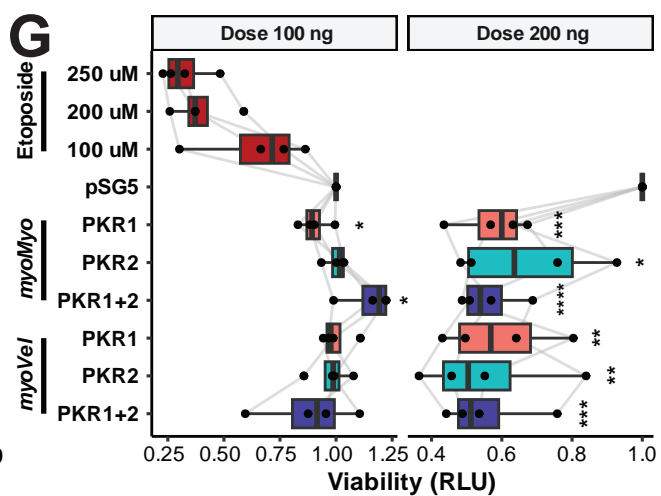
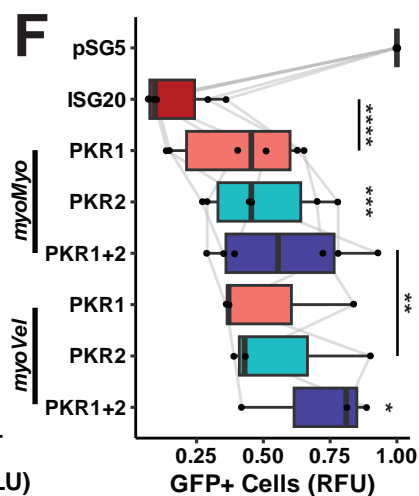
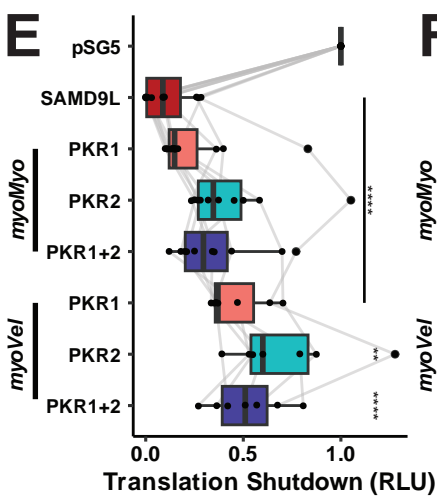
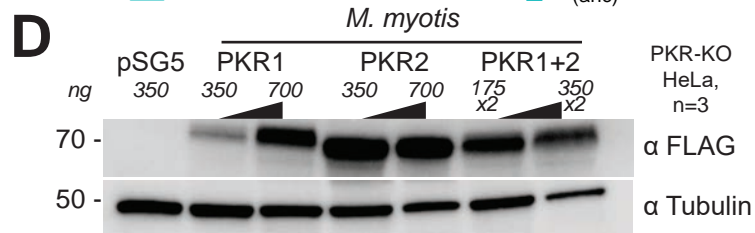
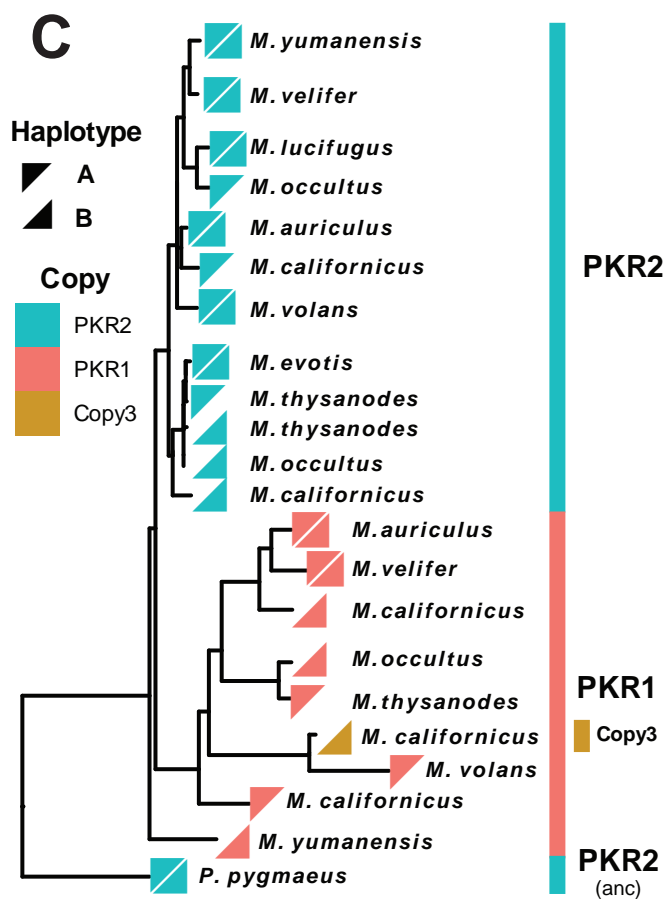
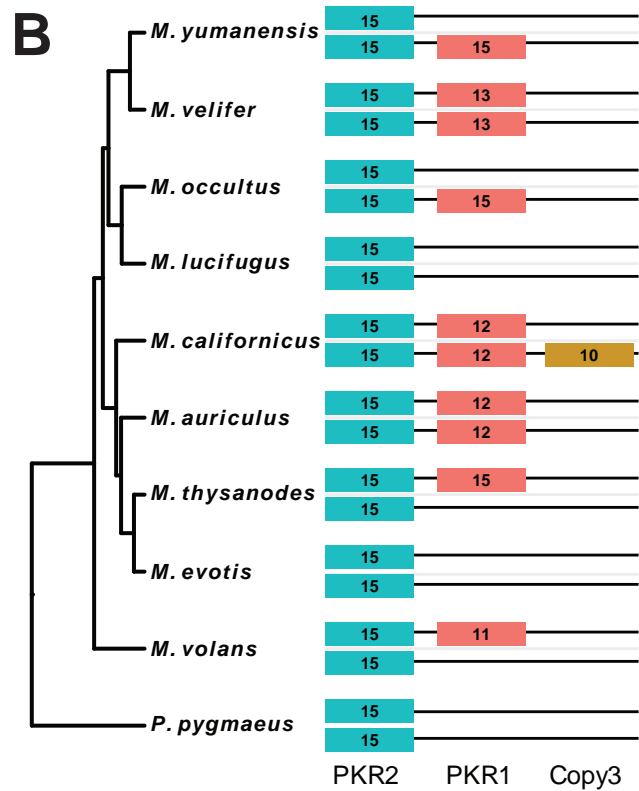
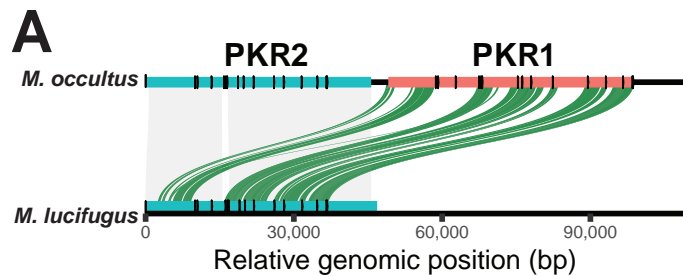




799 **Figure 4:** Adaptation to DNA viruses, but not RNA viruses, is enriched in *Myotis* and other bats. **A)** Diagram of an  
800 example VIP, CD45: a host cell transmembrane receptor that interacts with the human adenovirus protein sec49K.  
801 Previous work has shown that the amino acids of CD45 that participate in this direct interaction are under strong  
802 positive selection, as indicated in the graph above the cartoon. **B-F)** Enrichment plots showing the ratio of positive  
803 selection in VIPs versus matched sets of control genes at different p-value thresholds. The solid line shows the  
804 median ratio; the color of the line, and the number above each point, represents the number of VIPs with significant  
805 BUSTED-MH p-values at the given threshold; the grey band represents the 95% confidence interval generated by  
806 bootstrapping sets of matched control genes. Inset plots show the same for all bats in this study excluding *Myotis*.



807 **Figure 5:** A varied structural variation landscape across 9 nearctic *Myotis* species. **A)** Synteny between *Myotis*  
808 species on chromosome V15, showing syntenic regions (grey), inversions (orange), translocations (green), and  
809 duplications (blue). Regions with high proportions of telomeric repeats were masked prior to alignment. **B)**  
810 Distribution of transposable elements and segmental duplicates in mMyoVel1. Pie chart indicates overall genome  
811 proportions of TEs; histogram represents the size distribution of segmental duplications genome-wide. **C)** CAFE  
812 results among our Nearctic *Myotis* relative to single-copy human orthologs. Phylogeny is colored by the estimated  
813 birth/death rate ( $\lambda$ ) for all genes examined. Bar plot indicates the cumulative number of significant gain and loss  
814 events for each species. **D)** Per-genome copy numbers of all genes with over 6 copies in any Nearctic *Myotis*  
815 genome. Genes are classified into 5 categories (cancer, aging, immunity, VIP, translation, and “Other”) based on  
816 literature reviews on PubMed. **E)** Copy number estimates of *FBXO31* across 536 mammalian genomes identified  
817 using Reciprocal Best-Hit BLAT. **F)** Gene-tree reconciliation of *FBXO31* across mammals generated using  
818 GeneRax.





819 **Figure 6:** Evolutionary history and function of an actively segregating copy number polymorphism of *PKR* in *Myotis*.  
820 **A)** Structural comparison of the single- and dual-copy *PKR* haplotypes across two species. Orthologous regions  
821 between the two haplotypes are indicated by grey bands, while syntenic duplications are indicated in green. Exons  
822 in *PKR1* and *PKR2* are annotated with black marks. **B)** Cartoon of the *PKR* locus in the two phased haplotype  
823 assemblies of each species. While *PKR2* is present across all haplotypes, *PKR1* and *PKR* copy 3 are polymorphic  
824 within and across species. Each number indicates the number of exons identified for each gene in the haplotype.  
825 **C)** The reconciled gene tree for all copies of *PKR* across all haplotypes and species shown in **B**. The haplotype  
826 corresponding to the reference genome of each species (haplotype A) is represented by an upper-diagonal triangle,  
827 while the alternative haplotype (haplotype B) is represented by a lower-diagonal triangle. Nodes where both copies  
828 of a gene were sister to one another were collapsed into a single rectangle for clarity. **D)** Steady state protein  
829 expression levels in *PKR*<sup>-/-</sup> HeLa cells transfected with plasmids encoding FLAG-tagged *Myotis myotis* *PKR1* and  
830 *PKR2* plasmids. Western blots targeting FLAG or Tublin (loading control) in lysate of cells transfected with  
831 increasing amounts of either empty vector (pSG5), *PKR1*-FLAG, *PKR2*-FLAG, or an equimass mix of both *PKR*  
832 vectors. **E)** The effect of *Myotis* *PKR* copy number on the translation of luciferase, measured in Relative Light Units  
833 (RLU) and normalized to the empty vector control. Co-expression of both *PKR1* and *PKR2* has an additive effect  
834 on cell translation shutdown, with no synergy or dominant negative effects observed. Human SAMD9L-GoF was  
835 used as a positive control of cell translation inhibition<sup>251</sup>. **F)** The effect of *Myotis* *PKR* copy number on viral VSV  
836 infectivity. The percentage of VSV-GFP infected cells was measured by flow cytometry and normalized to the control  
837 pSG5 condition. Although all *Myotis* *PKR* conditions restrict VSV infection, expressing both *PKR1* and *PKR2* is not  
838 beneficial against VSV infection. ISG20 was used as a positive control of VSV-GFP restriction<sup>243</sup>. **G)** The effect of  
839 *Myotis* *PKR* copy number on cell viability, normalized to the empty vector control. While no effect on viability was  
840 observed at a lower total dose of plasmid, at higher doses of *PKR* there is a significant reduction in cellular viability.  
841 Etoposide at 3 doses (100  $\mu$ M, 200  $\mu$ M, and 250  $\mu$ M) were used as a positive control for cell death. For **E-F**, error  
842 bars indicate the means  $\pm$  SEM for at least three independent experiments. Statistical significance was assessed  
843 by unpaired t-test of each condition versus control.  
844

## 845 Supplemental Information

846 **Document S1.** Figures S1-S6

847 **Table S1.** Genome Statistics

848 **Table S2.** Phylogeny time calibration and evolutionary modeling data

849 **Table S3.** aBSREL significant gene lists and Reactome enrichments

850 **Table S4.** RERConverge and RELAX results and enrichments

851 **Table S5.** List of VIPs and VIP subclasses

852 **Table S6.** SyRI-identified structural variants (SVs)

853 **Table S7.** Experimental data for Neocarzinostatin and *PKR* experiments